2001

DESIGNING MOLECULAR RECOGNITION IN THE CONTEXT OF HYDROGEN BONDING AND MOLECULAR DYNAMICS

Peter G. Willis
University of Kentucky, pgwill0@pop.uky.edu

ABSTRACT OF DISSERTATION

Peter G. Willis

The Graduate School
University of Kentucky
2001

DESIGNING MOLECULAR RECOGNITION IN THE CONTEXT OF HYDROGEN BONDING AND MOLECULAR DYNAMICS

ABSTRACT OF DISSERTATION

A dissertation submitted in partial fulfillment of the
requirements for the degree of Doctor of Philosophy
in the College of Arts and Sciences
at the University of Kentucky

By

Peter G. Willis

Lexington, Kentucky

Director: Dr. Arthur Cammers-Goodwin, Associate Professor of Chemistry

Lexington, Kentucky

2001

ABSTRACT OF DISSERTATION

DESIGNING MOLECULAR RECOGNITION IN THE CONTEXT OF HYDROGEN BONDING AND MOLECULAR DYNAMICS

The effect of hydrogen bonding on the conformation of organic molecules unifies two projects in this thesis. In one project, the stability of the intramolecular hydrogen bond in derivatives of 2-guanidinobenzimidazole was studied by dynamic ^{1}H NMR spectrometry. The impact that this intramolecular hydrogen bond had on the bond order of the neutral guanidino group and on the dynamic conformation of these aromatic structures was related to the concept of hydrogen bond-assisted resonance. In another project, an oligomer possessing repetitive conformation and capable of much inter- and intramolecular hydrogen bonding was designed and synthesized. The sensitivity of this oligomer to changes in anion concentration, as well as its own propensity to self-aggregate were measured.

Hydrogen bonds found in many biological oligomers are connected though a system of conjugated bonds. Guanidinobenzimidazole is a conjugated system of carbon and nitrogen, connected by an intramolecular hydrogen bond. Several

derivatives of guanidinobenzimidazole were synthesized, and the effect of several simple alkyl for hydrogen substitutions were studied. Guanidinobenzimidazole was used as a model to study what effect the conjugation and the intramolecular hydrogen bond have on each other.

The formation of redundant low energy hydrogen bonds is universal in biological oligomers. In DNA and RNA multiple hydrogen bonds are formed with a typical energy contribution of only 1-2 kcal/mol. Individually, these interactions do not give the biological oligomers their conformational stability, but together they are very stable. The urea and amide based oligomers designed in the work and discussed in the thesis should form multiple hydrogen bonds with themselves and/or with anionic guests. Chiral oligoureas were designed to possess this characteristic of cooperative conformation that so many biological oligomers and polymers share.

KEYWORDS: Intramolecular hydrogen bond, Conformational design, Benzimidazole, Oligomers

_____

_____

DESIGNING MOLECULAR RECOGNITION IN THE CONTEXT OF HYDROGEN BONDING AND MOLECULAR DYNAMICS

By

Peter G. Willis

_____
Director of Dissertation

_____
Director of Graduate Studies

_____

RULES FOR THE USE OF DISSERTATIONS

Unpublished dissertations submitted for the Doctor's degree and deposited in the University of Kentucky Library are as a rule open for inspection, but are to be used only with due regard to the rights of the authors. Bibliographical references may be noted, but quotations or summaries of parts may be published only with the permission of the author, and with the usual scholarly acknowledgments.

Extensive copying or publication of the dissertation in whole or in part requires also the consent of the Dean of the Graduate School of the University of Kentucky.

A library that borrows this dissertation for use by its patrons is expected to secure the signature of each user.

Name	Date

DISSERTATION

Peter G. Willis

The Graduate School
University of Kentucky
2001

DESIGNING MOLECULAR RECOGNITION IN THE CONTEXT OF HYDROGEN BONDING AND MOLECULAR DYNAMICS

Dissertation

A dissertation submitted in partial fulfillment of the
requirements for the degree of Doctor of Philosophy
in the College of Arts and Sciences
at the University of Kentucky

By

Peter G. Willis

Lexington, Kentucky

Director: Dr. Arthur Cammers-Goodwin, Associate Professor of Chemistry

Lexington, Kentucky

2001

Dedicated to

My dad

Acknowledgments

The following dissertation, while an individual work, benefited from the insights and direction of several people. First, I would like to thank my Mentor, Dr. Arthur Cammers-Goodwin, for inspiring me to achieve to do quality work as a chemist and to drive me to always seek out knowledge. In addition, Dr. Robert Grossman provided timely and instructive comments and evaluation at every stage of my student career, allowing me to learn and to constantly reevaluate myself as an academic. Next, I wish to thank the complete Dissertation Committee, and outside reader, respectively: Dr. Mark Meier, Dr. Leonidas Bachas, Dr. John E. Anthony, Dr. Boyd E. Haley, Dr. Mark S. Meier and Dr. Malcom J. Avison. Each individual provided insights that guided and challenged my thinking, substantially improving the finished product.

Thanks go to current and former students in the Cammers and Grossman research groups. They have provided support and assistance that allowed me to achieve my goals as a chemist. Especially, Dr. Milind Sindkhedkar for his assistance in the synthesis of some of the oligoureas. I would also like to thank Dr. Hormuzd Mulla for his assistance with the guanidinobenzimidazole derivatives.

In addition to the technical and instrumental assistance above, I received equally important assistance from family and friends. My wife, Becky Lowery, provided on-going support throughout the dissertation process. My father, Raymond Willis, instilled in me, from our family conversations over the dinner table, the desire and skills to obtain the Ph.D.

Table of contents

List of tables

List of figures

List of files

Willis.Peter.Gordon.PhD.thesis.pdf	Adobe Acrobat portable document file

Chapter 1

A model system for intramolecular hydrogen bonds connected through a conjugated heteroatom system

1.1 Overview

The theme of this thesis is the exploration of hydrogen bonds as a controlling factor in the conformation of organic molecules. In most biological systems, including protein and DNA, hydrogen bonds help to form the complex biological structures necessary to sustain life. Regarding hydrogen bonding in protein and DNA, other factors including steric control lead to complex substructures including the α-helix, β-sheet and in DNA, the double helix. An understanding of the mechanisms and patterns involved in hydrogen bonding is crucial to the ability to understand and modify the activity of these biological structures.

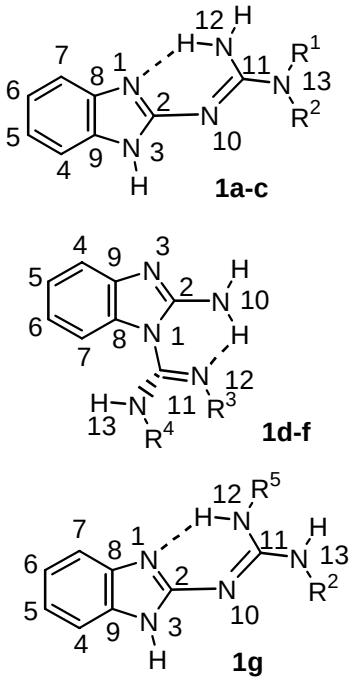

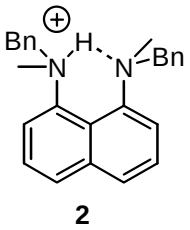

1: Derivatives of 2-aminobenzimidazole
1a: $R^{1,2}$ = H; **1b**: $R^{1,2}$ = Me; **1c**: $R^{1,2}$ = iPr; **1d**: $R^{3,4}$ = iPr; **1e**: $R^{3,4}$ = p-tol; **1f**: $R^{3,4}$ = Me (not isolated)
1g: $R^{2,3}$ = iPr
2: 1,8-bis(*N*-benzyl,*N*-methylamino) naphthalene

Figure 1.1 1,5-Diaminoaromatic structures

In the first part of the thesis, the reader will encounter a detailed analysis of the energetic contribution to overall conformational stability of six-centered intramolecular hydrogen bonds in nitrogen-based aromatic systems, which can have more than one tautomeric form. In this type of system the rate of hydrogen atom exchange is important because hydrogen atom exchange converts one tautomer to another. Furthermore, the hydrogen atom exchange tautomers possess different bond orders. A double bond greatly impedes bond rotation whereas a single bond allows bond rotation.

In chapter two there is a discussion on the details of syntheses of 2-aminobenzimidazole derivatives. These syntheses uses 2-aminobenzimidazole and 1,2-phenylenediamine with electrophiles including carbodiimides and dialkyl-dicyandiamides (*N,N*-dialkyl-dicyandiamides). The synthesis of these compounds was facile and included only one or two synthetic steps to get from a commercial

product to the desired chemical. In most cases only required crystallization for purification. For **1g** an initial purification was done, by column and a subsequent crystallization was required due to the tendency of these compounds to streak on the column.

In Chapter three this thesis moves from a problem in minute analysis to a problem in the global design of a family of oligomers (oligoureas) that can take on hydrogen bond-dependent conformations. The effort was directed toward the mimicry of the peptide backbone in its ability to bind anionic guests as in the case of sulfate[6,29] and phosphate binding proteins. Since it is the N-H contacts in the phosphate binding protein that stabilize the enfolded anions,[26] we reasoned that oligoureas should do this better. Oligoureas have twice as many N-H hydrogen bond donors per residue than the peptide chain. The work in this thesis scratches the surface of the full potential of this project to flower into a comprehensive study. Forays were made into the synthesis of the desired materials. Using the conformation and intermolecular hydrogen bonding in a crystal structure of a dimer as a footstool, we extrapolated to the conformation of extended structures using molecular modeling. Some physical studies (nuclear magnetic resonance spectrometry and circular dichroism spectrometry) were also performed to assay the hydrogen bonding interactions between oxo-anions and oligoureas.

Before we began this work there was discrepancy in the literature regarding the presence of an intramolecular hydrogen bond in guanidinobenzimidazole. In our studies we found indirect evidence for the existence of a weak, intramolecular hydrogen bond in guanidinobenzimidazole

through a study of derivatives for this molecule. Because this hydrogen bond is weak hydrogen atom exchange is an important phenomena in the control of the rate of hydrogen bond cleavage. The relative rates of exchange processes in guanidinobenzimidazole is therefore very solvent dependent.

In the other theme of this thesis, interactions between *de novo* oligomers and anions were studied by modeling and a few binding assays of various derivatives to determine the influence of the shape and conformation of the monomer units on the shape and resulting properties of the oligomer. The effect of intramolecular hydrogen bonds and aggregation were studied for their ability to lead to interesting conformations of oligoureas. The oligomers contained hydrogen bond donors and acceptors, as well as a significant volume of hydrophobic matter. We hope that aggregation and self-condensation of the monomer units will lead to cooperative effects in these large oligomers, leading to stronger hydrogen bond interactions and stable repeating conformations.

1.2 Introduction

Guanidinobenzimidazoles **1a-c, g** and 2-amino-1-carboxamidinylbenzimidazole **1d-f** offer a unique opportunity to study the effect of substitution patterns on the strength of an intramolecular hydrogen bond. The hydrogen bonds of these structures were analyzed to determine the conformational control that they exert over conjugated systems capable of tautomerization. The intramolecular hydrogen bonds in these structures are found in a general class of 1,3-diamino aromatic structures. A classic example of this type of hydrogen bond is found in ‘proton sponge’, **2**, in its protonated

form.[9,20,21] Crystal structures of protonated 1,8-diaminonaphthalene derivatives have an N-H-N hydrogen bond length of ~2.65 Å.[9] This value is close to the N-H-N bond distance in neutral guanidinobenzimidazole in the solid state (crown ether complex 2.69 Å[8], and uncomplexed 2.75 Å[35]). Isopropyl substituted guanidinobenzimidazole, **1c** and **1g** also had similar bond distances of 2.67 Å, and 2.78 Å (this work). The gas state calculated structure of **1f** had a N-H-N bond distance of 2.80 Å despite some steric issues that prevent a planar molecule. In the crystal structure of **1d** there were no intramolecular hydrogen bonds, indicating that the hydrogen bond should be weak.

The 1,8-diaminonaphthalene salts have raised questions about the possibility of low barrier hydrogen bonding. The major difference between these six-centered internal hydrogen bond acceptor pairs and the models studied in this work are the charge and the symmetry of the intramolecular hydrogen bond. Protonation of **2** reduces the strain caused by the steric crowding and the repulsion between the lone pairs of the nitrogen atoms, and lowers the energy required for protonation. The proton involved in the hydrogen bond in **2** is constrained to point at the hydrogen bond-acceptor nitrogen atom, strengthening the intramolecular hydrogen bond.[34]

Conjugated systems can increase hydrogen bond strength. When a system, like **1**, significantly perturbs the stability of an intramolecular hydrogen bond, the effect is referred to as resonance-assisted hydrogen bonding.[16,17,36,37] Our work indicated that the stability of the intramolecular hydrogen bond in model structures **1a-f** was intimately tied to the local structure.

This work compared the stability of the hydrogen bond in **1b-c,g** with analogous interactions in **1d-f**. The solvent effect was also considered. The hydrogen bond in **1a-c,g** had limited control of the dynamics of the structure, but slow proton exchange, and limited conformational mobility were required to explain how the hydrogen bond in **1d-f** appeared to contribute significantly to the dynamics of the structure.

1.2.1 The impact of hydrogen bonds on the conformation of organic molecules

Intramolecular hydrogen bonds are implicated in the control of the conformation of many biological molecules and are said to contribute to the interactions necessary for efficient molecular recognition.[11,12,25,32] Hydrogen bonds are a primary source of conformational stability in proteins and DNA, decreasing the mobility of helices, β-sheets, and β-turns. In DNA, the double helix is held together by multiple hydrogen bonds in a conjugated system. In these systems, each hydrogen bond has an estimated strength of 6-7 kcal/mol from mass spectrometric experiments.[18] All together, these interactions bind the strands together, and provide a basis for the genetic code. However, each hydrogen bond individually is weak enough for the changes in state necessary for the repair and packaging processes required by the biological mechanism.

The strength of an isolated hydrogen bond interaction is generally between 2.1 and 5.8 kcal/mol,[16] and is primarily an electrostatic interaction. The length of this type of hydrogen bond is between 2.65 Å and 2.84 Å from heteroatom to heteroatom.[15,16] X-ray diffraction analysis of derivatives of 2-

aminobenzimidazole analyzed in this work uncovered hydrogen bonds in this range of N–H–N distances. This indicates that **1b,c,g** possess mid-range, text book hydrogen bonds that may say something in general about the impact of hydrogen bonds on conformational stability. These derivatives were compared to another derivative that displayed similar dynamics, but was stericly inhibited from forming short hydrogen bonds. Hydrogen bonds that are longer than 2.84 Å are usually considered weak, and those that are shorter than 2.65 Å are considered strong. The crystal structure of **1d** indicated that **1d-f** might not necessarily have a strong hydrogen bond despite dynamics that indicate that exchange is slow between the two alkyl groups R^3 and R^4.

One of the reasons to study six-centered intramolecular hydrogen bonds is their putative usefulness in stabilizing designed conformations of molecules for the purpose of molecular recognition and drug design. The conformation instead of just the structure is often the target in the design of pharmacophores. This requires the ability to direct the molecular conformation, a task in which hydrogen bonds should prove useful. In pursuit of this task, five- and six-centered intramolecular hydrogen bonds can be used to induce greater stability in dendrimers with the goal of developing dendrimers that fold into stable ordered conformations.[23] Circular dichroism (CD) shows that the 2-aminobenzamide connectors, highlighted in bold in the figure below, increased the structural stability of this dendrimer. Without these connectors, the degree of helicity in the dendron was highly solvent dependant.[22,33] In addition, without the connector, changing to a polar solvent caused a decrease in the CD absorption of the

dendrimers. Addition of the connector in each generation of the dendrimer caused increased helical order with each new generation.[23] This comes despite the fact that the chromophore is concentrated at the periphery of the dendron.

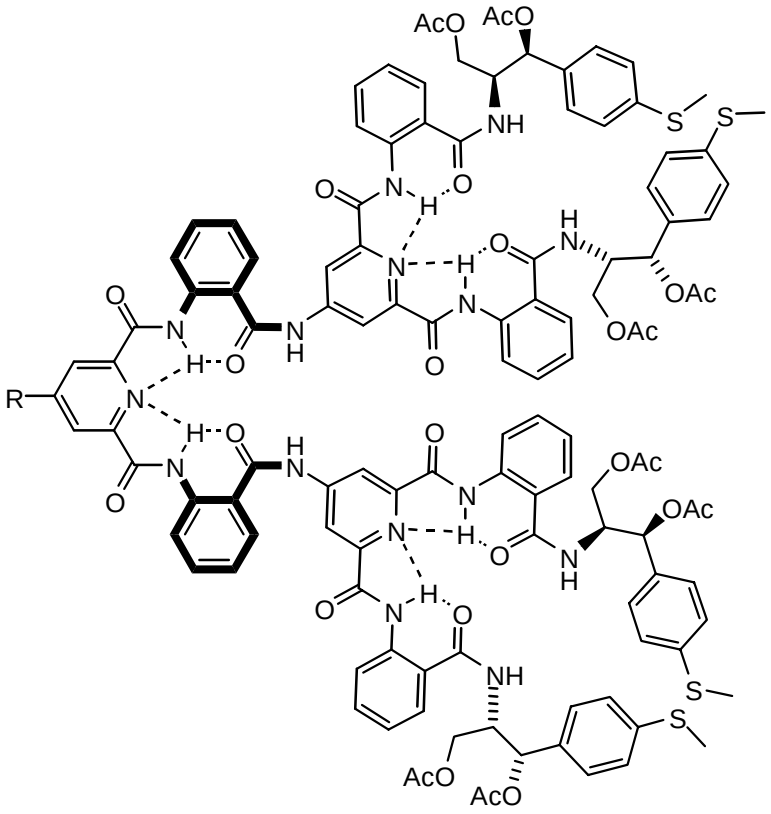

Figure 1.2 Conformational control of dendron packing with five and six-centered intramolecular hydrogen bonds in a second-generation dendron.

The conformation of the above dendron is directed by intramolecular hydrogen bonds.[22] If the internal structure of the dendron was stabilized in a helical form this would correlate to increased peripheral helicity. A 2-aminobenzamide turn unit highlighted in bold in the figure above was used to link each generational shell, and formed a stable six-centered intramolecular hydrogen bond between adjacent amides linked through this subunit. The linker induces a turn in the dendron that folds the outer dendritic shells.[22] The

conformational direction of the intramolecular hydrogen bond is assisted by the stiffness of the three bonds between the hydrogen bond donor and acceptor. This allows for a finite amount of conformers, and an enhancement of the conformational direction of the intramolecular hydrogen bond results.

A similar result comes from **2;** in it, the cleavage of the hydrogen bond is slow on the NMR time scale.[20] This proton sponge is protonated and deprotonated slowly and equilibration of the (d,l)[**2**H^+] to the thermodynamic mixture of meso and racemic forms takes about 10 min.[9] The free energy barrier to rotation does not decrease with increasing solvent polarity, and the strain energy, which is relieved upon protonation of the tetramethyl proton sponge analogous to **2,** has been calculated at 35 kJ/mol.[9] From these observations, it appears that these six-centered intramolecular hydrogen bonds are useful for controlling conformation in structures in which conformational options are limited.

1.2.2 The intramolecular hydrogen bond

Measurement of the distance between heteroatoms is quite useful in identifying strong hydrogen bonds inside proteins and other intramolecular hydrogen bonds. The parameter, d_{AB} is the distance between two electronegative atoms, A and B, in the species A—H---B. As d_{AB} decreases, the A-H bond length increases. In 1,3-diketones at a d_{OO} of 2.4 Å,[32] the proton is equidistant from both oxygen atoms, and the O-H distance decreases in length as d_{OO} increases (See Figure 1.3). The increased symmetry and decreased d_{OO} reduces the barrier to hydrogen atom exchange between the two oxygen atoms to the point where the barrier can become less than the zero point vibrational energy.[32]

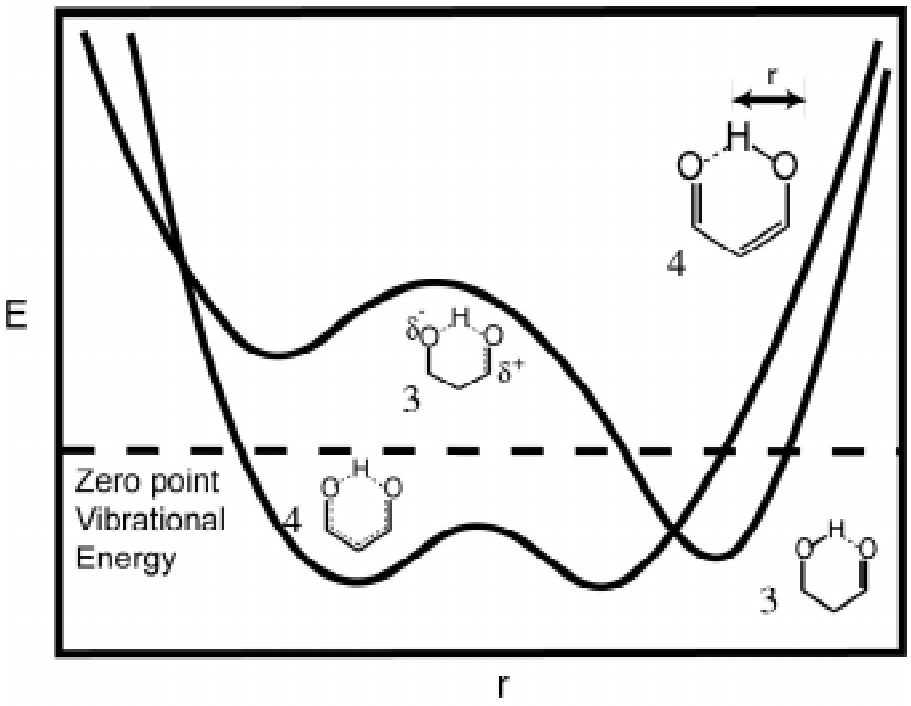

Figure 1.3 Normal hydrogen bonds versus the resonance assisted hydrogen bond showing a lowering of the energy barrier to proton exchange from resonance considerations.

This type of hydrogen bond is called a ‘low barrier hydrogen bond’ and is sometimes identified by a distinctive change in the ^{1}H NMR chemical shift of the protons of interest. The chemical shift of some of the NH protons in **1c** and **1g** moved downfield as the temperature of the sample was reduced. The large downfield chemical shift is not seen in **1d**. This is the derivative with greater conformational control, but no apparent hydrogen bond in crystal structure evidence. **1c** and **1g** are the chemicals in which a short intramolecular hydrogen bond was found in the crystal structure. In **1d** a short intramolecular hydrogen bond was not found in the crystal structure. This effect has been used to identify low barrier hydrogen bonds, but other evidence contradicts this conclusion. In one piece of evidence the downfield proton has a similar chemical shift at room

temperature as an imidazole proton, and this exists in the **1c**, and **1g**, not in **1d**. In a low barrier hydrogen bond, the proton oscillates equally between the two heteroatoms, and as the temperature is reduced, the proton spends more time exactly between the two heteroatoms. This effect decreases the electronic shielding of the hydrogen nucleus, which results in a downfield shift.

Intramolecular hydrogen bonds show a similar effect, but the magnitude is generally decreased compared to low-barrier hydrogen bonds. Thus, smaller downfield shifts are used to identify intramolecular hydrogen bonds.[19] In one system, VT-NMR and VT-IR were used to detect and identify free and intramolecularly bound amide NH.[19] The intramolecular hydrogen bond seen in **1c**, and **1g** however had little effect upon the dynamics of the guanidine moiety under protic conditions. Under conditions with no protic solvent and limited amounts of an analyte, conformational control increased.

1.2.3 Intramolecular resonance assisted hydrogen bonds

Intramolecular hydrogen bonds connected by a series of conjugated bonds can be much stronger than the normal hydrogen bond with the same two atoms not electronically connected by a π-system. This hydrogen bond is typically called a ‘resonance assisted hydrogen bond.’ Hydrogen bonds can affect changes in covalent bond order. Figure 1.3 shows **4,** which is a typical resonance assisted hydrogen bond. Compound **4** is connected by a series of conjugated bonds and when compared to **3**, has the stronger hydrogen bond. The carbonyl in **4** is lengthened, and in fact, this trend is general. The smaller the O-O distance, the longer the carbonyl stretching frequency.[15,16]

In this part of the thesis we probe the differences in stability between two types of six-centered intramolecular hydrogen bonds both possessing π-conjugated N1-C2-C3-C4-N5-H6 connectivity **1a-c,g** and **1d-f**. We found that the relationship between the two different types of six-centered intramolecular hydrogen bonds was tentative and differences could not be directly compared. In **1a-c,g** proton exchange obscured the energy of the intramolecular hydrogen bond, but evidence does suggest that the hydrogen bond and the hydrogen atom exchange that accompanies it is adds more electron density between C2 and N10 and less between C11 and N10.

1.3 Determination of the conformational stability of a six-centered aromatic system with an intramolecular hydrogen bond.

Six-centered aromatic structures with an intramolecular hydrogen bond have proven to be useful in the design of conformationally stable molecules. This functionality, seen in structure **1a-g,** was investigated experimentally though an analysis of the dynamics of these molecules. The hydrogen bond in **1a** should be stable in solution, but the chemical literature gives conflicting evidence regarding the stability of the intramolecular hydrogen bond of guanidinobenzimidazole. The crystal structures of **1a** show an N1-N12 distance of 2.75 Å,[35] and show the molecule to be planar.[1] This implies that the hydrogen bond can obtain optimal conformation.[16,17] However, in solution there is little evidence for a strong intramolecular hydrogen bond or for a static planar structure.[1,7,35,38] Solution state ^{15}N, ^{13}C and ^{1}H NMR studies indicate a weak or non-existent intramolecular hydrogen bond for **1a** because the $^{15}N12$/ $^{15}N13$ exchange is rapid and

accelerated by protic solvents.[1,5,10] The exchange of ^{15}N1/ ^{15}N3 in **1a** at the imidazole ring correlates with protic exchange, but is not mechanistically related to guanidino ^{15}N12/ ^{15}N13 exchange. In **1a** dissolved in CD_3OD, both processes are fast on the NMR time scale; however, $DMSO_{d6}$ suspends ^{15}N1/ ^{15}N3 exchange and allows ^{15}N12/ ^{15}N13 exchange. This behavior indicates that proton exchange is a bimolecular process in the absence of protic polar species. In $DMSO_{d6}$ intermolecular proton exchange is suspended by impeding the aggregation of **1a**. Our studies of the guanidinobenzimidazole derivatives also indicate that exchange of the benzo hydrogen atoms is more strongly related to proton exchange than exchange of the alkyl groups attached to the guanidine terminus.

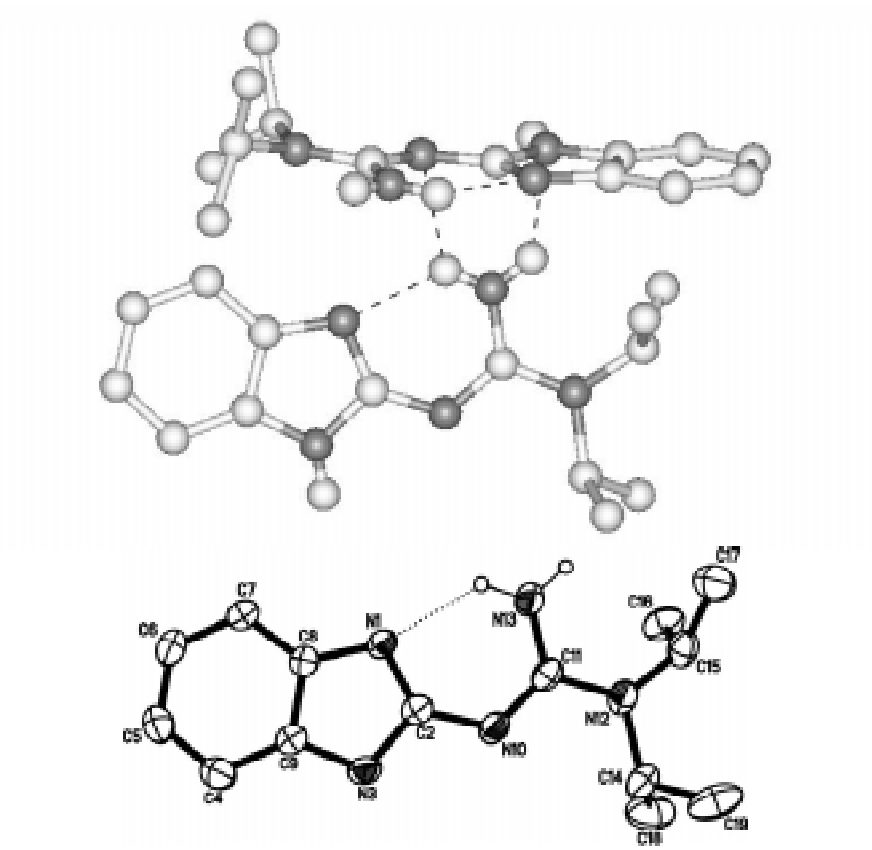

Figure 1.4 Crystal structure of 1c

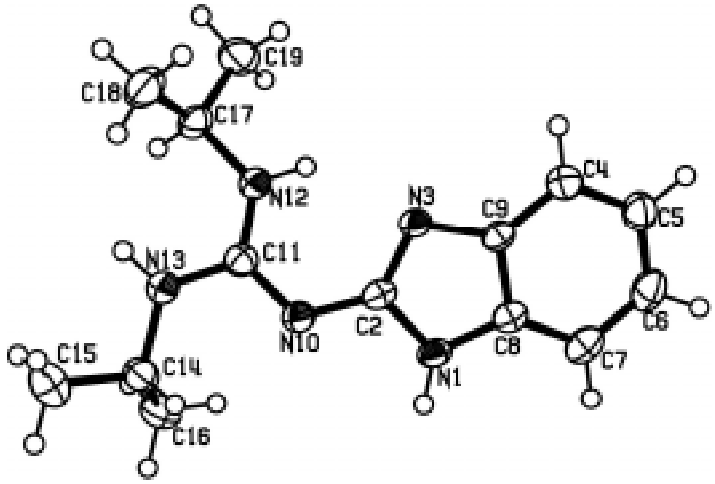

Figure 1.5 crystal structure of 1g

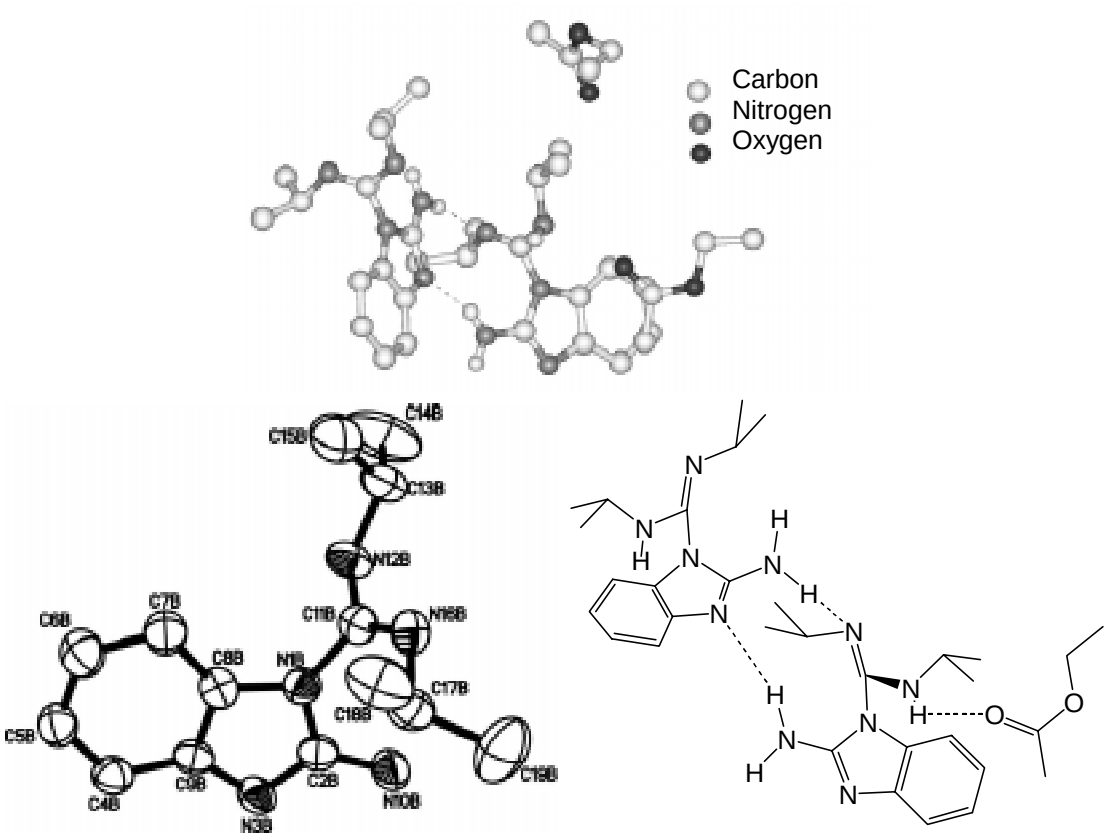

Figure 1.6 Crystal structure of 1d

Figures 1.4 and 1.5 show that the guanidinobenzimidazole derivatives **1c,g** are planar in the solid state, while Figure 1.6 shows that **1d** was not. The intermolecular hydrogen bonds in the crystal structure of **1c** did not interfere with the planarity of the molecule as seemed to be the case in **1d** Figure 1.6. Molecules of **1c** stacked in antiparallel fashion hydrogen bonded with each other to form a T-shaped aggregate. This interaction could have been of the cation-π or proton-π type that have been recently investigated.[14,28,31,40]

In contrast to the molecule **1c**, in one molecule of **1d** N3 and N10 hydrogen bonded with a symmetry-unrelated molecule of **1d** at N12 (16). In the crystal structure determination of **1d** the dihedral angle of axis V (see Figure 1.7) was close to 90° with 4 different intramolecular hydrogen bonds with other

molecules of **1d**, and one with the carbonyl oxygen of a molecule of ethyl acetate. This occurs despite the fact that esters tend to be very poor hydrogen bond acceptors. In solution, the amount of tight intermolecular hydrogen bonds should have been reduced and the packing forces of the crystal eliminated. In fact, the two isopropyl methine protons were distinctly different in the proton spectra. This may be attributed to an intramolecular hydrogen bond, however in contrast to what is observed for the **1a-c,g**, exchange rates were unaffected by the polarity and proton availability of the solvent. A gas phase calculation minimized to a dihedral angle of 36-42° for rotation about axis V for the **TT** conformer of **1d** shown in Figure **1.9**. This calculation was run with Gaussian at b3lyp/631G* theory level. The structure was optimized at this theory level using the standard minimization protocol for all possible conformers described in the text under Figure 1.10.

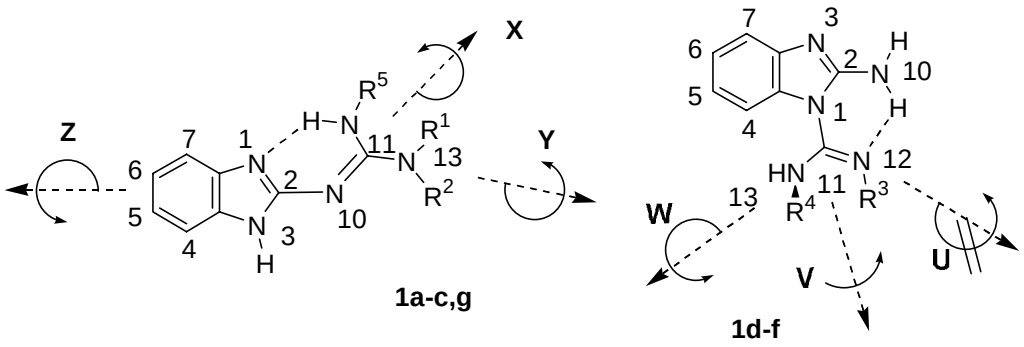

Figure 1.7 Axes of rotation observed to exchange protons in ^{1}H NMR

This work studied the impact of small changes in the substitution pattern of a conjugated heteroaromatic system and an intramolecular hydrogen bond in guanidinobenzimidazole on the structure and dynamics of the molecule. The barriers and rates were determined by monitoring the exchange of a set of alkyl

protons or a set of benzo protons on the derivative of **1**. For derivatives **1b,c** the rate of exchange by rotation was determined for two bonds, N13-C11 and N10-C2 (axis Y and Z in Figure 1.7) using VT-H^1NMR for acquisition of kinetic data. For derivatives **1g,** the rate of exchange by rotation was determined for two bonds, N10-C11 and N10-C2 (axis X and Z in Figure 1.7) using VT-H^1NMR for acquisition of kinetic data. Exchange was assumed to occur around axis Y but the rates were too fast or the chemical shifts too similar for interpretation of the exchange rates. Exchange rates were also determined for the rotation around N13-C11 and N1-C11 (axis W, V in Figure 1.7) for **1d,e**. In **1a-c**, rotation around axis X and Z broke the intramolecular hydrogen bond, but rotation around axis Y did not. Rotation around axis X was not favored because this rotation would have resulted in a sterically strained structure instead of a hydrogen-bonded structure. Only rotation around Y and Z were observed. In **1d,e** rotation about axis U and V broke the hydrogen bond, and W did not. However, proton exchange was required for the exchange to occur. The molecule only registered one pKa at about pH 7 and none at a low pH. Proton exchange may be very slow at the carboxamidine nitrogen atoms in this situation. Again, two rotations were observed W and V. Rotation around the axis U by itself would work against a double bond. To get to a ground state from this conformation would require another rotation around axis V. With a proton exchange, rotation U combined with V would be the same as a simple, single rotation around W. This issue is discussed in detail in the text under Figure 1.9.

The CN double bond in **1d,e** appeared to direct the conformation of alkyl groups. One alkyl group was held over the benzo part of the heterocycle, and the other near the amine. The hydrogen bond could not be strong due to the significant steric hindrance that prevented planarity in **1d**. With **1b,c** there were more degrees of rotational freedom for the six-centered intramolecular hydrogen bond than for **1d,e**. The molecule **1b,c** appeared to rotate about axis Z with almost no hindrance from the intramolecular hydrogen bond under protic conditions.

Table 1.1 Rate of exchange for the derivative at the indicated axis in the indicated solvent.

Solvent / Bond	CD_3OD	$CDCl_3$	Conc. Of protic material in CDCl3 sample per 750 ul
1b Y	72.5 Hz (213 K)	*	8 mg **1b**
1c Z	81.1 Hz (213 K)	16.3(218 K) 60.2 (243 K) *	8 mg **1c** 8mg **1c** 20 mg **1c**
1c Y	962.8 Hz (225 K)	1332.9 Hz (228K)	20 mg **1c**
1c (N13–*i*Pr)	967.5 Hz (214 K)	*	20 mg **1c**
1d V	722 Hz (328 K)	406.2 Hz (305K)	8 mg **1d**
1d W	132.8 Hz (250 K)	100.0 Hz (257K)	8 mg **1d**
1e V	156.2 Hz (290 K)	123.1 Hz (296K)	8 mg **1e**
1e W	14.9 Hz (230 K)	ND	8 mg **1e**
1g X	116 Hz (223 K)	283 (263 K)	8 mg **1g**
1g Z	158 Hz (223 K)	7 Hz (263 K)	8 mg **1g**

1.3.1 Determination of the energy barriers for guanidinobenzimidazole derivatives by VT-^{1}H-NMR.

The above rates of exchange in table 1.1 were used to determine the barriers to exchange for all the derivatives of 2-aminobenzimidazole. Exchange rates were determined from the equation $k=\pi\Delta_{AB}/2^{1/2}$ where Δ_{AB} is the difference

in chemical shift of the resonances undergoing chemical exchange. Limiting values for Δ_{AB} in many cases were determined by plotting the difference in chemical shift over a range of temperatures. Substituting the exchange rate, k, into the Eyring equation, $k=(k_BT/h)exp(-\Delta G^{\ddagger}/RT)$, allows for the determination of $\Delta G^{\ddagger}$. The error in the rate measurement was about 6-9% as given by gNMR™ for the accuracy of its full line shape analysis. The concentration of the analyte is given, because the rates are at least partly dependant upon proton availability.

For cases in which the two peaks did not coalesce, and for double checks of the accuracy of the coalescence method, the rate of exchange was found by analyzing the shape of the peak with the program gNMR™. The program estimated the rate of exchange required to simulate a peak with the required peak width and position, from the low temperature chemical shifts and from imported real data points of the peaks of interest into gNMR™. A limited amount of exchange information could be processed from the current system. With the systems **1d,e** the simulations program was not set up to handle all the protons and the multiple conformers for determination of rotation around axis V. The presence of multiple conformations was simulated with line broadening which was consistent over multiple temperatures.

1c also had multiple conformers at low temperatures in CD_3OD and $CDCl_3$. These conformers were well resolved in methanol but not in chloroform, which has a smaller working range of temperatures for VT-NMR. As a result, only the methanol set was resolved into its component rates. **1g** had the potential for having multiple conformers in low temperature solution. The average position of

the two isopropyl methine resonance peaks in chloroform and in methanol shifted slightly as the temperature was lowered. This may indicate an unequal population of two sets of conformers. To compensate for this, and to reduce error in the calculation, the chemical shift of the two peaks was set as a variable and simulated in gNMR™.

To determine the exchange rate of two inequivalent isopropyl methine protons, they were coupled with six equivalent protons, and the two methine protons were exchanged to match the peak shape of the spectrum, thus simulating the coalescence of two methine protons. The peaks for the part of the spectrum of interest were imported into the program and the program matched the shape and the size of the peaks by automatically calculating a probable exchange rate to change the size and shape of the peaks, then recalculating the exchange from the difference in the calculated and the experimental spectra. Solvent and other extraneous peaks are truncated to avoid confusing the program

Table 1.2 Experimental energy barriers for the derivative at the indicated axis in the indicated solvent.

	$\Delta G^{\ddagger}_{rotation}$ (kcal/mol)		
Solvent / Axis	CD_3OD	$CDCl_3$	Conc. Of protic material in CDCl3 sample per 750 ul
1b Y	10.5 (213K)	*	8 mg **1b**
1c Z	10.2 (213K)	Low exchange catalyst 11.4 (218 K) 12.1 (243 K) High exchange catalyst *	8 mg **1c** 8mg **1c** 20 mg **1c**
1c Y	10.5 (225K)	<10.1 (228K)	20 mg **1c**
1c (N13—*i*Pr)	9.5 (214K)	*	20 mg **1c**
1d V	14.4 (298K)	14.2 (305K)	8 mg **1d**
1d W	12.1 (250K)	12.6 (257K)	8 mg **1d**
1e V	14.0 (290K)	14.5 (295K)	8 mg **1e**
1e W	12.1 (230K)	*	8 mg **1e**
1g X	10.8 (223K)	12.4 (263 K)	8 mg **1g**
1g Z	10.7 (223K)	14.3 (263 K)	8 mg **1g**

In the table above the symbol * indicates that the NMR peaks did not separate at temperatures at which $CDCl_3$ is in the liquid state, or there was not

enough information to determine the rate of exchange. The pK_a values for **1a-d** were 7.2, 7.3, 8.2, and 7.4, respectively. The pK_a of **1e** was not determined due to low aqueous solubility.

1.4 Mechanism of exchange

The X-ray structures of **1a,c,d,** and **g** show a material with nitrogen atoms that have a flat trigonal pyramidal geometry. This indicates that N12 and N13 (numbering from Figure 1.1) have significant p character. Furthermore, the mechanism of geometrical isomerization of C=N apparently switches from inversion to rotation as the CN bond order decreases.[2,30] Three resonance structures distribute electrons in guanidine, so that the three CN bonds have bond orders greater than one and less than two.

1.4.1 Inversion or rotation

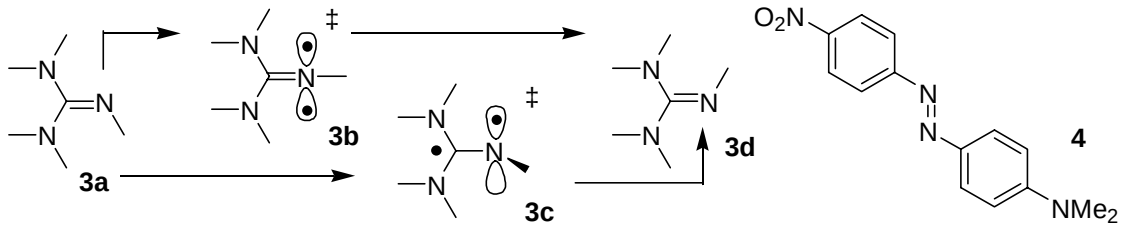

Figure 1.8 Mechanisms of exchange for substituents on guanidine.

Inversion (**3a** to **3b** to **3d**) (see Figure 1.8) has been promoted as the best mechanism for exchange of substituents on monosubstituted nitrogen atoms of guanidine, whereas rotation (**3a** to **3c** to **3d**) is the only mechanism for disubstituted nitrogen atoms in neutral guanidine and in all guanidinium species.[24] In one case, the barrier to rotation in a guanidine was estimated to be 12 kcal/mol higher than the barrier to inversion![24] This result seems incredible given that sp^2 hybridized nitrogen atoms in charge-neutral 4-nitro-4'-

dimethylaminodiphenyldiazene **4** rotate in polar solvents and invert in apolar solvents.[39] One of two compelling pieces of evidence for inversion in guanidine derivatives comes from Hammett free energy correlations in which σ_r stabilizes the transition state through electron withdrawal.[2,24] Other evidence comes from trends observed in known barriers to inversion and rotation. Steric hindrance usually impedes rotation and facilitates inversion, and steric strain in neutral guanidine facilitates exchange of substituents on nitrogen atoms in which inversion is feasible. When the two disubstituted guanidine nitrogen atoms are connected with an ethylene linker in a basic guanidine molecule, the barrier to rotation is decreased by approximately seven kcal/mol.[4,30]

The mechanism of geometrical isomerization of C=N apparently switches from inversion to rotation as the CN bond order decreases.[2,30] This correlates well with a mechanism of heterolytic or a homolytic cleavage of the pi-bond as in the transformation of **3a** to **3b** in Figure 1.8. The isomerization barrier of phenyl-carbonimidic acid dimethyl ester, $(MeO)_2CNPh$, 14.4 kcal/mol, was found to be higher than that of phenyl dithiocarbimidoic acid dimethyl ester, $(MeS)_2CNPh$, with a barrier of 13.8 kcal/mol.[30] Therefore, greater resonance stabilization leads to a lowered barrier to rotation around the CN double bond.

General sentiment in the literature is that disubstituted amines in guanidine bases rotate.[3,4,30] The above mechanisms only require rotation at disubstituted amines. The exception to this rule is the rotation along axis Z in derivatives **1b,c**, and along axis X and Z in **1g**. Calculated barriers for this rotation are similar to the experimentally determined value for the barrier to

exchange. Again, **1b,c** are tautomerizible compounds and proton exchange can produce the high-energy tautomer **15**. The dynamics of **15**, described below, demonstrate another believable mechanism for the rotation around axis Z.

Dynamic studies of **1a-g** also indicated that rotation and not inversion was the best (most simple) explanation for the exchange of nuclei. On the *N,N*-derivatives **1b,c** exchange was observed between alkyl groups on N13, and between protons on benzo carbons C4, C7 and between C5,C6. Rotation of axes **Y** and **Z** made the observed exchange match the mechanism of exchange. With the intramolecular hydrogen bond intact in the ground state, inversion at N10 makes a high-energy structure, which must then rotate to get to a lower energy structure or invert to return to the original configuration. Calculations revealed in the ground state structure of **1b,c** that N10-C2 had a bond order closer to 1 than to 2. A lower bond order generally means rotation and not inversion.[30]

There are two possible explanations for the dynamics of **1d,e**. In one, the hydrogen bond influences the dynamics of the molecule differentiating the two alkyl groups on the carboxamidine functional group. In this scenario, proton exchange is fast, and rotation is slow along axis V. Therefore, the steric hindrance should also prevent the carboxamidine group from aligning parallel to the benzimidazole. However, this system did not act like the other systems **1c,g**, the system was not affected by any increase in a weak proton exchange catalyst like methanol. In the other scenario, alkyl groups are not differentiated by the hydrogen bond, but by the stable imine. In this scenario, rotation is slow along axes U and W, and proton exchange is slow. The carboxamidine NH may be

much more stable than the imidazole or guanidine NH. This is the simplest explanation and is explained below.

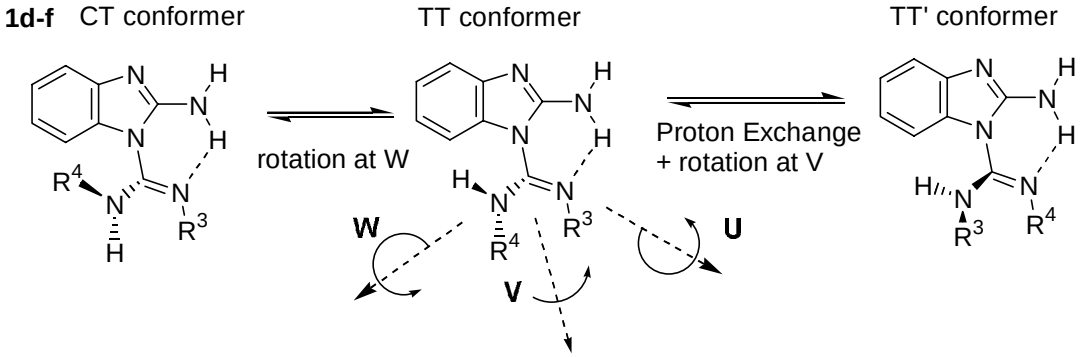

Figure 1.9 Observed species in solution for derivatives 1d,e

The dynamic behavior of **1d,e** could be explained by the structures in Figure 1.9. There were two possible conformers, the **CT** and the **TT** conformer, and both were detected in solution at low temperatures. The **CT** conformer has one isopropyl group cis and one trans to the benzimidazole. The **TT** conformer has both groups trans to the benzimidazole. The exchange at axis V was a high temperature phenomenon and at axis W, a low temperature phenomenon. The proton the nitrogen atom adjacent to R^4 was a controlling factor in all conformations of the molecule. The presence of this proton in **1d-e** broke the symmetry across the plane containing the 2-aminobenzimidazole moiety in **1d-e**.

This rendered the two R groups in the **TT** conformer diastereotopic in magnetically distinct conformational space. The R groups in the **CT** conformer are of course diastereotopic regardless. In the *ca.* 1: 1 mixture of **TT** to **CT** two pairs of *i*Pr methine signals are visible at low temperature. If proton exchange was very slow on the carboxamidine moiety then the presence or absence of the proton exchange is important for the exchange phenomena that occur between

R^3 and R^4. Steric interactions between the benzo CH and the carboxamidine NH or R^4 keep R3 and R4 diastereotopic. The rotation of the carboxamidine group along axis V of the **TT** conformer perpendicular to the benzimidazole makes the two R groups equivalent assuming fast proton exchange. Dynamic 1H NMR supported these conclusions.

1.4.2 Conjecture regarding the rotational transition state of 1b-c

A set of tautomers was investigated computationally for **1b,d**, and **f** to determine which was the lowest in energy and had the lowest barrier to rotation. The barriers to rotation could be determined experimentally for a set of structures, and *ab initio* calculations determined the barrier for individual tautomers. Barriers to rotation could be experimentally determined by monitoring the slow exchange of a set of protons in the ^{1}H-NMR, and calculated *ab initio* with a modeling program that optimized the structure at 6-31G* theory level. Calculations were run by the method described below, to determine the rotational transition state. VT-NMR experiments, as described section 1.5 in were used to experimentally determine the barriers to rotation. The comparison of the barriers determined by experimental and *ab initio* methods were used to generate theories on the strength of the intramolecular hydrogen bond and the mechanisms of exchange in the ^{1}H-NMR.

1.4.3 *Ab-initio* studies of energy barriers to rotation about C-N partial double bonds

Using the Gaussian98 program[13] for molecular modeling a barrier to rotation was determined for *N,N*-dimethyl-*N'*-2-benzimidazoyl at two different

bonds. First the ground state for the molecules was found by an optimization of the molecule starting from a planar state and optimizing at the B3LYP/6-31G* level of theory. For this conformation, the energy was calculated at the MP2/6-311++(2d,2p) level. To determine the barrier to rotation about the Z-axis, the N1-C2-N10-C11 dihedral angle was set and frozen at 90º and then optimized, at the B3LYP/6-31G* level of theory, with that dihedral angle still frozen. The energy for this conformation was then calculated at the MP2/6-311++(2d,2p) level; subtracted from the calculation of the energy of the planar structure also calculated at this theory level. This procedure was repeated for the C2-N10-C11-N12 dihedral angle for **1b**.

The intramolecular hydrogen bond appears to still affect the molecule even with the dihedral angle of C2-N10-C11-N12 set to 90º out of the plane. N1-N12 bond distance for 1b was 3.33 Å versus 2.70 Å when the dihedral angle is not constrained. N1-N12 bond distance was 2.67 Å in the crystal structure for 1c. Both of these distances are within the definition of a hydrogen bond.

Table 1.3 Energy (kcal/mol) of tautomers vs. a ground state tautomer from *Ab initio* modeled structures.

Bond / Compound	C2−N10 Flat	C2−N10 Twisted	N10−C11 Twisted
13b or **1b**	0.0	9.0	17.1
15b	13.9	14.2	No calculation
1f	0.0	9.4	18.7

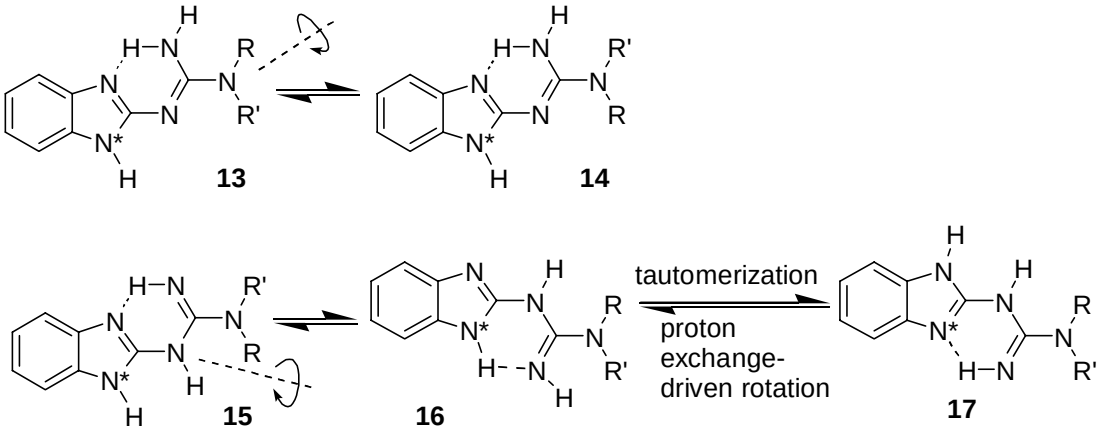

Figure 1.10. Mechanisms for exchange in *N,N*-substituted guanidinobenzimidazole

In table 1.3 and 1.4 all energies are referenced to the ground state tautomer **1b** and **1f**, which are the *N,N*-dimethyl derivative, and *N,N'*-dimethyl derivatives. Calculations were done at MP2/6311G++(2d, 2p) in the gas phase. Subtract the flat ground state energies from the twisted transition state energies to calculate particular energy barriers. Subtract the energies of the tautomers to appreciate which tautomer may likely dominate the equilibrium mixture. Bear in mind that the observations were made in solution, not the gas phase.

Table 1.4 Energies calculated with simulated solvent PCM method

Bond / Compound	C2−N10 flat	ΔH of solvation
1b or **13b**	0	-12.66
15b	12.8	-15.58
1f	0.0	-12.75

Calculated energies (kcal/mol) of tautomers in Figure 1.10. The lowest energy tautomer in each substitution pattern was assigned zero energy; the energies of the other tautomers were referenced to these. Calculations were done at the 6−31G* theory level using the Polarized Continuum (overlapping spheres) model (PCM) with water dielectric. The cavity was built up by putting a sphere around each solute atom, using UAHF radii when available and UFF radii otherwise with a scaling factor of 1.0 for protic hydrogen atoms and 1.2 for all other atoms. For a complete discussion of these methods see: http://www.gaussian.com/00000474.htm.

The exchange between tautomers **13-17**, shown in Figure 1.10, represent the two observed exchange mechanisms for *N,N*-dialkylated guanidinobenzimidazoles, and the tautomeric pair that most likely undergoes the rotational exchange. For calculations sake tautomers **13b, 15b,** and **16b** were calculated using R=methyl for tautomers of **1b** to reduce calculation time and memory requirements. *Ab initio* calculations show that tautomer **15b** should have facile rotation around axis Z, and the intramolecular hydrogen bond in **15b** should be very weak. Calculations showed that rotation along axis Z only raises the

energy of **15b** by 0.3 kcal/mol. Tautomers **13b**, **14b** were lower in energy in the gas phase than **15**,**16** by 10.0 and 13.9 kcal/mol, respectively, but conversion of **15b** to **16b** is energetically downhill by 3.9 kcal/mol. The calculated barrier to rotation along axis Z for **13b** was 9.0 kcal/mol and was within 1.2 kcal/mol of the experimental value of 10.5 kcal/mol. In solution, **15b** maybe accessible, but rotation of axis Z from **13b** seems to be the best explanation of the dynamics of the C2-N10 bond.

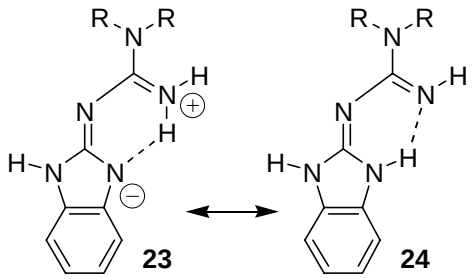

Figure 1.11 Is proton exchange occurring in the crystal structure?

The crystal for **1c** showed a feature in the difference maps of the **1d** crystal that indicated possible proton exchange along the intramolecular hydrogen bond in the crystal structure. The feature was in the right position to indicate proton exchange was occurring. If proton exchange does occur there would be extra electron density on the N10-C2 bond. Figure 1.11 shows the electronic structure that explains the effects of proton exchange on the rotation at axis Z. A normal proton exchange can occur under the conditions of bond vibration of the intramolecular hydrogen bond. Proton exchange along the intramolecular hydrogen bond of the low energy tautomer **1b** would generate structure **24**. This vibration should be possible even under the tight packing conditions of a solid crystal because motion along the hydrogen bond trajectory

does not produce much motion in the entire molecule. In solution, this tautomer was transient and did not appear to have any impact on the dynamics of the molecule.

Most measurements were taken in the presence of fast proton exchange using CD_3OD. Running the experiments at low dilutions raised the barriers for **1d** by 1 to 2 kcal/mol for the benzo protons. **1g** had a greater change in its barrier to exchange. The change from protic to aprotic conditions increased the barrier to exchange for the alkyl groups R^5, R^2 by two kcal/mol to 12 kcal/mol and the benzo protons by four kcal/mol to 14 kcal/mol.

CT and **TT** conformers of **1f** were analyzed using an *ab initio* calculation; methodology was the same as for the above conformers. Calculations showed the **CT** to be 1.3 kcal/mol lower in energy than the **TT** conformer. Both conformers of **1f** were seen in solution with the ratio changing with different solvents. **TT** was preferred in methanol, and **CT** was preferred in chloroform.

1.5 VT Data and analysis

1.5.1 Solvent dependant conformational preference of 1d

^{1}H-NMR spectra were taken at low temperatures to identify the ground state conformation, to investigate solvent sensitivity, and to explore the differences between different substitution patterns of 2-aminobenzimidazole. Solvent had an obvious influence on some of the conformers of **1d**. The solvent affected changes in the conformation of the isopropyl groups, when the solvent was changed from CD_3OD to $CDCl_3$. The **TT** conformation was preferred over the **CT** conformation in CD_3OD, and in $CDCl_3$ a less sterically hindered **CT**

conformer was preferred. Spectrum C, Figure 1.13, taken at -50 ˚C in CD_3OD shows the **CT** conformer was slightly favored over the **TT** conformer. Apolar solvents like $CDCl_3$ switched the equilibrium to favor the **CT** conformer over the **TT** conformer (see Figure 1.11 spectrum b); compare the methine signals of the *i*Pr groups at 4.2-3.0 δ in spectrum b in Figure 1.12 ($CDCl_3$) to those in spectrum c in Figure 1.13. Conformers **CT** and **TT** were assigned by NOE. At -50 °C in $MeOD_{d4}$, **TT** and **CT** produced separate ^{1}H NMR signals (1.3: 1.0 ratio, **TT**: **CT**). A NOESY experiment at -70 °C (see appendix) confirmed the proximity of the two *i*Pr substituents in **TT**. The two most intense *i*Pr methine protons were assigned to **TT** because these correlated with two methyl signals in the NOESY experiment. The other two methine *i*Pr signals shared cross peaks with one methyl signal. Cross peaks from chemical exchange between the two methine protons from the major and the minor rotamer appeared in the NOESY spectrum. The low-temperature NOESY spectrum is available in the appendix.

1.5.2 Variable temperature ^{1}H NMR of 1d in $CDCl_3$

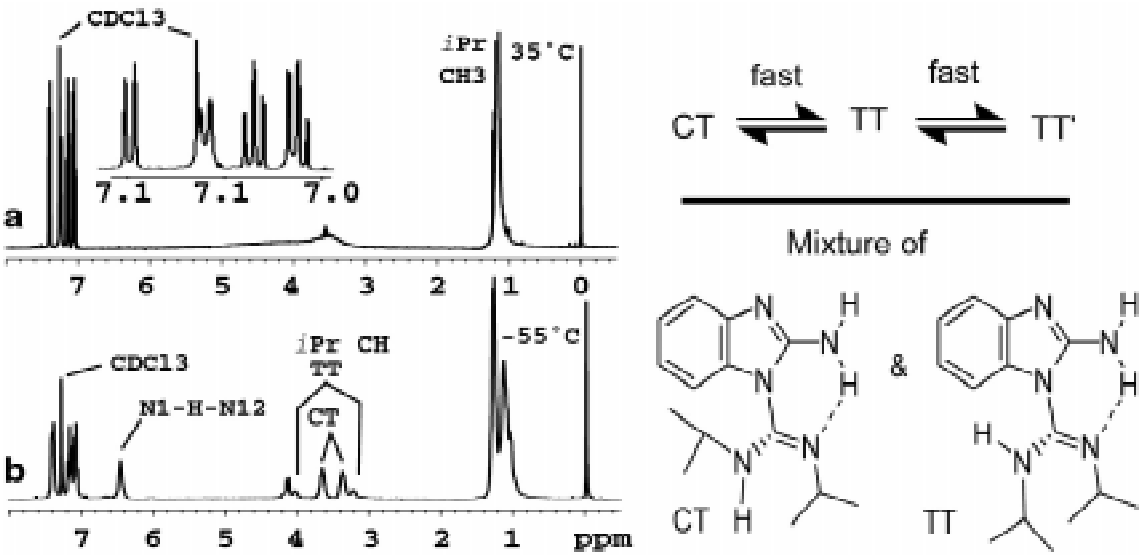

Figure 1.12. Stacked spectra showing the dynamic exchange in 1d in $CDCl_3$.

Stacked spectra in Figure 1.11, showed the dynamic exchange in **1d** in $CDCl_3$ as the temperature was decreased. The inset at 35 °C (spectrum a) clearly showed the first order pattern in the benzo protons. A single benzo proton was broadened by the presence of the two different conformers. The signals from the isopropyl groups were broad features at 35 °C, but cooling to -55 °C (spectrum b) suspended the exchange in the methyl and methine protons on the NMR timescale. There was a broad protic signal riding on the downfield edge of the most downfield methine signal at ~4.1 δ. The protic peak at 6.5 δ was assigned to the intramolecular hydrogen bond.

In **1c,g** the exchange rate of exchangeable benzo protons increased as a proton exchange catalyst was added in aprotic solvents like $CDCl_3$. Addition of DMSO, an inhibitor of proton exchange led to a downfield shift of the downfield chemical shifts in **1c**. In **1c,g** the protic chemical shifts varied as a function of temperature. In **1d,** one of the protic signals (~2H, δ 6.5, -55 °C) changed -11.1 ppb/K in $CDCl_3$, which was approximately 6.3-fold larger than the temperature-dependence of the chemical shift of an upfield protic signal, approximately -1.8 ppb/K (1H, δ 4.05). Temperature-sensitivity of the analogous downfield protic signals in **1c** (1H, δ 10.0, -30 °C) and (2H, δ ~7.3, -30 °C) in $CDCl_3$ was -25 ppb/K for the downfield shift. The upfield protic shift at δ 7.3 was much less temperature-dependent, but broadened considerably upon cooling. These protons behaved like the quickly exchanging protic signal of $methanol_{d3}$ in CD_3OD NMR solvent. The upfield protic signal in **1d** behaved differently than the

protic signal in the free solvent and was probably due to the proton in intramolecular hydrogen bond. Attempts to unambiguously assign these protic signals failed.

1.5.3 Variable temperature ^{1}H NMR of 1d in CD_3OD

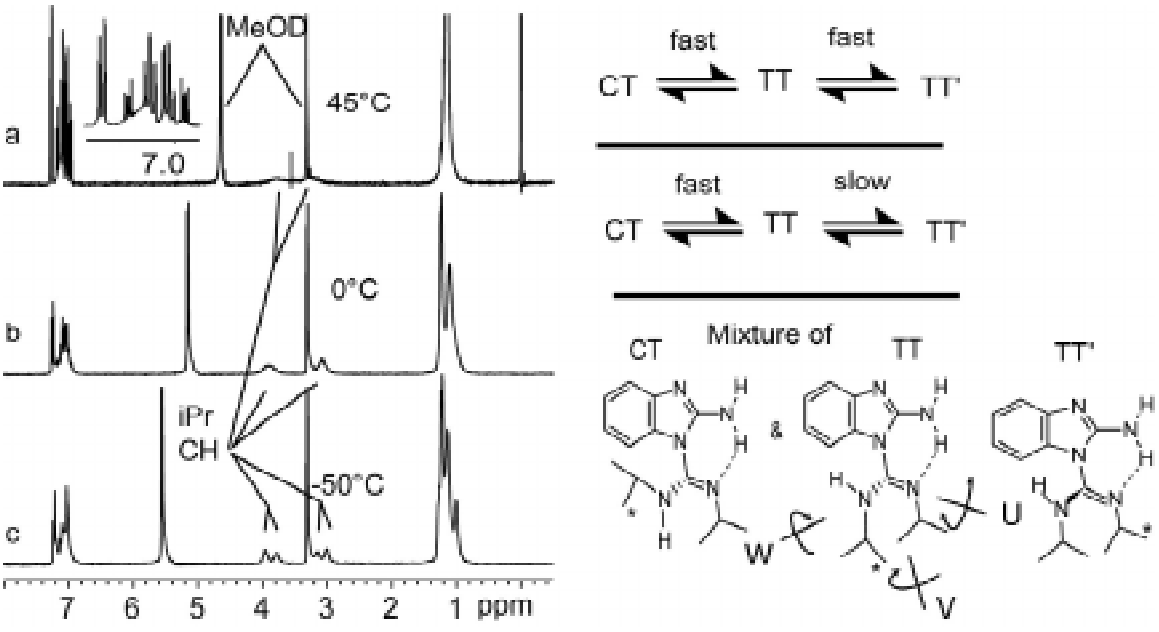

Figure 1.13. Stacked spectra showing the dynamic exchange in 1d in CD_3OD.

Stacked spectra showed the dynamic exchange in **1d** in CD_3OD as the temperature was decreased. The series from spectrum a at 45 °C to spectrum b at 0 °C to spectrum c at -55 °C clearly showed two dynamic processes. The first exchange (spectrum c to b) involved an equilibrium of **CT** and **TT,** and the next exchange (spectrum b to a) involved **TT** and **TT'**.

There were four signals, two pairs (1.2: 1.0), for the *i*Pr methine protons of **1c** in CD_3OD at -50 °C. These appeared to arise from hindered rotation of the *i*Pr substituents. One of the *i*Pr methine protons in **CT** and **TT** was proximal to the benzimidazole deshielding cone. Probably the deshielding cone of the

benzimidazole shifted these methine protons downfield by ~ 1 ppm of the other *i*Pr methine signals. Molecular modeling demonstrated that the interatomic distance between benzimidazole H4 and the methine proton in **CT** was ~2.6 Å, and the analogous distance for **TT** was ~2.8 Å. Stark changes in magnetic anisotropy tend to occur above or below the π-system, and the isopropyl groups were restricted into those areas.

1.5.4 Variable temperature ^{1}H NMR of 1b in CD_3OD

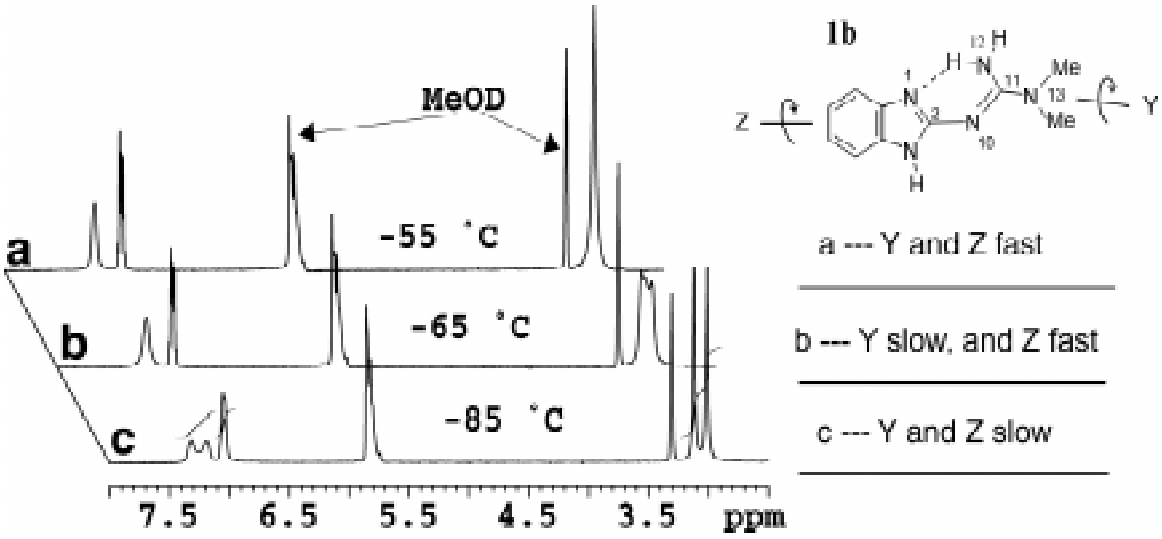

Figure 1.14 Stacked spectra showing the dynamic exchange in 1b

Stacked spectra showed the dynamic exchange in **1b** in CD_3OD as the temperature was decreased. Two mechanistically unrelated asynchronous processes exchanged the methyl substituents on the guanidino terminus and the protons in the benzene ring. From spectrum a to spectrum c the pattern in this aromatic region changes from AA'BB' to ABCD, and protons C and D were broadened but still occurred at the same frequency. Only an upper limit could be placed on the exchange of the protons in the benzene ring.

1.5.5 Temperature sensitivity of protic peaks

Exalted temperature-sensitivity in chemical shifts of intramolecular hydrogen bonds has been reported.[37] Chemical shifts of hydrogen bonded protons occur downfield of analogous protons bound to only one electron donor because the hydrogen atom partially dissociates from the hydrogen bond donor atom toward the hydrogen bond acceptor atom. The chemical shift of a proton involved in a hydrogen bond varies inversely with temperature, if the hydrogen bond is not a low barrier hydrogen bond.[27] The hydrogen in the intramolecular hydrogen bond in **1d** in $CDCl_3$ was found 2.2 ppm downfield of the next most downfield protic signal in **1d**. The slope of the temperature dependence of the chemical shift for the intramolecular hydrogen bonded proton was -11.1 ppb/K in CDCl3, which was approximately 6.3-fold larger than the temperature dependence of the chemical shifts of the other protic signals, approximately -1.8 ppb/K.

1.6 Conclusion.

An intramolecular hydrogen bond was analyzed under conditions of fast and slow hydrogen atom exchange. We determined that the rate of exchange of the alkyl groups and benzimidazole protons was influenced by the amount and rates of hydrogen atom exchange in **1a-g**, making an analytical determination of the hydrogen bond strength difficult. Despite the obvious influence of proton exchange, the molecule's dynamics was influenced by the hydrogen bond.

The explanation for the dynamics of guanidinobenzimidazole is a combination of the effects of a dynamic intramolecular hydrogen bond, hydrogen

atom exchange, and quite possibly solvent polarity. If guanidinobenzimidazole and its derivatives had the dynamics that would correspond to a structure indicated by the tautomer shown in Figure 1.1, then the rotation about axis Y and Z would be fast, and rotation about axis X would be very slow. However, the situation is not that simple and the dynamics of the system are more complex. The effect of a resonance-assisted hydrogen bond (RAHB) was useful in the explanation of the dynamics of the molecule. Although a direct measurement of the strength of the intramolecular hydrogen bond was not possible, the dynamics of the molecule was useful in finding evidence for the presence of the RAHB in solution. If the RAHB is present, it does not possess the normal strength of a RAHB. Even under slightly protic conditions of 8 mg / 750 μL chloroform, the exchange is faster for the alkyl groups along axis X than along axis Z. This implies that bond order has been reduced between C11 and N10 (numbering from Figure 1.1) and a tautomer like structure 24 in Figure 1.11 is found. In lower polarity aprotic solvents, this mechanism may be promoted while in polar protic solvents many tautomers exist with other mechanisms for exchange exist. Therefore, with redundant mechanisms the potential for exchange increases, as does the rate of exchange. Our dynamic results are similar to those described earlier for the dynamics of ^{15}N-NMR spectroscopy of **1a** described earlier in chapter 1.

In **1d,e** the exchange of the alkyl groups is remarkably well controlled in comparison to the conformational control offered by the hypothetical planar resonance stabilized hydrogen bond did not appear to contribute as much to the

conformational stability as the hydrogen bond that was not resonance stabilized or planar. This was a rather remarkable discovery, but the explanation was quite simple. The carboxamidine functional group had a different pKa than the guanidine and this led to remarkable dynamics, which appeared unchanged by differing amounts of a weak proton exchange catalyst. There were at two least two possible explanations for this behavior. The first rationalization focuses on the differences between the intramolecular hydrogen bond acceptors in the derivatives of **1** studied in this thesis. Other arguments were more complex. In another explanation, the secondary imine nitrogen atom may participate in a kinetically more stable hydrogen bond than the primary imine nitrogen atom. The second rationalization focuses on the nature of the hydrogen bond in planar, five or six centered intramolecular hydrogen bonds. The heteroatoms in these species may simply be too close for optimal hydrogen bonding. This may be born out in calculations since the atoms are not all coplanar after optimizing the atomic positions at a high level of theory. If the bonding pattern positions the heteroatoms involved in the hydrogen bond too close, the hydrogen bond is established at the expense of conjugation (non-planar structure) and conjugation is optimized at the expense of the hydrogen bond. In the absence of the solvent shell, (x-ray structures, gas-phase calculations) the optimum distance d_{AB} of the hydrogen bond likely shortens, making the hydrogen bonds give rise to more planar structures. The third explanation says that the mechanisms and the rates of exchange are different for the three types of six-centered intramolecular hydrogen bonds.

Rotation was found to be the best mechanism for basic guanidines involved in a six-centered intramolecular hydrogen bond. The barrier to rotation was measured for two different heterocycles. Barriers to exchange matched well with the calculated values for the barrier to rotation. These studies provided a realistic vision of what to expect of intramolecular hydrogen bonds in the control of *de novo* designed conformations. If any hydrogen bond will operate to control conformation, the ones that participate in planar aromatic structures should contribute the most to conformational control. In general, the six-centered intramolecular hydrogen bonds studied here were not stable enough to be used for the design of compounds needing conformational stability.

1.7 References.

(1) Acerete, C.; Catalan, J.; Sanchez-Cabezudo, M. *Heterocycles* **1987**, *26*, 1581-1586.

(2) Asano, T.; Furuta, H.; Hofmann, H.-J.; Cimiraglia, R.; Tsuno, Y.; Fujio, M. *J. Org. Chem.* **1993**, *58*, 4418-4423.

(3) Asano, T.; Okada, T.; Herkstroeter, W. G. *J. Org. Chem.* **1989**, *54*, 379-383.

(4) Bauer, V. J.; Fulmor, W.; Morton, G. O.; Safir, S. R. *Tetrahedron Lett.* **1968**, *90*, 6846-6847.

(5) Bedford, G. R.; Taylor, P. J.; Webb, G. A. *Magn. Reson. Chem.* **1995**, *33*, 383-388.

(6) Bidwell, L. M.; McManus, M. E.; Gaedigk, A.; Kakuta, Y.; Negishi, M.; Pedersen, L.; Martin, J. L. *J. Mol. Biol.* **1999**, *293*, 521-530.

(7) Caira, M. R. *Top. Curr. Chem.* **1998**, *198*, 164-208.

(8) Caira, M. R.; Watson, W. H.; Vogtle, F.; Muller, W. *Acta Crystallogr.* **1984**, *C40*, 1047.

(9) Charmant, J. P. H.; Lloyd-Jones, G. C.; Peakman, T. M.; Woodward, R. L. *Eur. J. Org. Chem.* **1999**, *1999*, 2501-2510.

(10) Contreras, R.; Andrade-Lopez, N.; Ariza-Castolo, A. *Heteroatom Chemistry* **1997**, *8*, 397-410.

(11) Folmer, B. J. B.; Sijbesma, R. P.; Kooijman, H.; Spek, A. L.; Meijer, E. W. *J. Am. Chem. Soc.* **1999**, *121*, 9001-9007.

(12) Forés, M.; Duran, M.; Solá, M. *J. Phys. Chem. A.* **1999**, *103*, 4525-4532.

(13) Frisch, M. J.; Trucks, G. W.; Schlegel, H. B.; Scuseria, G. E.; Robb, M. A.; Cheeseman, J. R.; Zakrzewski, V. G.; Montgomery, J. A.; Stratmann, R. E.; Burant, J. C.; Dapprich, S.; Millam, J. M.; Daniels, A. D.; Kudin, K. N.; Strain, M. C.; Farkas, O.; Tomasi, J.; Barone, V.; Cossi, M.; Cammi, R.; Mennucci, B.; Pomelli, C.; Adamo, C.; Clifford, S.; Ochterski, J.; Petersson, G. A.; Ayala, P. Y.; Cui, Q.; Morokuma, K.; Malick, D. K.; Rabuck, A. D.; Raghavachari, K.; Foresman, J. B.; Cioslowski, J.; Ortiz, J. V.; Stefanov, B. B.; Liu, G.; Liashenko, A.; Piskorz, P.; Komaromi, I.; Gomperts, R.; Martin, R. L.; Fox, D. J.; Keith, T.; Al-Laham, M. A.; Peng, C. Y.; Nanayakkara, A.; Gonzalez, C.; Challacombe, M.; Gill, P. M. W.; Johnson, B. G.; Chen, W.; Wong, M. W.; Andres, J. L.; Head-Gordon, M.; Replogle, E. S.; Pople, J. A. *Gaussian 98 (Revision A.6)*; Gaussian, Inc.: Pittsburgh PA, 1998.

(14) Gallivan, J. P.; Dougherty, D. A. *J. Am. Chem. Soc.* **2000**, *122*, 870.

(15) Gilli, G.; Bertolasi, V.; Gilli, P.; Ferretti, V. *J. Chem. Soc., Perkin Trans. 2* **1997**, 945-952.

(16) Gilli, G.; Bertolassi, V.; Gilli, P.; Ferretti, V. *Chem. Eur. J.* **1996**, *2*, 925-934.

(17) Gilli, G.; Gilli, P.; Bertolassi, V.; Ferretti, V. *J. Am. Chem. Soc.* **1994**, *116*, 909-15.

(18) Gould, I. R.; Kollman, P. A. *J. Am. Chem. Soc.* **1994**, *116*, 2493-2499.

(19) Gung, B. W.; Zhu, Z.; Zou, D.; Everingham, B.; Oyeamalu, A.; Crist, R. M.; Baudlier, J. *J. Org. Chem.* **1998**, *63*, 5750-5761.

(20) Hodgson, P.; Lloyd-Jones, G. C.; Murray, M.; Peakman, T. M.; Woodward, R. L. *Chem. Eur. J.* **2000**, *6*, 4451-4460.

(21) Howard, S. T.; Platts, J. A. *J. Org. Chem.* **1998**, *63*, 3568-3571.

(22) Huang, B.; Parquette, J. R. *Org. Lett.* **2000**, *2*, 239-242.

(23) Huang, B.; Parquette, J. R. *J. Am. Chem. Soc.* **2001**, *123*, 2689-2690.

(24) Kessler, H.; Leibfritz, D. *Tetrahedron Lett.* **1970**, 1423-1426.

(25) Kim, B. H.; Cho, S. G.; Ha, T.-K. *J. Org. Chem.* **1999**, *64*, 5036-5041.

(26) Ledvina, P. S.; Yao, N.; Choudhary, A.; Quiocho, F. A. *Proc. Natl. Acad. Sci. USA* **1996**, *93*, 6786–6791.

(27) Lluch, J. M.; Garcia-Viloca, M.; Gelabert, R.; González-Lafont, À.; Moreno, M. *J. Am. Chem. Soc.* **1998**, *120*, 10203-9.

(28) Ma, J. C.; Dougherty, D. A. *Chem. Rev.* **1997**, *97*, 1303-1324.

(29) Macedo-Ribeiro, S.; Hemrika, W.; Renirie, R.; Wever, R.; Messerschmidt, A. *J. Biol. Inorg. Chem.* **1999**, *4*, 209-219.

(30) Marullo, N. P.; Wagener, E. H. *Tetrahedron Lett.* **1969**, 2555-2558.

(31) Ngola, S. M.; Dougherty, D. A. *J. Org. Chem.* **1998**, *63*, 4566-4567.

(32) Perrin, C. L.; Nielson, J. B. *Annu. Rev. Phys. Chem.* **1997**, *48*, 511-44.

(33) Recker, J.; Tomcik, D. J.; Parquette, J. R. *J. Am. Chem. Soc.* **2000**, *122*, 10298-10307.

(34) Solà, M.; Luque, F. J.; Forés, M.; Duran, M.; Orozco, M. *J. Phys. Chem. A* **1999**, *103*, 4525-32.

(35) Steel, P. J. *J. Heterocycl. Chem.* **1991**, *28*, 1817-18.

(36) Tóth, G.; Szöllösy, A.; Almásy, A.; Podányi, B.; Hermecz, I.; Breining, T.; Mészáros, Z. *Org. Mag. Res.* **1983**, *21*, 687-693.

(37) Wachter-Jurcsak, N.; Detmer, C. A. *Org. Lett.* **1999**, *1*, 795-8.

(38) Watson, W. H.; Galloy, J.; Grossie, D. A.; Voegtle, F.; Mueller, W. M. *J. Org. Chem.* **1984**, *49*, 347-53.

(39) Wildes, P. D.; Pacifici, J. F.; Irick, G.; Whitten, D. G. *J. Am. Chem. Soc.* **1971**, *93*, 2004.

(40) Zoltewicz, J. A.; Maier, N. M.; Fabian, W. M. F. *J. Org. Chem.* **1998**, *63*, 4985-4990.

Chapter 2

Synthesis of benzimidazole derivatives

Guanidinobenzimidazole has complex chemical reactivity. The guanidine moiety is difficult to selectively alkylate, and the basicity is more like imidazole than guanidine. Guanidinobenzimidazole has a pK_a of 7.09,[1] while that of benzimidazole is 5.56[1], and that of guanidine is 14.38[1]. Alkylated derivatives can be formed in several ways. The optimum method used to form the guanidinobenzimidazole depends upon the substitution pattern desired. The most nucleophilic atom on 2-guanidinobenzimidazole is the non-protonated imidazole nitrogen (N1, numbering system shown in Figure 1.1). The nucleophilicity of N1 was used to methylate this nitrogen, using a strong unhindered electrophile like methyl iodide. Other derivatives formed from this reaction were not isolated due to difficulty in purification.

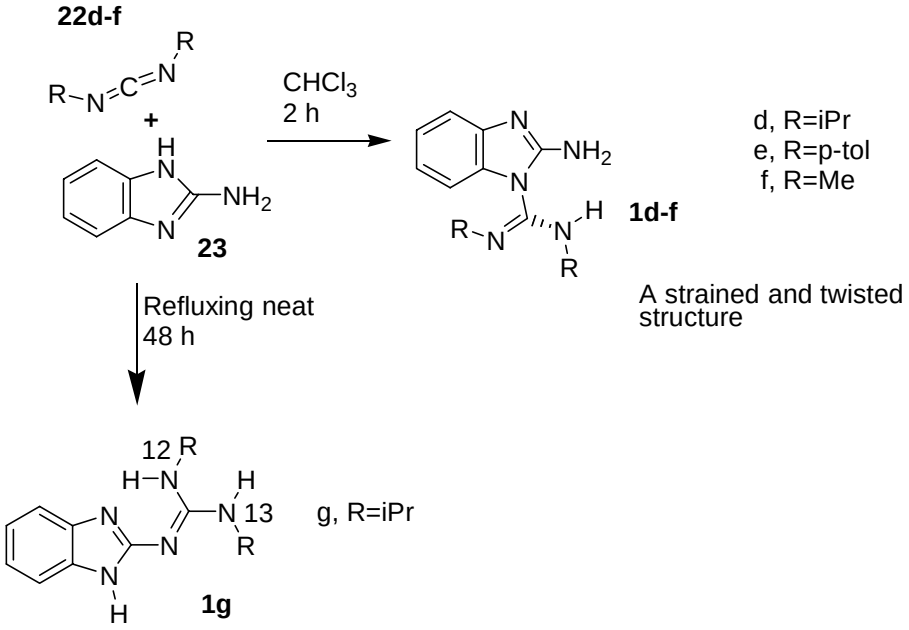

Figure 2.1 Synthesis of 2-amino-1-benzimidazole-*N,N'*-dialkylcarboxamidine derivatives

Methods to selectively and directly alkylate the terminal nitrogen atoms on the guanidine moiety, N12, N13 have not been discovered, due to their lower nucleophilicity. With reactivity again reflective of the nucleophilicity of N1, **1d-f** were synthesized by the condensation of the corresponding *N,N'*-disubstituted carbodiimide **22d-f**. **22f** appears to be particularly labile to solvolysis for *N,N'*-derivative **1f**. These derivatives required a moderately bulky substituent for isolation of a product. Larger alkyl groups appeared to decelerate the solvolysis of **1d-f**. *N,N'*-Dimethyl derivative **1f** was detected in solution, but purification methods decomposed the chemical. *N,N'*-Diisopropyl derivative **1d** decomposed over several hours at raised temperatures in protic solvents, but was stable to silica chromatography. However, because it crystallized pure from non-polar aprotic solvents, chromatography was not necessary, and the material could be

obtained in excellent purity. p-Tolyl derivative **1e** was less stable to silica and small impurities persisted after silica chromatography, presumably due to the decomposition on the column.

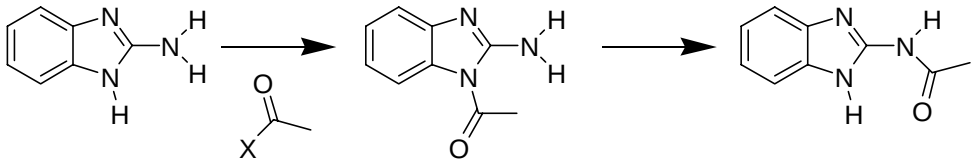

Figure 2.2 Literature evidence for 2-amino substitution.

Substitution at N1 was unexpected for the reaction of carbodiimides with 2-aminobenzimidazole. Dimethylcyanamide reacted with 2-aminobenzimidazole when heated in neat dimethylcyanamide at 105 °C at the 2-amino position to form **1b** granted in low yield and impure. Acetylation of the same molecule proceeded with substitution at N1, but heat caused a rearrangement with substitution at the 2-amino position.[2] With the carboxamidine cation being more stable than the *N*-acetyl cation the rearrangement should have been more facile. 2-Amino substitution was expected. In the crystal structure, seen below in Figure 2.3, the product was highly strained with no favorable intramolecular hydrogen bonding interactions and decreased π-conjugation.

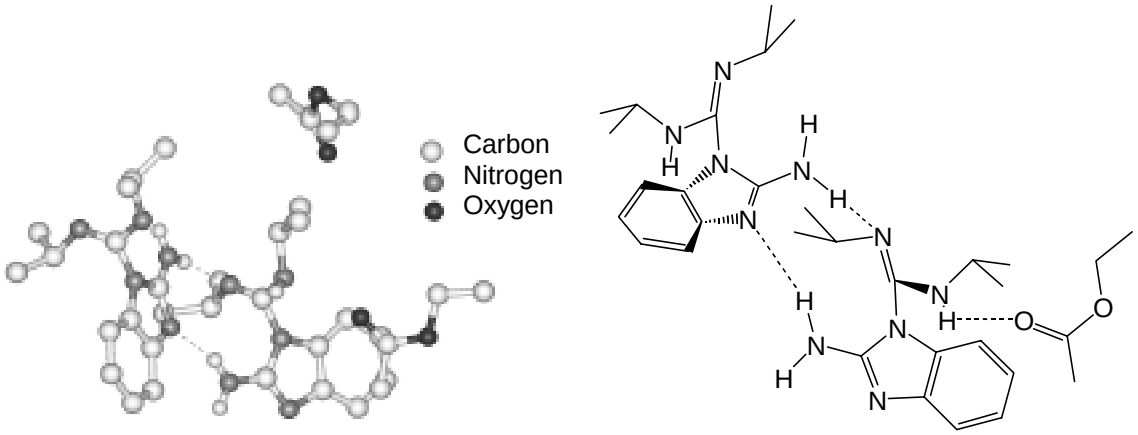

Figure 2.3 Crystal structure of 2-amino-1-benzimidazole-*N,N'*-diisopropylcarboxamidine

There are at least four different intermolecular hydrogen bonds for every molecule of **1d**. This does not include another hydrogen bond to the carbonyl of a molecule of ethyl acetate. Planarity and the cohesion of the intramolecular hydrogen bond between the carboxamidine and the 2-amino protons in **1d** is probably disturbed by the intermolecular hydrogen bonding just described.

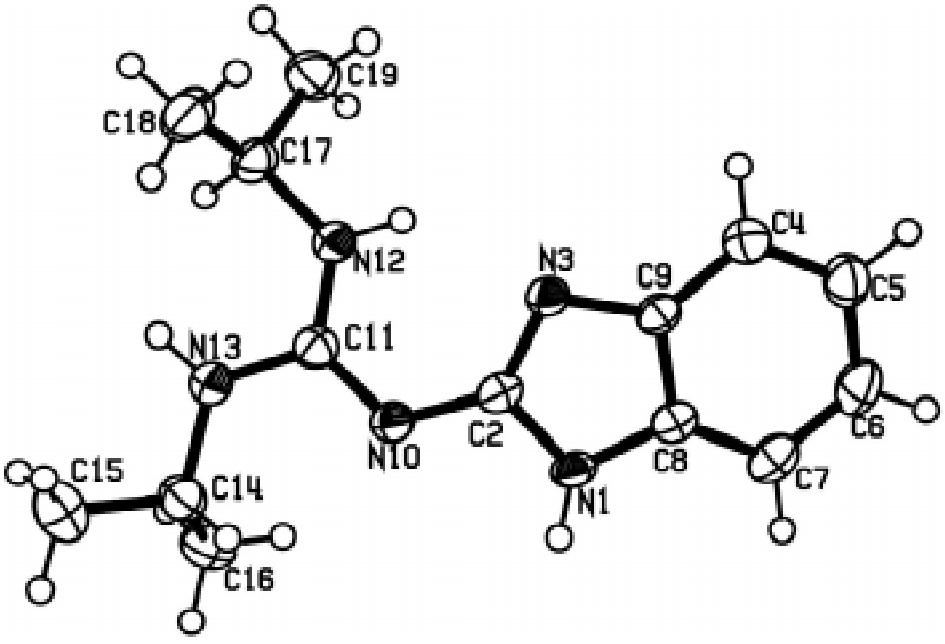

Figure 2.4 Crystal structure of 1g.

Another product is formed when the reaction to make **1d** was repeated at 110 °C, refluxing a melt of the two starting materials. This product was identified as the 2-aminobenzimidazole with the carbodiimide substituted at the 2-amino position, **1g**, shown in figure 2.1. Although the yield was low at around 12% yield, improvements in the methodology should improve the yield. The crystal structure for **1g** is shown above in Figure 2.4.

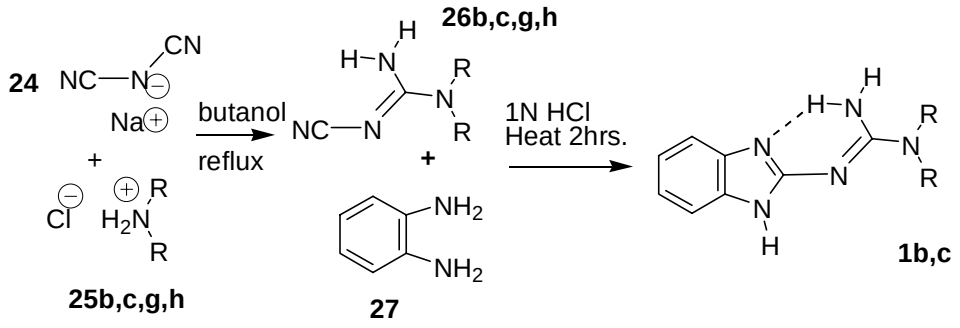

Figure 2.5: Synthesis of *N,N*-dialkyl guanidinobenzimidazoles

Substitution at only N13 was accomplished with alkyl groups of moderate to high steric hindrance. *N,N*-dialkyl-2-guanidinobenzimidazole derivatives **1b**,**c** were synthesized, as shown in Figure 2.4 above, by the condensation of ortho-phenylenediamine and an *N,N*-dialkyl-dicyandiamide. This method has been shown to be useful in the synthesis of 2-(*N*-isopropylguanidino)benzimidazole[3] and also to make the corresponding dimethyl, isobutyl, piperidino, cyclohexyl, and morpholino derivatives.[4]

1b was also synthesized using a similar method with 2-aminobenzimidazole and dimethylcyanamide. *N,N*-Dimethylguanidino-*N'*-(2-benzimidazoyl) **1b** was formed by the condensation of 2-aminobenzimidazole and dimethylcyanamide in low yield. Synthesis of **1c** using diisopropylcyanamide

was unsuccessful. Heat and Lewis acid catalysis resulted in starting material and decomposed starting material.

Two 2-amino-1-benzimidazole-*N,N'*-dialkylcarboxamidine derivatives were synthesized by the condensation of *N,N'*-dialkylcarbodiimides **22** and 2-aminobenzimidazole **23**. The synthesis of **1d,e** by the reaction of 2-aminobenzimidazole with a carbodiimide with alkyl substituents of high steric bulk (for example, **22d**) ran in high yield. For the synthesis of 2-(*N,N*-dialkylguanidino)benzimidazoles with large alkyl substituents the reaction of phenylenediamine and *N,N*-diisopropyldicyandiamide ran in poor yield. For the synthesis of 8-(*N,N*-dialkylguanidino)purines, the reaction of 4,5-diaminopyrimidine and *N,N*-isopropyl, t-butyldicyandiamide ran in high yield.

2.1 Synthesis of *N,N*-dialkylguanidinobenzimidazoles from *N,N*-dialkyl-*N'*-cyanoguanidines and *o*-phenylendiamine.

Cyanoguanidines (Dicyandiamides) are typically made from the reaction of an amine hydrochloride and sodium dicyanamide in refluxing alcohol. The yields for this reaction are moderate, however decomposition products at the end of the reaction do not hamper isolation. The only impurities in the product are the starting materials. The *N,N*-dialkyl-*N'*-cyanoguanidine product also called *N,N*-dialkyldicyandiamide can be purified by extraction into ethyl acetate and crystallization. A series of *N,N*-dialkyl-*N'*-cyanoguanidines were made with the varying yields shown in Table 2.1.

Table 2.1 Synthesis of *N,N*-dialkyl-*N'*-cyanoguanidines

Derivative	Alkyl group	% yield

26b	R = Methyl	25
26g	R = Ethyl	50
26c	R = *iso*Propyl	42
26h	R = *tert*Butyl	17

The less sterically hindered *N,N*-dialkyl-*N'*-cyanoguanidines were useful in the synthesis of *N*-(1H-benzimidazol-2-yl)-*N',N'*-dialkyl-guanidines. When the *N,N*-dialkyl-*N'*-cyanoguanidines were refluxed in water with 4 equivalents of HCl and one equivalent of *o*-phenylenediamine the cyanoguanidines condensed with the *o*-phenylenediamine losing ammonium chloride. When *N*-*t*-butyl,*N*-*iso*propyl-*N'*-cyanoguanidine and *N,N*-di*t*-butyl-*N'*-cyanoguanidine were submitted to the same conditions, no reaction took place. The following derivatives were isolated in the following yields.

Table 2.2 Synthesis of *N,N*-dialkylguanidinobenzimidazoles

Derivative	Alkyl group	% yield
1a	R = Methyl	10-25
1c	R = *iso*Propyl	10-16
1h	R = *t*Butyl	0

2.2 Synthesis of 2-amino-1-benzimidazole-*N,N'*-dialkylcarboxamidine from 2-aminobenzimidazole and *N,N'*-dialkylcarbodiimides or *N,N'*-dialkyluronium chloride salts.

Guanidines can also be synthesized by using carbodiimides and uronium chloride salts. These reactions were facile and high yielding when the alkyl group on the carbodiimide had moderate steric bulk. 2-Amino-1-benzimidazole-*N,N'*-diisopropylcarboxamidine (**1d**) was synthesized using commercially available *N,N'*-diisopropylcarbodiimide and 2-aminobenzimidazole. Within 12 h the reaction had gone to completion by TLC. The crude yield was about 85%. The crude residue was purified by recrystallization with ethyl acetate. The ethyl acetate was removed by dissolving in $CHCl_3$, pumping off the residue under high vacuum, crushing the residue to a powder and again evaporating under high vacuum.

N,N'-Di-*p*-tolylcarbodiimide, **22e** also reacted with **23** in refluxing THF overnight, and was crystallized from wet ethyl acetate. A small amount of hydrolyzed product also resulted from this crystallization, but other methods only precipitated powder. The yield of this product was good at 76%. The more

sterically hindered *N,N'*-di-*tert*-butylcarbodiimide did not react with **23** under refluxing THF, or DMF heated to 60 °C.

N,N'-Dimethylcarbodiimide was synthesized according to a literature procedure[5] for the synthesis of 2-amino-1-benzimidazole-*N,N'*-dimethylcarboxamidine, **1f**. *N,N'*-dimethylthiourea and HgO (dried at 150 °C for 2 h) were stirred at 0 °C to room temperature over 45 min The precipitate was filtered and concentrated by slow distillation from a bath temperature of 50-55 °C. This material was used as is and stirred with 2-aminobenzimidazole in $CHCl_3$ overnight under N_2. The resulting product was filtered and dried under vacuum. The ^1H NMR in $DMSO_{d6}$ showed mostly the 2-aminobenzimidazole with a product that could not be isolated pure.

The *N,N'*-dimethyluronium chloride was synthesized according to a literature procedure[6] for the synthesis of **1f**. *N,N'*-Dimethylthiourea (107.3 mg, 1.030 mmol) was dissolved in 10 mL dry THF. Triphosgene (328.5 mg, 1.107 mmol) in 5 mL dry THF was added to the thiourea slowly by syringe. The reactions was stirred for 1 h and refluxed for 3 more. The reaction formed a precipitate that was dissolved with $CHCl_3$, and again precipitated with THF. The precipitate was filtered under nitrogen and recrystallized with the $CHCl_3$ and THF solvent mixture for a total yield of 202.6 mg, 1.901 mmol or 68% yield with respect to the thiourea. When stirred with 2-aminobenzimidazole the *N,N'*-dimethyluronium chloride reacted in a manner similar to *N,N'*-dimethylcarbodiimide. The reaction was incomplete and the product was unstable to purification.

2.3 Synthesis of N,N'-diisopropylguanidinobenzimidazoles

2.3 Synthesis of 1-methyl-2-guanidinobenzimidazole

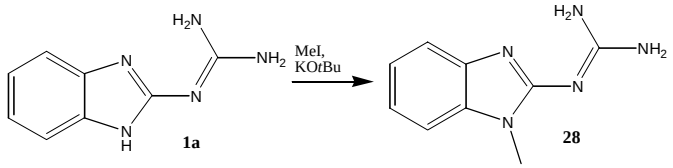

Figure 2.6 Alkylation of 1a with methyl iodide

Deprotonation of the imidazole nitrogen N1, in **1a**, resulted in *N*-methylation of N1 upon treatment with methyliodide. This reaction was regioselective for alkylations at the imidazole nitrogen. One equivalent of **1a**, and Potassium tert-butoxide and a catalytic amount of 18-crown-6 was dissolved in THF. An equivalent of methyliodide was added drop-wise to the reaction at 0 °C. After 5-10 minutes a white precipitate had formed. 1-methyl-2-guanadinobenzimidazole, **28**, was neutralized and purified by crystallization from ethyl acetate and hexane (53% isolated yield).

2.4 Synthetic procedures and data

2.4.1 Synthesis of *N*-(1H-benzoimidazol-2-yl)-*N'*,*N'*-dimethyl-guanidine (1b)

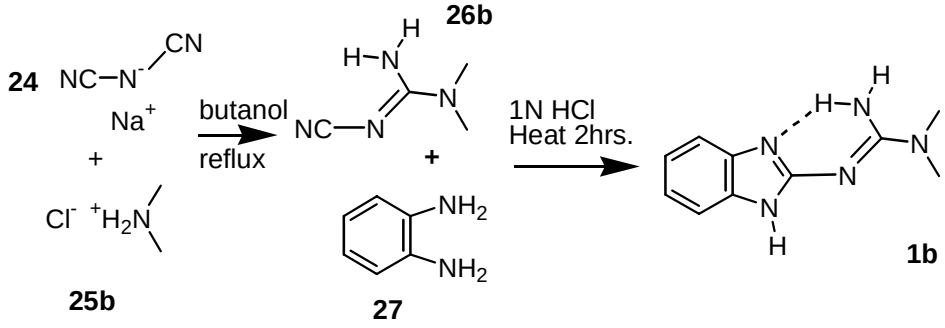

Figure 2.7 Synthesis of 1b

Dimethylamine (2.60 mL, 40% aqueous solution) sodium dicyanamide (1.78 g, 20.0 mmol), and HCl (1.76 mL, 37% aqueous solution) were refluxed for 24 h. This solution was neutralized with Na_2CO_3 (2M) and extracted into n-butanol. The n-butanol layer was washed with brine and evaporated. The crude *N,N*-dimethyldicyandiamide (0.566g, 5.05 mmol, 25% yield) was crystallized from n-butanol and ethyl acetate. *N,N*-dimethyldicyandiamide (431 mg, 3.85mmol) and phenylene diamine (401 mg, 3.71 mmol) and 310 µL of conc. HCl was dissolved in 4.0 mL distilled water. The reaction was refluxed for 6 h then neutralized with sodium carbonate and water, extracted with ethyl acetate and dried with $MgSO_4$. After silica gel chromatography (5% TEA in EtOAc) the solution was concentrated and *N*-(1H-benzoimidazol-2-yl)-*N',N'*-dimethyl-guanidine (84.1 mg, 0.381 mmol, 10% yield) was obtained as crystalline material.

^{1}H-NMR (300 MHz; $CDCl_3$) δ 7.22 (2H, dd, J=6.1, 3.2 Hz), 6.94 (2H, dd, J=6.0, 3.2 Hz), 3.27 (6H, s) m/z (EI) 259 (M^+, 1%), 133 ((M - diisopropyldiimidyl)$^+$, 83%) ^{13}C NMR (75.4 MHz; $CDCl_3$) δ156.702, 156.0, 117.3, 109.7, 33.8. IR(KBr pellet)2924.9, 2867.5, 1529.9, 1459.3, 1388.6, 1261.2, 1215.2, 1051.5 cm^{-1} *Anal. Calcd.* For $C_{10}H_{13}N_5$ C, 58.80, H, 6.91, N, 34.29 found C, 58.97, H, 6.47, N, 34.07.

2.4.2 Synthesis of *N*-(1H-benzoimidazol-2-yl)-*N′,N′*-diisopropyl-guanidine (1c)

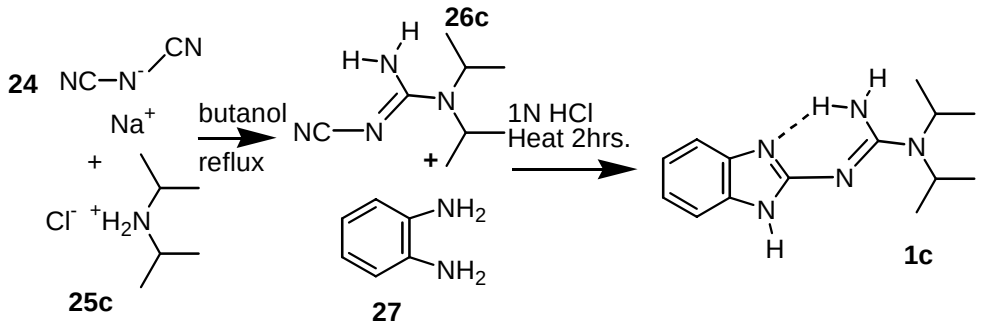

Figure 2.8 Synthesis of 1c

Sodium dicyanamide (4.34 g, 49.3 mmol) and diisopropylamine (4.85 g, 48.0 mmol) and 4.0 mL concentrated HCl (50 mmol) were refluxed in n-butanol for 28 h. The solution was washed with distilled water and then 3x with brine resulting in a pink aqueous phase and a pale clear yellow organic phase. *N,N*-diisopropyldicyandiamide (2.33 g, 13.8 mmol, 29%) was crystallized from hot ethyl acetate. *N,N*-Diisopropyldicyandiamide (211.7 mg, 1.26 mmol) was refluxed for 2 h with o-phenylenediamine (140.8 mg, 1.30 mmol) in 2 equiv. $HCl_{(aq)}$ (2.0 mL, 0.66 M). The reaction was worked up with Na_2CO_3 washed three times with ether, and then with brine. The solution was concentrated and purified by flash silica gel chromatography (4: 1, hexane: EtOAc and 5% TEA). The first fraction (232 mg, 0.894 mmol) 71% crude yield was recrystallized from hexane and EtOAc.

^{1}H NMR (300 MHz; CD_3OD) δ 7.99 (dd, 2H, 7.1 Hz, 25.5 Hz), 7.61 (dt, 2H, 2.2 Hz, 6.9 Hz), 4.21 (septet, 2H, 6.8 Hz), 1.34 (d, 12H) ^{13}C NMR (75.3 MHz; $CDCl_3$) δ 156.7, 146.6, 131.3, 129.3, 59.0, 26.5, 22.4 IR(KBr pellet) 3493.6,

3393.2, 3120.11, 2973.0, 1626.2, 1606.8, 1516.2, 1486.3, 1457.9, 1388.6, 1272.1, 1215.2, 1136.2 cm^{-1} *Anal. Calcd.* for $C_{22}H_{21}N_5$ C, 64.84, H, 8.16, N, 27.00 found C, 64.76, H, 8.06, N, 26.92.

2.4.3 Synthesis of 2-amino-1-benzimidazole-*N,N'*-diisopropylcarboxamidine(1d)

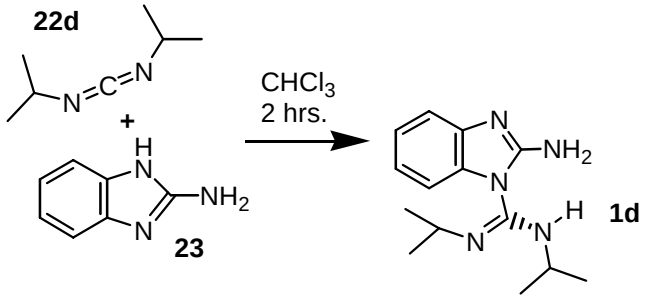

Figure 2.9 Synthesis of 1d

2-amino-benzimidazole (1.11 g, 8.31 mmol) was dissolved in a solution of THF with two molar equivalents of *N,N'*-diisopropylcarbodiimide. Within 12 hours the 2-amino-benzimidazole was completely used up by TLC. Water was added to the mixture and the product was extracted into $CHCl_3$. The crude yield was about 85%. The crude residue was purified by recrystallization with ethyl acetate. The ethyl acetate was removed by the pump freeze thaw method several times.

^{1}H NMR (300 MHz; $CDCl_3$, 25 ˚C) δ 7.40 (d, 1H), 7.27 (broad d, 1H), 7.14, (t, 1H), 7.05 (t, 1H), 5.2-6.0 (broad s, 2H, NH), 3.2-4.2 (broad m, 4H),1.0-1.4 (broad s, 12H); ^{13}C NMR (75.4 MHz; $CDCl_3$) δ 160.6, 153, 141.9, 133.1, 122.6, 116.7, 109.7 (vb), 47.0 (vb), 24.1 (b); IR -3500-3300, 3080, 1640-1700, 1554, 1458, 740; *Anal. Calcd.* for $C_{14}H_{21}N_5$ C, 64.83, H, 8.16, N, 27.01 found C, 64.51, H, 8.31, N, 26.55.

2.4.4 Synthesis of 2-amino-1-benzimidazole-*N,N'*-ditolylcarboxamidine (1e)

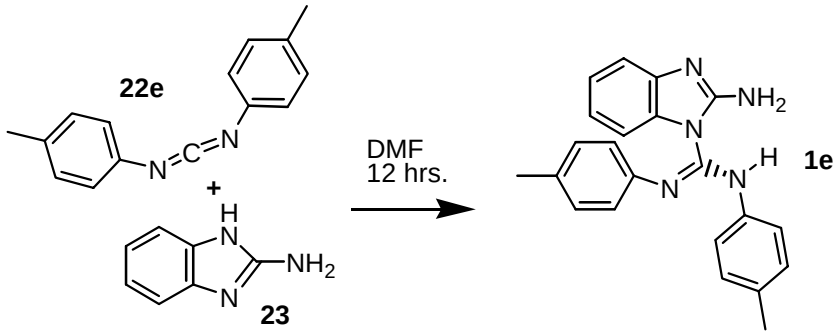

Figure 2.10 Synthesis of 1e

2-Amino-benzimidazole (299.1 mg, 2.25 mmol) was dissolved in a solution of 2.5 mL DMF with an excess of *N,N'*-ditolylcarbodiimide (499.9 mg, 2.25 mmol). The DMF was evaporated under high vacuum, and the resulting solid was crystallized from wet ethyl acetate. **1e** (607.3 mg, 1.71 mmol) was recovered for a yield of 76.1%. This material was recrystallized with ethyl acetate and hexane and ethyl acetate and chloroform. The ethyl acetate was removed by the pump freeze thaw method several times.

^{1}H NMR (300 MHz; $CDCl_3$) δ 7.29 (t, 1H, 8.0 Hz), 7.22 (t, 1H, 8.0 Hz), 7.14 (vb, 4H, 9.8 Hz), 7.07 (t, 1H, 9.8 Hz), 7.05 (t, 1H, 6.8 Hz), 6.90 (vb, 2H), 6.66 (vb, 2H) , 2.31 (vb, 3H), 2.17 (vb, 3H), 1.34 (d, 12H) ^{13}C NMR (300 MHz; $CDCl_3$) δ 172.3, 172.2, 138.7, 132.5, 131.6, 129.3, 125.2, 71.5, 29.4 *Anal. Calcd.* for $C_{22}H_{21}N_5$ C, 74.34, H, 5.96, N, 19.7 found C,74.48, H,6.30, N,19.62.

2.4.4 Synthesis of *N*-(1H-benzoimidazol-2-yl)-*N′,N′*-diisopropyl-guanidine (1g)

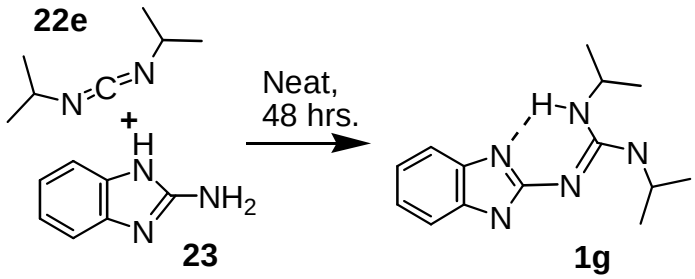

Figure 2.11 Synthesis of 1g

2-Amino-benzimidazole (522.8 mg, 3.93 mmol) was stirred with diisopropyl carbodiimide (450 mg, 4.0 mmol) neat for 48 h at 110 °C. The reaction was held under a static nitrogen atmosphere with the carbodiimide held under a condenser. Excess carbodiimide, **22e**, was evaporated under high vacuum, the resulting solid was dissolved in 100 ml ethyl acetate filtered and addition of a small amount of hexane caused the formation of a suspension which over time, formed an oily layer on the bottom of the flask. The liquor was decanted and further addition of hexane caused the crystallization of **1g** from ethyl acetate. **1g** (117mg, 0.45 mmol) was recovered for a yield of 12%. This material was further purified by crystallization with ethyl acetate and hexane. The crystals were of a yellow brown color and melted at 162°C. X-ray analysis revealed the form of the chemical shown above in Figure 2.10. Residual ethyl acetate was removed by dissolving with chloroform and evaporating under high vacuum, crushing this material into a powder and again evaporating under high vacuum.

^{1}H NMR (400 MHz; CD_3OD) δ 7.20 (m, 2H, 3.2 Hz), 6.95 (m, 2H, 3.2 Hz), 4.02 (septet, 2H, 6 Hz), 1.23 (d, 12H, 7 Hz) ^{13}C NMR (400 MHz; CD_3OD) δ 158.76, 155.15, 137.54, 120.07, 111.91, 42.61, 22.10; IR 3431, 2971, 1598, 1529, 1461, 1402, 1367, 1273, 1176, 736; *Anal. Calcd.* for $C_{14}H_{21}N_5$ C, 64.83, H, 8.16, N, 27.01 found C, , H, , N, ; EI Mass Spectra m/z 259 (~70%), 244 (20%), 159 (100%), 158 (45%), 134 (20%).

2.4.5 Synthesis of 1-methyl-2-guanadinobenzimidazole (28)

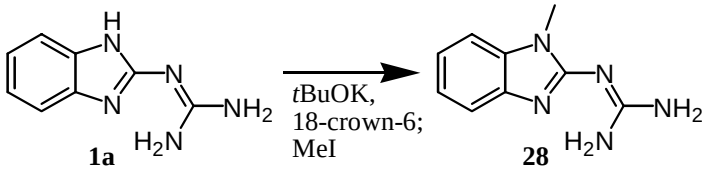

Figure 2.12 Synthesis of 1-methyl-2-guanadinobenzimidazole (28)

1-Methyl-2-guanadinobenzimidazole, **28** was synthesized from 2-guanidino-benzimidazole (**1a**), with methyl iodide as an electrophile 1.63 g (9.30 mmol) **1a**, 1.04 g potassium tert-butoxide (9.27 mmol) and 0.172 g (0.651 mmol) 18-crown-6 was dissolved in 40 mL THF. This solution was chilled to the temperature of melting ice. Methyl iodide (0.580mL, 9.30mmol) was added drop wise and the reaction was allowed to rise to room temperature. After 5-10 minutes a white precipitate had formed. The volume of the THF was reduced and the material was neutralized with 1 M $NaHCO_3$. The organic layer was then extracted with CH_2Cl_2 and H_2O 3 times. An amount of 0.94 g (5.0 mmol) 1-methyl-2-guanadinobenzimidazole product was purified by crystallization from ethyl acetate and hexane (53% yield). Spectral properties of the product were identical to those previously reported in the literature.[1,7]

2.5 References

(1) Acerete, C.; Catalan, J.; Sanchez-Cabezudo, M. *Heterocycles* **1987**, *26*, 1581-1586.

(2) Graubaum, H.; Martin, D.; Csunderlik, C.; Glatt, H.-H.; Bacaloglu, R.; Malurea-Munteanu, M. *Z.Chem.* **1984**, *24*, 57-58.

(3) King, F. E.; Acheson, R. M.; Spensley, P. C. *J. Chem. Soc.* **1948**, 1366-1371.

(4) Kataoka, H. *2-(3N-substituted guanidino)benzimidazole derivatives*; Taisho Pharm.: Japan, 1962; Vol. 64, pp 19629d.

(5) Heilmayer, W.; Sterk, H.; Kollenz, G. *Tetrahedron* **1998**, *54*, 8025-8034.

(6) Eilingsfield, H.; Neubaur, G.; Seefelder, M.; Weidinger, H. *Chem. Ber.* **1964**, *97*, 1232-1245.

(7) Contreras, R.; Andrade-Lopez, N.; Ariza-Castolo, A. *Heteroatom Chemistry* **1997**, *8*, 397-410.

Chapter 3

Design, synthesis, and evaluation of an oligomeric helical receptor

This chapter focuses on the design of a conformational motif for molecular recognition of anions. Synthetic challenges were encountered in the work so the experimental progress was limited. However, much of the iterative design hinged on sound experimental results.

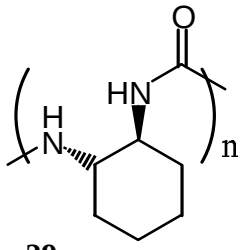

29

Figure 3.1 Oligourea receptor

3.1 Introduction

Hypothetical oligomer **29** should possesses repetitive conformational motifs capable of switching between inter and intramolecular hydrogen bonding. Molecular modeling studies showed that these oligomers had a high propensity to form multiple cooperative hydrogen bonds, and a helix was the most favored conformation. Furthermore, the helical conformation, should be stabilized relative to other conformers in the presence of anionic species. A differentially protected dimer of **29**, n=2, showed a very organized pattern of self-aggregation in the solid state by x-ray diffraction. Using the dimer of **29** and extrapolating to n-mers in molecular mechanics calculations provokes the notion that β-sheet-like

aggregation will be a low energy conformer of this material. When the dimer of **29** was extended to n>7, a material was formed which was similar in the structure to a β-sheet. In the extended dimer, multiple intramolecular hydrogen bonds were formed between the two oligomers. This creates an organized aggregation pattern, creating a material, that is much less soluble in solution than the monomeric units.

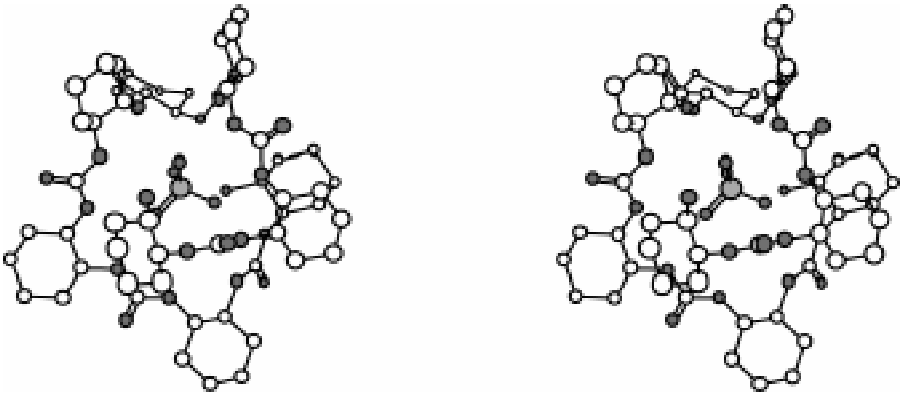

Figure 3.2 Hypothetical octamer structure 29, n=8 and a stereo diagram of the calculated interaction between 29, n=8 and HPO_4^{2-}.

Enantiomerically pure C_2 symmetric 1,2-diamines were used in attempts to construct the chain of oligomers. The 1,2-diamines possess C_2 symmetry as the only point group operation. The same is true for the helix. Helical symmetry should result when an anion is present to bind to the oligomer (see figure 3.2). Multiple hydrogen bonds could form with the multiple hydrogen bond acceptors on the oxoanion. This structure would fold with a helical bias like natural proteins. Another positive aspect to using C_2 symmetric subunits is the simplicity of the construction. Synthesis should be based on N-C amide bond formation. The constituent 1,2-diamines due to the C_2 symmetry avail both nitrogen atoms as nucleophiles. If either one reacts the same chiral product is obtained. The work

began with commercially available 1,2-diaminocyclohexane, however the work will continue with synthetically available 1,2-diaryl-1,2-diaminoethanes and other C_2 symmetric diamines. Another graduate student will continue this project in our labs.

In this work we sought to perturb the conformation of the oligomers by changing the media and introducing guest anions. The preferred method of detection of these conformational changes was CD spectroscopy. CD can be used to monitor the conformation of biopolymers in solution.[1] Bands in the CD spectrum at 190 and 220 nm that correspond to the λ_{max} of the amide carbonyl of an α-helix.[1] These peaks are mostly independent of the amino acid composition. Given this, a similar change would be expected from a secondary structure formation in oligomers of **29**. The sensitivity of this oligomer to changes in anion concentration as well as its own propensity to form a conformation analogous to a β-sheet should be investigated.

In the analysis of the CD results, the goal of molecular modeling computation was to relate observed changes upon the titration of the oligomers with anions to conformational changes that cause the observable. α-helix gives 3 distinctive peaks at 191, 207 and 221 nm. β-conformation gives two peaks at 194, and 216 nm.[2] The CD spectra for an α-helix is essentially constant from one protein to the next, assuming the absence of chromophoric side chains or solvent interactions.[1] This is the primary reason for the expectation that a conformational change will result in an observable change in the CD spectra for polyamides.

The amide bond and the carbonyl are the primary chromophores that

generate CD signals. In the α-helix there are two transitions, which are aligned, parallel and perpendicular to the screw axis of the helix. This generates the two transitions at higher wavelength. Titration caused a change in the CD and NMR spectra for both pentamers. For extended oligomers of **29** the material was expected to form helices, which should increase the R-value, or the rotation of light in one direction per mole of oligomer, for that oligomer. CD titration data was more complicated than this, so further investigation of the bound and the unbound structures was needed.

3.2 Biomimetics

Oligomers of **29** were synthesized to mimic the conformations of biological molecules. Biologically derived molecules show the ability to greatly accelerate reactions with a phenomenal specificity, and to tightly and specifically bind to large or small molecules. These extreme properties drive chemists to study biomolecules to understand and mimic their properties. Biomolecules can generate much complementary surface area that is useful in forming pockets to catalyze or bind to specific molecules. The architectural diversity that comes from α-amino acids is rather remarkable. A diverse array of interesting globular structures comes from chains of α-amino acids. RNA, and proteins take advantage of conformational motifs that generate stable 3D structures that can do interesting chemistry.

3.2.1 Design of a biomimetic host

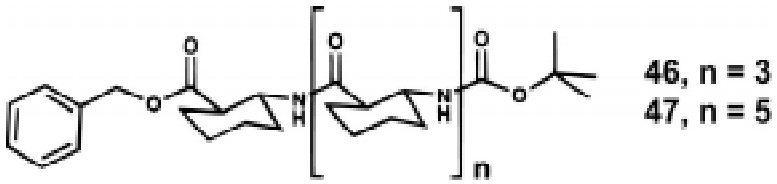

Figure 3.3 Structurally related helical foldamers.

Foldamer is a term that can be used to describe any polymer that has a strong tendency to adopt a general conformation. In general, the conformation is repetitive, but not necessarily the sequence.[3] In the design of **29,** a goal was set for a system which would be simple to make, but would still lead to complex structures. Modeling of **29** and comparison[4,5] to the above β-peptides, in Figure 3.3, and the natural proteins led to the notion that **29** would also form helices similar to those of proteins. Calculations, of the above systems, predict that they are relatively rigid and form tight helices. In Figure 3.2 a hypothetical octomer is produced with Monte Carlo simulations. The conditions of the modeling are described later in section 3.4.1. The general conditions included the use of the Amber* force field and the GB/SA solvent model for water; modeling procedure are described in detail in sections 3.4.2, and 3.4.3. The octamer structure was not tightly constrained and could form a pocket to nearly encapsulate the modeled oxoanions. Monte Carlo simulations showed multiple low energy conformers with significant coverage of the phosphate molecule. Changing the solvent model from water to chloroform only improved the energy of the binding. The polar oligoureas formed weak hydrogen bonds that should collectively work to bind the oxoanions. An oligourea appeared well suited for anion recognition.

The modeling studies showed encapsulation, via helix formation in Figure 3.2. The encapsulation was nearly complete with an oligourea only 8 units long. Multiple hydrogen bonds formed with the oxoanion allowing the oligourea to mimic the normal solvation shell of the oxoanion in a hydrogen bonding solvent. Ordering in the binding pocket appeared to improve upon use of a single enantiomer of trans-1,2-diaminocyclohexane, implying there could be some cooperativity in the helix formation. Oxoanions are more difficult to coax into intermolecular association with de novo molecular guest than cations, the size and directionality of the solvation shell requires a complex molecule, from a design and a synthesis standpoint. Oxoanions also possess large negative free energies of hydration, keeping them hydrated instead of in an associated state. Foldamers are able to form complex complementary surface area from a relatively simple linear chain. Despite the large and negative free energy of hydration, many biological foldamers[6] are able to bind strongly to oxoanions.

3.2.2 Foldamer concept

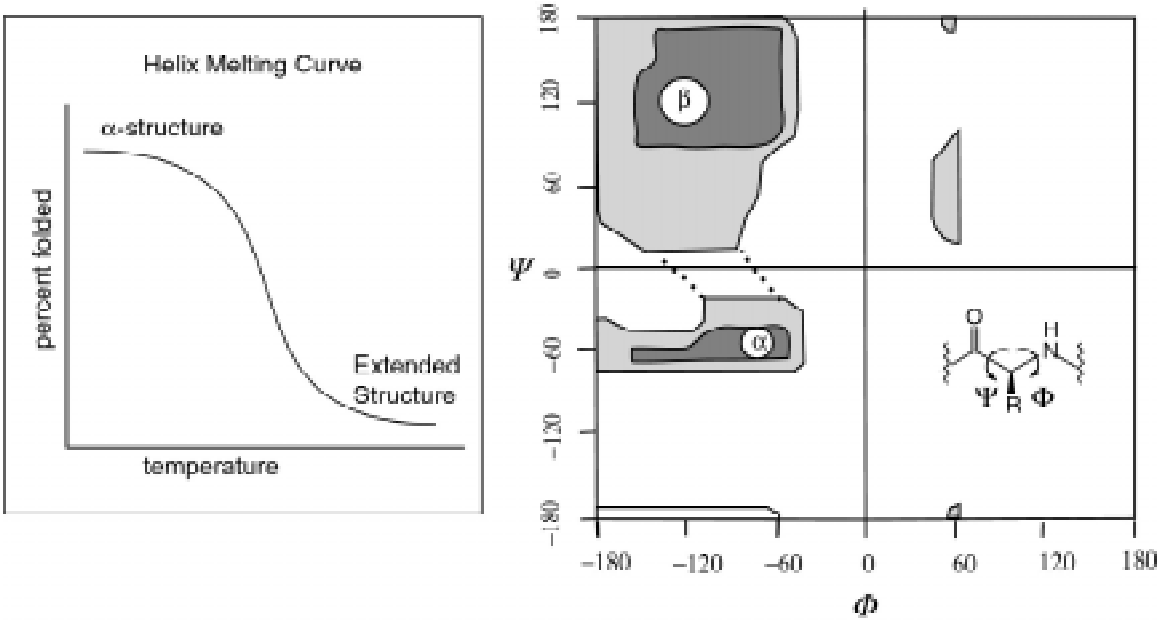

Figure 3.4 Ramachandran diagrams show the limited conformational space in polypeptides. Two state behavior in chiral conformational space results from this limited chain entropy.

Biological systems use the foldamer concept to package genetic information in DNA oligomers. In DNA, chemical diversity at the level of the primary sequence transmits information. This system compacts, folds the information for storage, and allows the information to be read, copied, and repaired. As a foldamer, DNA can behave like a homogeneous polymer despite the fact that it is composed of four different monomers in a plethora of different sequences. Likewise foldamers (α-helices, β-sheets, β-turns, β-barrels, and Ω-loops) in proteins effectively allow 1D sequences to birth complex, functional 3D architectures. Diversity in protein conformation is surprising when one considers the limited nature of Ramachandran conformational space in peptides (see

Figure 3.4).[7] On the other hand, the peptide foldamer may be useful for biological architecture only because its conformational space is limited. This may be a general statement regarding the dynamic behavior of molecules that fold in biologically relevant ways. Limited conformational space appears to be an important factor in the formation of the biological foldamer and the suitability of the foldamer to strong 2D structure formation, not only in proteins but also in RNA.[8]

3.2.3 Foldamer models

These general principles can be applied to the design of non-biological oligomers. Biological oligomers are not the only interesting, or biologically relevant foldamers other foldamers have been formed from oligoamides constructed from β-amino acids or β-peptides.[9] The conformation of these peptides was studied and compared to the natural α-peptides using the diversity inherent in the α-peptide system. Several examples of biological activity and therapeutic application of β-peptides have been found. One of Gellman's cyclopentane derived β-peptides, β-17 displayed unique antibacterial activity in its ability to kill the drug-resistant strains, *Enterococcus faecium* and *Staphylococcus aureus*.[10] The antibiotic activity appears to derive from the fact that the β-peptide folds into helix which disposes hydrophobic side chains on one side and cationic side chains on the other, similar to a family of antibiotic peptides, the magainins. Seebach has also found biological activity in β-

peptides.[11] These materials obviously resemble their natural peptide cousins and interact with the body in a manner similar to the α-congeners.

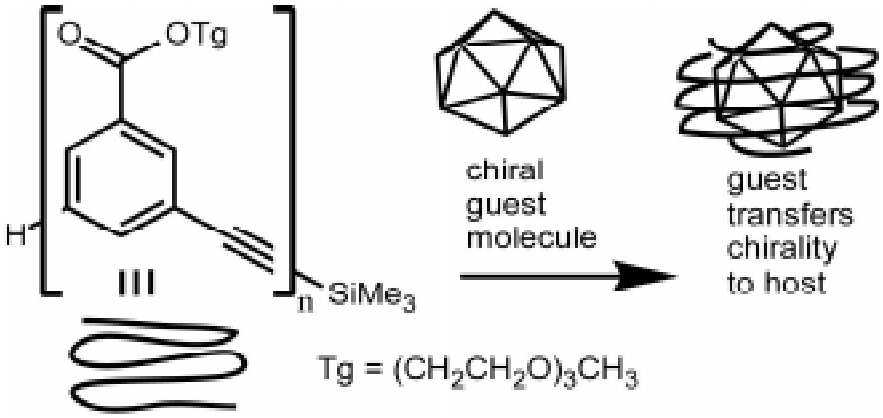

Figure 3.5 Foldamer-based molecular recognition.

If β-peptides are scientifically interesting,[9] other conformationally constrained oligomers bearing peptide-like properties should be considered in this regard as well. In fact some other non-peptide foldamers have been studied and were found to form some unique and interesting 3D forms.[12-15] The foldamer in Figure 3.5 was synthesized by Moore to demonstrate that foldamers could be used to establish cooperative molecular recognition.[12-15] Work with this foldamer established that this class of materials could be used to form a three dimensional cavity, for pocket binding of guest molecules. In these well-balanced systems, the electronic nature of the internal space, the external surface and the solvent molecules differed little. Furthermore, the chiral conformation in the foldamer came from the chiral guest. This foldamer differs from the ideas involved with the foldamer system **29**. Moore's foldamer explores achiral hydrophobic spaces and chirality is induces in the molecular host by chiral guests; see Figure 3.5. In contrast, in the development of foldamer **29**, the

objective was to achieve a chiral conformational change by binding an achiral anion to a chiral foldamer; see Figure 3.2.

3.2.4 Building a biologically-inspired foldamer

Enantiomerically pure *trans*-1,2-diaminoethane units were used as building blocks for the synthesis of **29**. (1R,2R)-1,2-diaminocyclohexane and (1R,2R)-1,2-diamino-1,2-diphenylethane (to be reported elsewhere) were used as monomers. The functionality of the monomers was similar to peptides both contain sp^2 hybridized hydrogen bond donors, the amide or urea NH functionality, and hydrogen bond acceptors, the carbonyl oxygen. The material was applied to a foldamer-based molecular recognition of oxoanions. Here, the local chirality of the monomer, C_2, predisposes the chain to take on conformations capable of doing molecular recognition.

In the proposed interactions between an oligourea and biologically relevant anions, the urea N-H functionality will point toward the axis of the helix and the aliphatic portion of the oligomer will occupy the perimeter of the helix. In suitable solvent, the guest will be enveloped by the oligourea. Conformational tendency in these oligomers should be controllable. The chiral 1,2-dimino ethane derivatives will have a tendency toward helicity, if each unit is either (R,R) or (S,S). In this manner, by virtue of its conformation, the oligomer will define the physical-chemical nature of inner and outer space. We see this property as potentially useful to the development of smart solids for chemo sensors and drug delivery of biologically relevant anions.

The molecular recognition scheme outlined above is biomimetic. The proposed conformational bias in the oligomers under consideration involves the principle of hydrogen bond cooperativity. This important characteristic of biological oligomers consists of numerous weak interactions contributing additively to a bioactive conformation.[16,17] The establishment of each atomic contact between the helix and the guest molecule should contribute synergistically to the stability of the ensemble.

Designed molecular recognition between large, non-biological and biological molecules has not received enough attention. Usually investigators pursuing molecular recognition target small guests toward small hosts. Likewise, the most important targets in the pharmaceutical community fall under the category of ‘small molecule drugs.’ Minimally complex molecules work well when searching for drug candidates because they are well suited for molecular libraries and high throughput screening. However, the majority of life processes involve the chemistry of polymers or oligomers. This principle is self-evident when one considers the central importance to the organism of materials like DNA, RNA, proteins, polypeptides, polyketides, tubulin, collagen, hyaluronan (and other oligosacharides) and lipid membranes. A living cell is not a solution of proteins and other biological substances; a cell is a gel due to the plethora of interactions between biological molecules. Clearly, most biochemical processes and much molecular recognition in the biological context occur at interfaces between solid and solution. There is much space for scientific thought and molecular design

between 'small molecule' drugs and the kind of substances that biologists and chemists consider oligomers.

3.3 Synthesis

A foldamer, **29** was synthesized using the synthetic intermediate (1R)-1-amino-(2R)-2-isocyanatocyclohexane as a template for the formation of an oligourea. Using different protecting and activating groups different oligomers were synthesized. Synthetic problems prevented the facile synthesis of oligoureas greater than 4 units in length. Long oligoureas were needed to be able to form a helix around the oxoanion. This conformational change would result in a detectable changes in the circular dichroism spectra of the complex. To overcome these problems, isophthalic acid, and 1,3-phenylenediisocyanate were used as spacers to increase the chain length. Amine protection with Boc anhydride and ethyl trifluoroacetate was used to control reactivity at either end of the molecule to enable effective elongation of the oligomers. Isophthalic acid was mono protected as the methyl ester. Convergent syntheses after each major step should have led to new binding candidates.

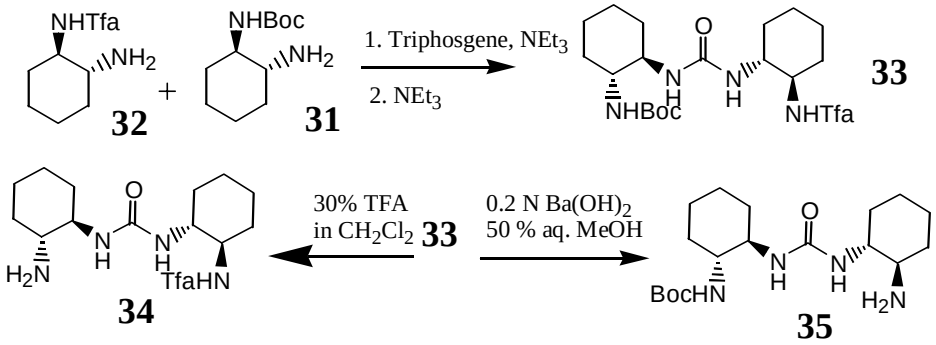

Figure 3.6 Synthesis of a differentially protected dimer.

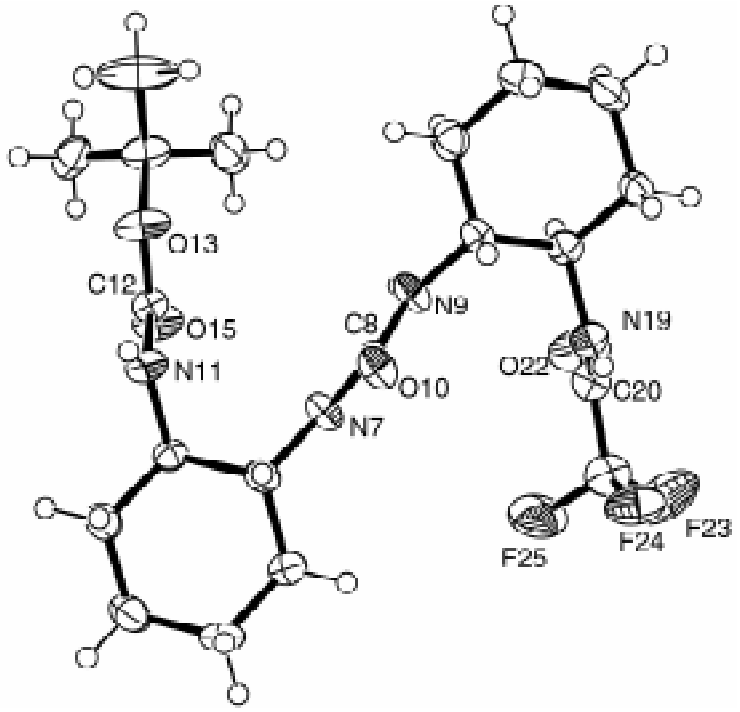

Figure 3.7 Crystal Structure of 33

Trans-1,2-Diaminocyclohexane was dimerized by adding 1-trifluoroacetamido-2-aminocyclohexane **32**, slowly to a solution of triphosgene, converting the unprotected amine into an isocyanate. This isocyanate reacted in a facile manner with **31** when the amine was added quickly to the isocyanate of **32**. This material could be crystallized from methanol/ethyl acetate in 60% yield. The crystal structure is shown above in Figure 3.7. The differentially protected dimer, **33**, could then be quantitatively differentially deprotected with the use of a 20% v/v solution of TFA/CH_2Cl_2 for removal of the *t*-Boc protective group and 0.2 N barium hydroxide in 50% aq. methanol for removal of the trifluoroacetamide protective group. Deprotection of the trifluoroacetamide protection group gave a chloroform soluble amine, **35**, which was used to proceed further in the synthesis.

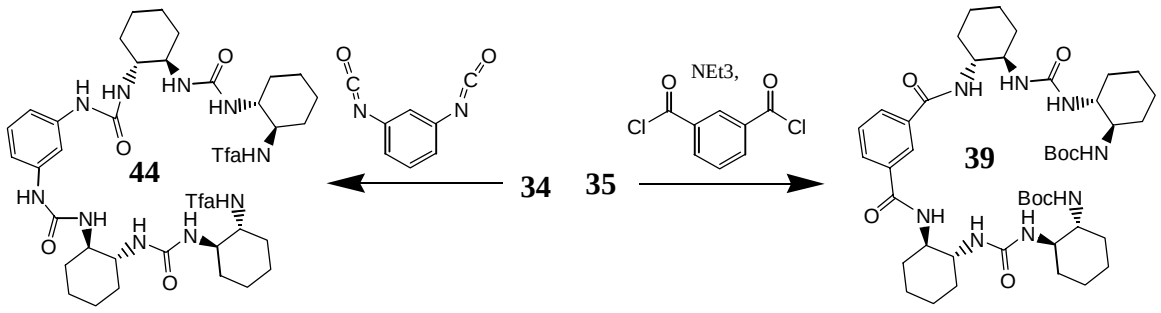

Figure 3.8 Synthesis of protected pentamers with spacers

Spacers were employed to make pentamers **39**, and **44** after the heterocoupling of **34**, and **35** with triphosgene did not result in a well-defined chemical species **60** (see Figure 3.9). Dimer **33** and pentamers **39**, and **44** gave well-defined ^{1}H, ^{13}C, and MALDI-TOF spectra. **34** reacted in a facile manner with isophthaloyl chloride to form pentamer **39** in good yield. **31** was also reacted with isophthaloyl chloride, and **32** condensed with 1,3-phenylenediisocyanate in good yield to form their respective trimers.

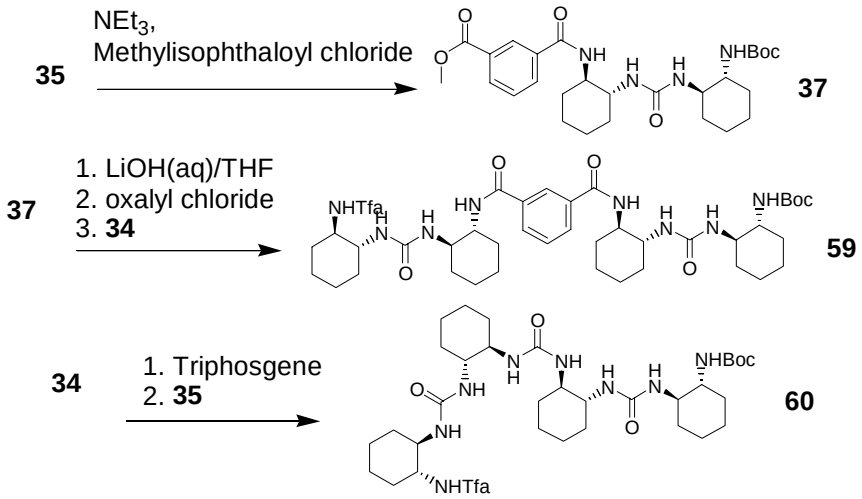

Figure 3.9 Synthesis of differentially protected oligomers

The methyl ester **37** was easily deprotected with 4 equivalents of lithium hydroxide, converted to the acid chloride and reacted with the trifluoroacetamide

protected dimer, **34**, forming a differentially protected pentamer. Unfortunately, this material was not well defined by MALDI-TOF, despite the fact that the symmetrically protected pentamer **39** above was well defined. NMR of **59** had 8 amide type NH peaks, but purification of the material by flash chromatography gave a material which was similar to **35**.

Hetero-protected oligourea **60** was not obtained by using triphosgene or carbonyldiimidazole coupling regents. Current work on the synthesis of these oligomers is currently being done by others in the group. This work is briefly discussed in the addendum. Carbonyldiimidazole produced only dimerized product and was ineffective at producing a heterocoupled product. Triphosgene was also ineffective at producing a heterocoupled product due to the low solubility of Tfa-protected dimer **34**. A protected diamine has been synthesized activated and isolated using p-nitrophenyl-chloro-formate as an activating reagent.

The sensitivity of the conformations of free amine derivatives **40** and **45** to the concentration of PO_4 were compared to those of shorter derivatives **43** and **38b** (Figure 3.26). These studies should have evaluated the ability of dimer **33** to function as substructural units in the molecular recognition of oxo-anions. The linkers were long enough to allow the two ends of the oligomer to meet in modeling studies, and should be more effective than a simple homocoupled oligourea from a dimerizing activating agent like carbonyl diimidazole.

3.4 Computation and modeling

Computation was used in the design and analysis phases of this research. Modeling directed the synthesis toward oligoureas that were helical in the presence of phosphate (see Figure 3.2). Modeling also sought to investigate the possible two-state behavior of the oligoureas.

3.4.1 Monte Carlo simulations

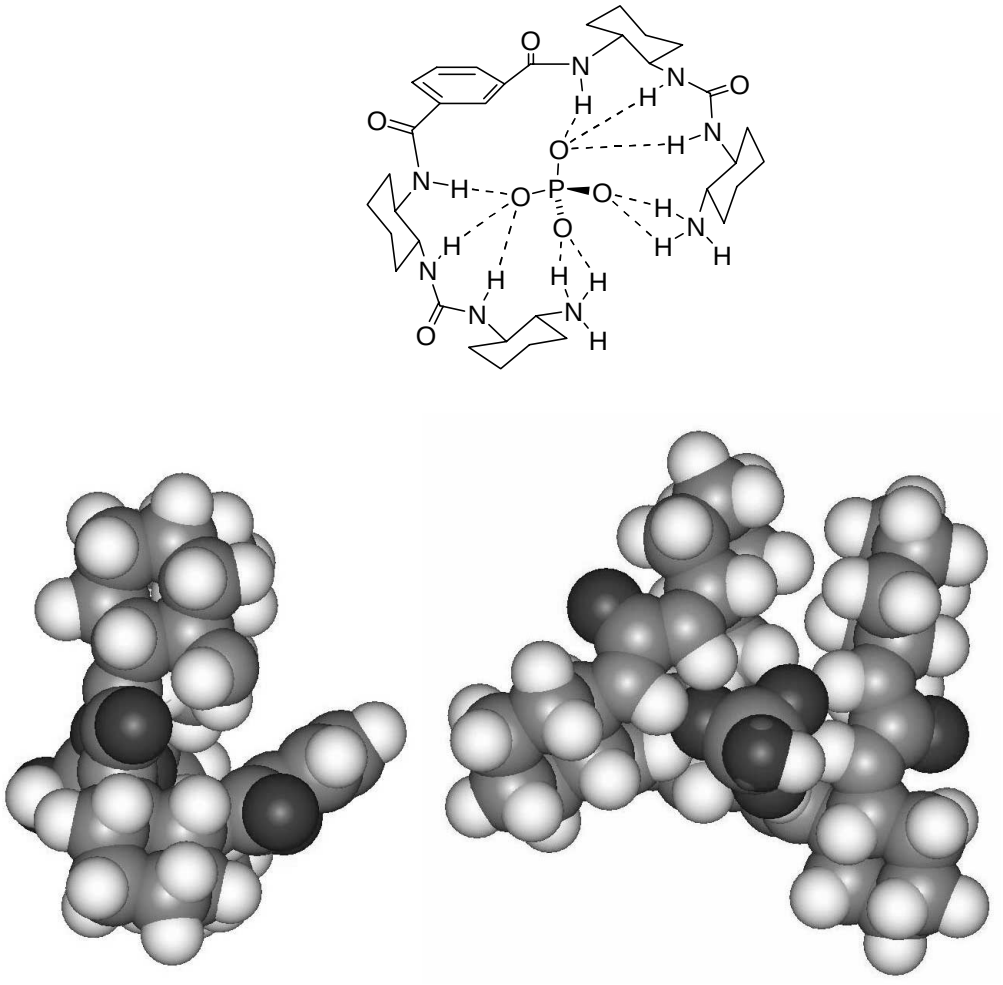

Figure 3.10 Monte Carlo simulation of the low energy structure pentamer 40 with HPO_4^{2-}

Monte Carlo simulations done on 200 trial conformations of **40**, procedures, and theoretical details as described below, found 12 low energy

conformations within 3 kcal/mol of the lowest energy structure shown above in Figure 3.10. Variations between the low energy conformers, found by the Monte Carlo search routine, of phosphate-bound pentamer were small. Structures lacked the length to wrap the phosphate in a helix, which would require the oligomer to wrap greater than 360° around the phosphate. **40** formed an interesting cup like structure in which the pentamer wrapped the phosphate, and the phenyl ring held the phosphate in the cup. Other conformers moved the position of the phosphate in the cup, or moved the amine of the terminal cyclohexane ring in or out of the cup.

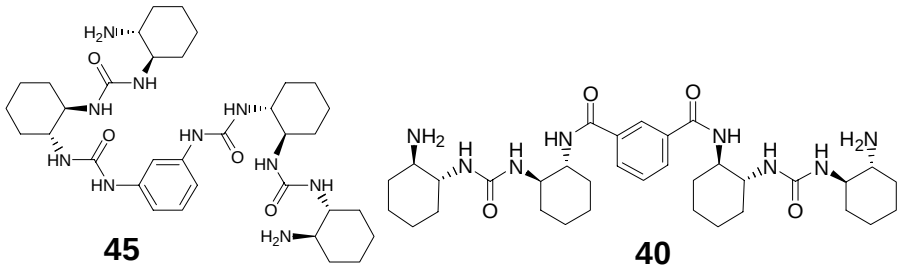

45 **40**

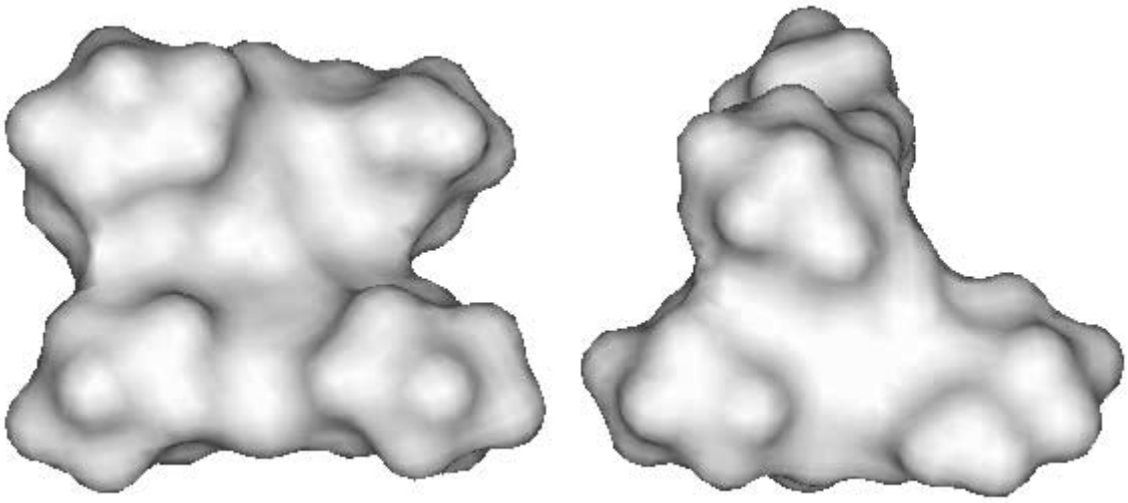

Figure 3.11 Pentamers 45, 40 with solvent exposed surface (1.4 Å probe radius)

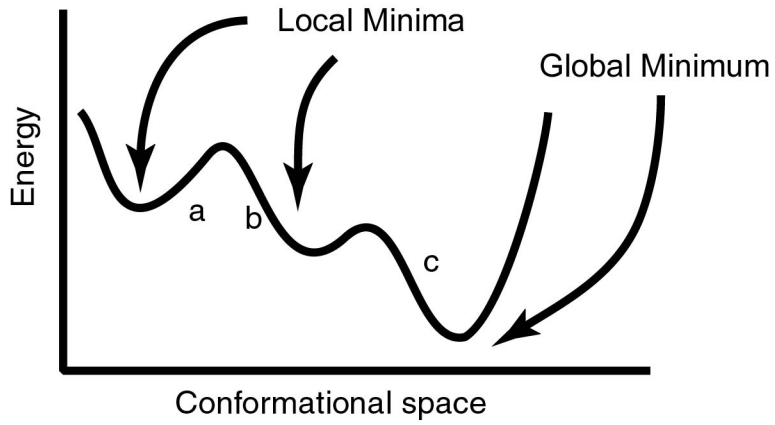

Figure 3.12 Description of conformational searching with Monte Carlo simulations

One of the primary goals of molecular modeling is to find the global minimum structure for any given oligomer. Unfortunately, because of the way that modeling programs find energy minima, the structure that results may not be the lowest energy conformation for the molecule. The lowest energy conformation given by the minimization can be referred to as the global minimum. The global minimum shown in the above figure is the deepest energy well. Local minima, shown above, as the smaller wells can also be important for chemical reactivity and, if the barriers to the interchange between the different conformational isomers are low, then the molecule may spend part of its time in one or more local minima.

Monte Carlo simulations explore the dynamics of the molecule. Most minimization programs calculate a derivative of the energy at a particular conformation. The conformational variables are then adjusted based on that derivative. This allows for fast determination of minima. Using this technique local minima are found if starting from a or b in conformational space or the global

minimum if starting from c. Users of modeling software defeat the predisposition to achieve local minima by intelligent choices of starting points. Monte Carlo simulations attempt to simulate heat energy to explore the dynamics of the molecule. A Monte Carlo simulation[18] takes a set of rotatable bonds and applies a random change, such as a rotational increment between 0 and 360°, or an atom displacement. If there are no high-energy steric interactions, then a minimization is run, and the energy compared to the lowest previously found minima. If a minimum structure is found then this is the new starting point and this structure is adjusted. Otherwise, the Metropolis algorithm[19] is used to determine if the trial configuration is accepted as the new starting point.[20] This algorithm generates a random number between 0 and 1, then compares this to a probability given by the Boltzmann distribution. $\exp(-\Delta E_i/kT)$ If the random number is smaller, then the new conformation is accepted as the new starting point.

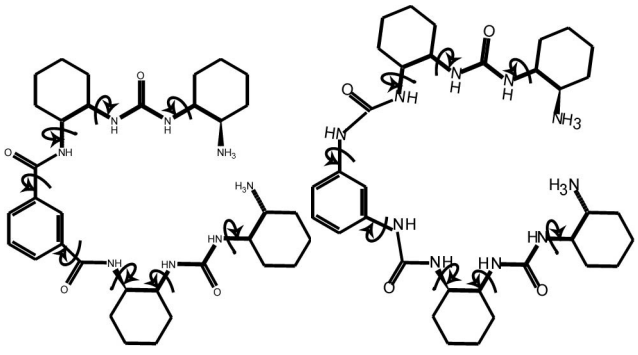

Figure 3.13 Pentamer 40, 45 with arrows to indicate the dihedral angles simulated in Monte Carlo calculations

Monte Carlo simulations ran trial configurations of pentamers **40**, and **45** with the Amber* force field, and the chloroform solvent parameter set.

Calculations set to find all conformations within 50 kJ/mol of the found global minimum. Pentamer minimizations calculated in a fashion similar to those of the Ramachandran plots shown below. Monte Carlo simulations ran with the constraints for torsinons marked with curved arrows, seen in Figure 4.13 above to reduce multiple high energy conformers and reduce the time required to find low energy conformers.

3.4.3 AMBER*

The AMBER* torsional parameterization set was employed with the program Macromodel Interactive Molecular Modeling System Version 5.0® to determine the low energy conformation of the oligomers. Amber is a molecular mechanics force field that is widely used for modeling biological oligomers. Like most molecular mechanics force fields this one is quite dependent on experimentally determined variables. Stability is conferred to the molecule if it can come close to the optimal bond length, bond angle and dihedral angle. A 12-6 parameter set is used to mimic the effects of the van der Waals forces. The sum of these effects gives an overall energy for the conformation of the molecule. This and other improvements in the parameters for the peptide backbone allow for optimal results for peptides.

3.4.4 Solvation treatment

Solvent can have a major affect upon the relative energy of many substances. Macromodel uses the GB/SA model to describe the effects of solvent. A chloroform parameter set was used for the analysis of oligomers of **29**. The free energy associated with solvent, G_{sol}, is the sum of three terms,[21]

including a solvent-solvent cavity term, G_{cav}, a solute-solvent cavity term, G_{vdW}, and a solute-solvent polarization term, G_{pol} ($G_{sol} = G_{cav} + G_{vdW} + G_{pol}$). For saturated hydrocarbons G_{sol} is linearly related[22,23] to the solvent accessible surface area (SA). G_{cav} and G_{vdW} can be calculated by a determination of the solvent accessible surface area and the solvation parameter for each atom. The other parameter modifies the electrostatic attraction of a system of widely separated charges. The generalized Born equation[21] relates the dielectric constant of the solvent to a contraction of the attractive or repulsive forces of separate charges. An article[21] by Still and Thompson describes well the generalized Born equation and its relation to G_{pol}. 3.6.11 Molecular modeling of oligomers (29)

Oligomers were modeled using MacroModel,[24] a molecular mechanics program to find optimum (minimum energy) conformations. Molecular mechanics uses sets of force fields that have been optimized using experimentally, and *ab initio* determined molecular constants. Molecular modeling is primarily used to examine molecules that are large of have many degrees of freedom that make them difficult to minimize using more computationally intensive methods. A force constant is used to put an energy value to torsion and bond length parameters. Molecular mechanics also uses experimentally determined values for the van der Waals radii and electrostatic attractions are also used to determine the low energy structure.

Monte Carlo simulations were run with unbound pentamers **40** and **45**. Simulations gave the conformational energy minima shown by the conformers in

Figure 3.11 above. These structures had varying degrees of compactness and helicity. Pentamer **45** appeared to be more stable in the most compact forms. Pentamer **40** appeared to be more stable in less compact conformations. In pentamer **45,** each dimer arm is conformationally stabilized with a 7-membered ring formed between the amide NH of one urea and the carbonyl CO of another. **40** was not as globular in its minimum energy conformation, and the two dimer arms crossed each other at a higher angle than that of **45**. See below for a diagram of the difference between **45** and **40**, in Figure 3.14. The change in the angle of the two dimer arms and the chain length caused by the change from an amide to an urea around the phenyl ring caused the molecule to go from a tight ball to a molecule that looks like a set of arms crossed.

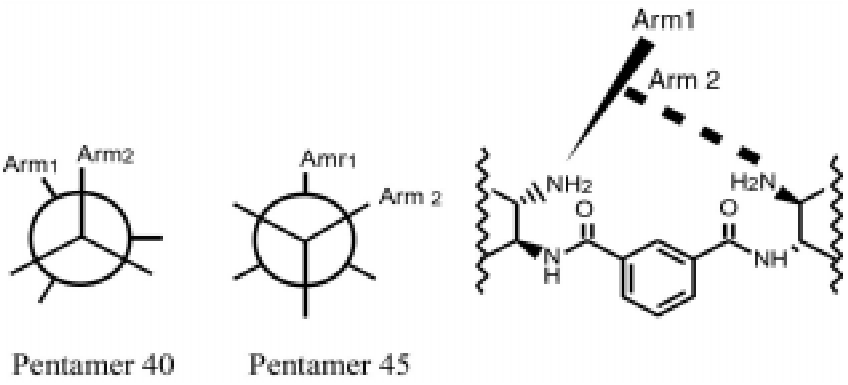

Figure 3.14 Diagram of position of cyclohexane arms in the pentamer 40 and 45

Like the biological molecules, the change in the dynamic globular structure of the two pentamer bodes a change in the rotation of circularly polarized light. Despite the small size of the molecules, they do appear to have a definite conformational preference. The ball shaped conformation of structure **40**

appeared to have little effect on rotationally polarized light, but the crossed arms of the conformation of pentamer **45** had a larger effect.

3.4.5 Conformational motifs and predictions of two-state behavior

Ramachandran plots, like the one shown in figure 3.4, indicate conformational propensity in complex conformational space as a function of two rotatable bonds. Limiting the conformational space is very important to biological molecules. This limited conformational space governs the ability of biomolecules to adopt native (functional) or extended (denatured) states. Using this type of plot Ramachandran and coworkers[7] defined an upper limit on the conformational space of peptides. Ramachandran defined the atoms in his dipeptide as spheres that have a hard shell and are not allowed to penetrate the shell of another atom. If a conformation causes two atoms' shells to penetrate then the conformations is not allowed. Large portions of the map are excluded using this method, but the sections that are not excluded can be used to categorize the various folding patterns in peptides. It is also possible to use the chart to predict if certain folding patterns are or are not allowed. The plot predicts the common right-handed α–helix, shown in the bottom left hand corner of the plot in Figure 3.4, as an allowed structure. The not so common left-handed helix, in the small lightly gray patch in the upper right-hand corner was predicted as an allowed but rare structure. The gamma helix lies outside the outer limit for the minimum contact distance and therefore is not allowed. The extended or β-structure labeled part of the plot in allowed conformational space for the dipeptide. It is difficult to see in the plot in Figure 3.4 but the α-helix has a deeper well (more stable) than the β-

structure. However, the β-structure covers more area in conformational space. Therefore, the β-structure should be entropically favored and thus favored at higher temperatures. Basically this gives rise to the two state behavior of peptide and protein folding.

Peptides that are longer than two amino acids in length have long-range steric interactions.[25] The long-range interactions of larger peptides impose further restrictions on the motion of the peptide. The packing of the chains of **29** should increase the order of the molecule with increasing length. The Ramachandran plot data for **56** showed a conformational preference for one of the four energy wells, and changing the solvent increases this preference.

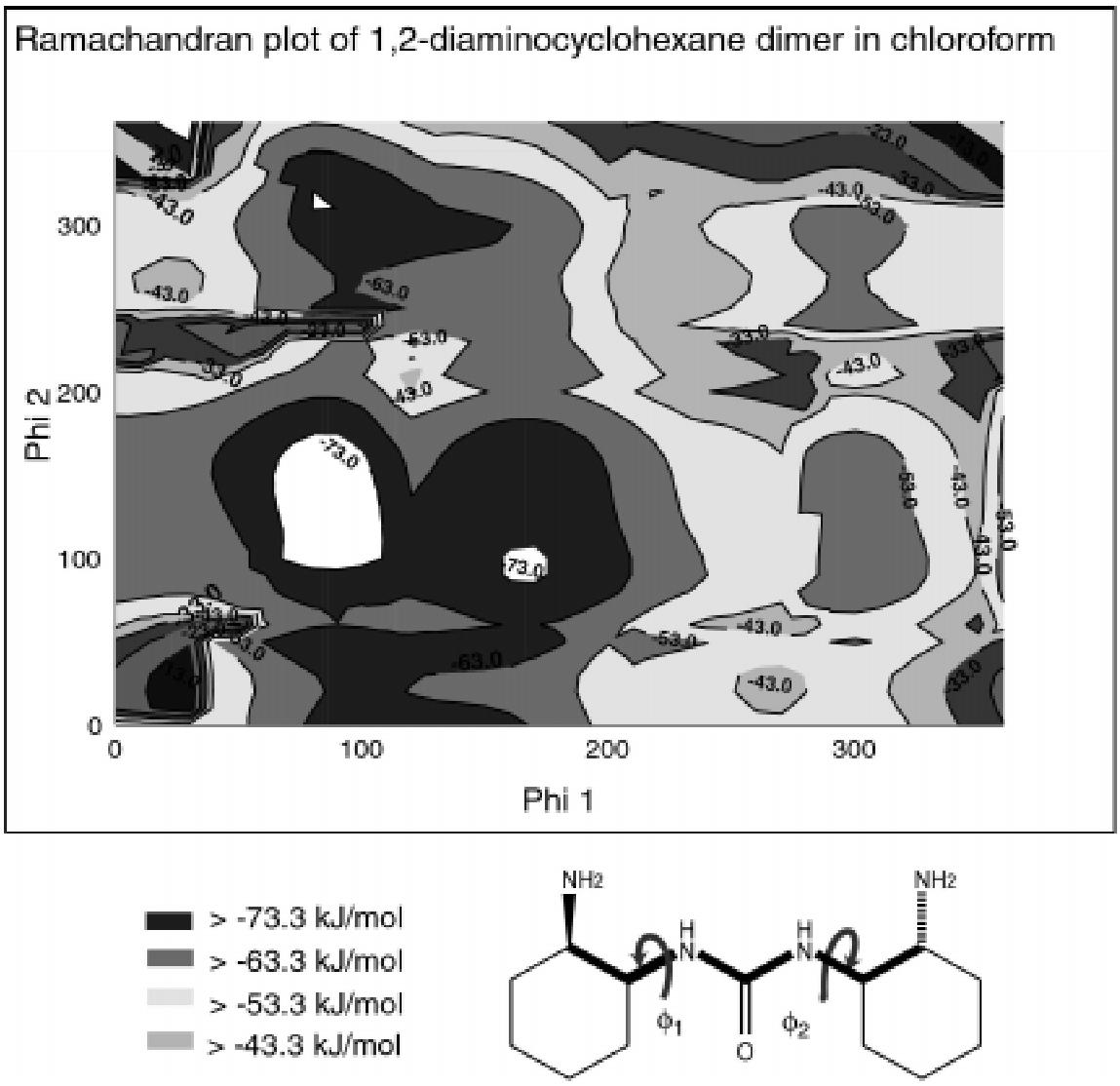

Figure 3.15 Ramachandran plot of the rotation of Φ_1 and Φ_2 in structure 56 using the GB/SA chloroform parameter set.

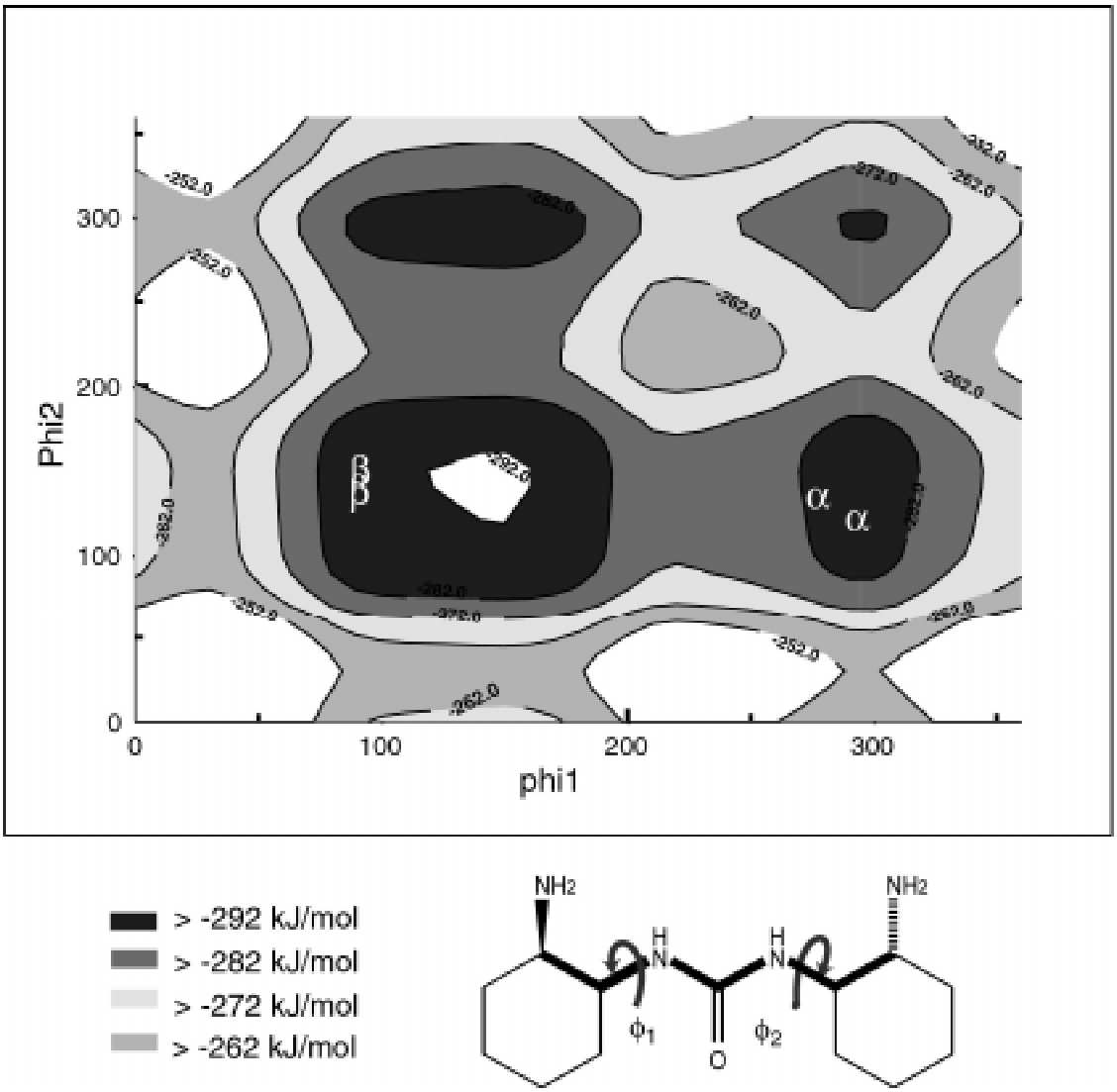

Figure 3.16 Ramachandran plot of the rotation of Φ1 and Φ2 in structure 56 using the GB/SA water parameter set.

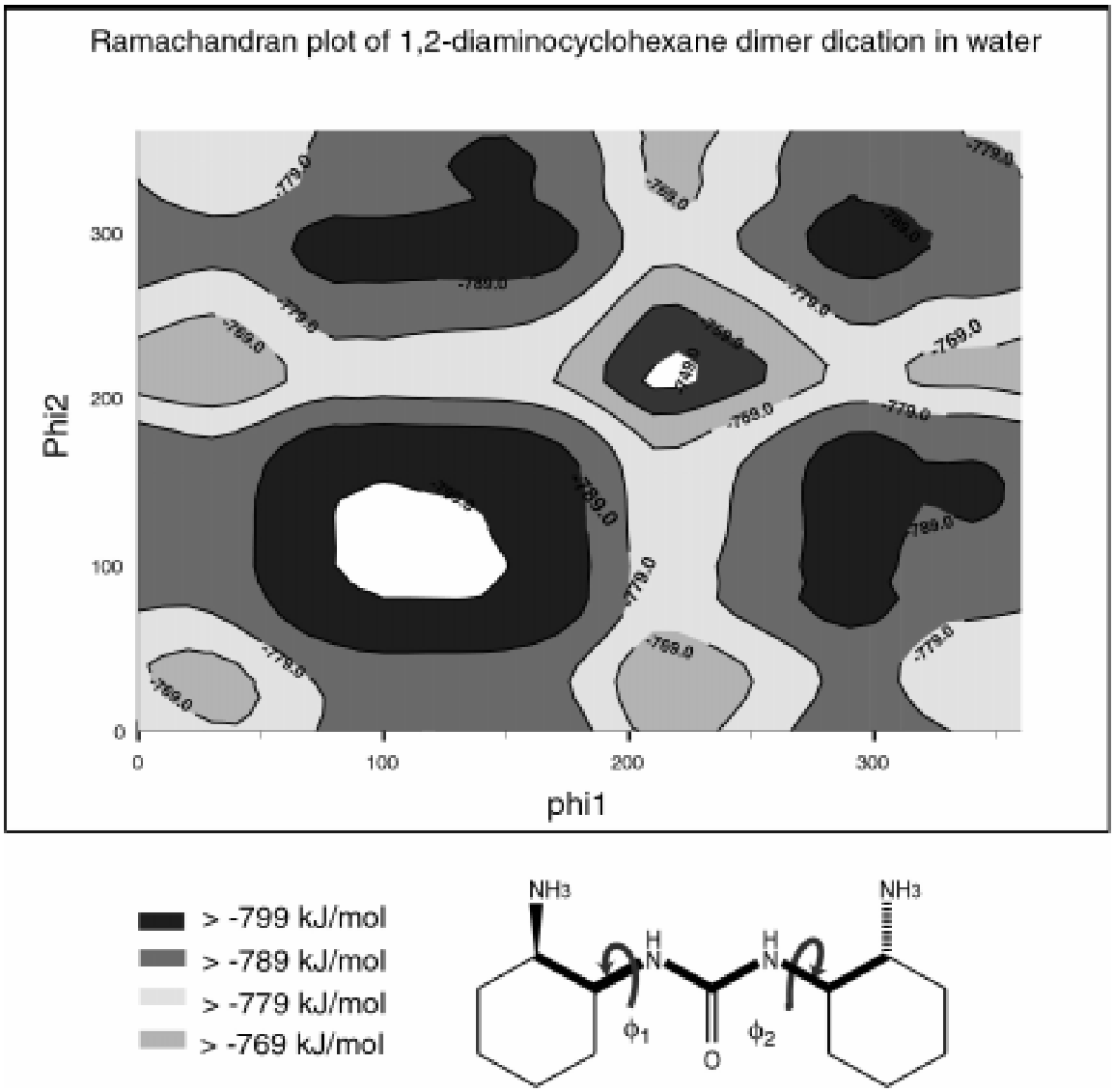

Figure 3.17 Ramachandran plot of the rotation of Φ1 and Φ2 in structure 56 + 2HCl using the GB/SA water parameter set.

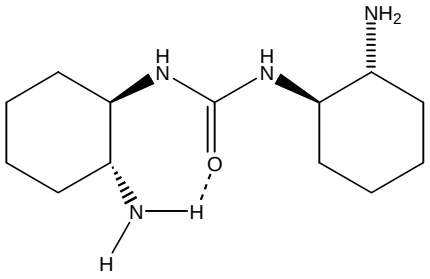

Figure 3.18 Low energy intermediate

Ramachandran plots of the dimer **56** showed the effects of conformation and solvent upon the hydrogen bond strength. Figure 3.16 showed that chloroform increases the effect of the intramolecular hydrogen bond on molecular conformation. In Figure 3.16 some of the energy wells are much deeper than others. The conformations correspond to the establishment of hydrogen bond donors and acceptors. The conformation shown in Figure 3.19 was one of the common energy wells shown in the RC plots. The seven member ring constrained by a hydrogen bond is also found in some of the high energy intermediates, presumably due to high energy atom contacts from the proton and nitrogen which are pushed too close to the amide NH. In Figure 3.16 and 3.17, the RC plots showed a decreased influence of the intramolecular hydrogen bond due to the solvent change from chloroform to water on the molecular conformation. The molecule can more easily explore four different regions of conformational space in water. Conformation appeared to be controlled primarily by the steric arguments.

Folding in apolar solvents appears more promising, and some helix inducing alcohols like trifluoroethanol or hexafluoroisopropanol may induce these conformational changes in mostly aqueous solvents.[26-28] The RC plot of the dimer in chloroform solvent gave low energy conformations in a smaller portion of the chart, with higher barriers between different energy wells. Some of the regions in the chart were explored with molecular modeling to identify forms that will come from them. The α–region and the β-regions of the chart were indicated in Figure 3.17. The determination of α- versus β-regions was determined by the

analysis of the compounds modeled from the crystal structure of the dimer **33**. Regardless, the Ramachandran space characteristic of the dimeric oligourea hint that conformational motifs reminiscent of natural polypeptide chains should be possible for the planned oligomers. The hypothetical structures below were modeled and the dihedral angles of the resulting structures were sampled.

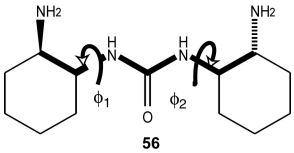

56

To find the Ramachandran plot for a dimer of the oligomer **29, 56** was minimized and the two dihedral angles for the two CN bonds immediately adjacent to the urea, ϕ_1, and ϕ_2 were adjusted. First ϕ_1 then ϕ_2 is rotated from 0° to 360° in increments of 10° to make 1296 energy measurements. Energy is determined for each conformation, and the data can be plotted on a contour plot like that of the well-known Ramachandran plot for ϕ, and ψ in proteins.

3.4.6 Protein like conformations of oligourea (29) n=8

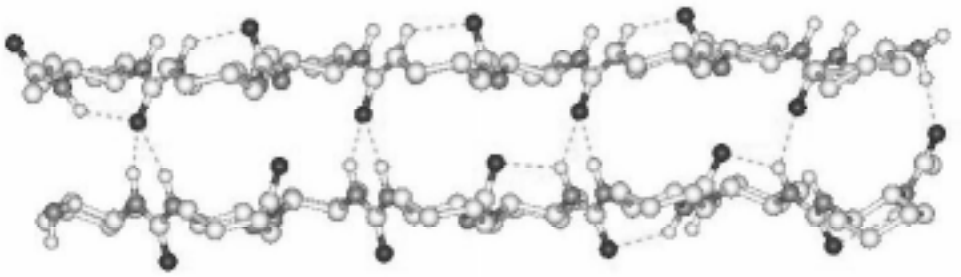

Figure 3.19 Extended dimer crystal structure

Modeling of oligourea **29** showed the propensity of the molecules to mimic protein forms. Of these forms, the β-sheet seems most obvious. The protected dimer formed a thick gel when added to halogenated solvent with a small percent

alcohol. The structure in Figure 3.20 shows a stable β-sheet like structure found for **29** n=8. This structure came from another modeling study. Two adjacent molecules of **33** from the crystal structure shown in Figure 3.7 were deprotected and elongated to eight units in length. They were then modeled with an Amber* force field, and water was modeled by the GB/SA solvent parameters. The resulting conformation of structures resembled a set of β-sheets in the way they formed a short network of perpendicular hydrogen bonds. The resulting aggregate was highly stable and could form a gel in solution. Urea compounds often form gels in solution. These gels may mimic the protein-protein interactions of the cellular environment.

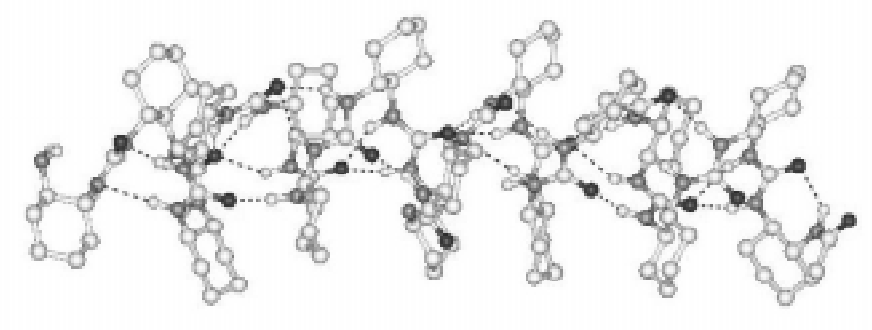

Figure 3.20 Hexadecamer helix conformer

Figure 3.21 shows a helical conformer of **29** n=8 with the right hand end acetylated. The above structure was a highly favorable conformer found through molecular modeling, which was lower in energy than the β conformation shown in Figure 3.20. Rotating the CN bonds so that NH bonds made contact with unit N+1 formed the α-structure. A minimization was then carried out using the same parameters as the β conformer, resulting in the conformation shown in Figure 3.21.

3.5 Evaluation and conclusions

3.5.1 CD titrations

In the modeling phase of this experiment it was hypothesized that upon addition of significant amounts of oxoanion, oligomers would bind and cause a gross change in the circular dichroism spectrum. CD spectroscopy required a low concentration of the oligomer for analytical determination of the CD spectra. To test the binding of the pentamer to phosphate an organic soluble source of phosphate was required. The tetrabutyl ammonium dihydrogen phosphate salt was an excellent source for solvents from methanol to acetonitrile to chloroform. Although the oligomers were modeled in a chloroform solvent field, that solvent was not transparent to UV light at wavelengths of less than 240 nm. The window of wavelengths in which urea absorbs is 200 to 240 nm; therefore this is the the region where we would like to detect the CD spectra. Acetonitrile is transparent for this section of the UV spectrum, so it was used for this titration. Titration methodology to detect binding of deprotected pentamers **40**, and **45** is described later in section 3.5.2.

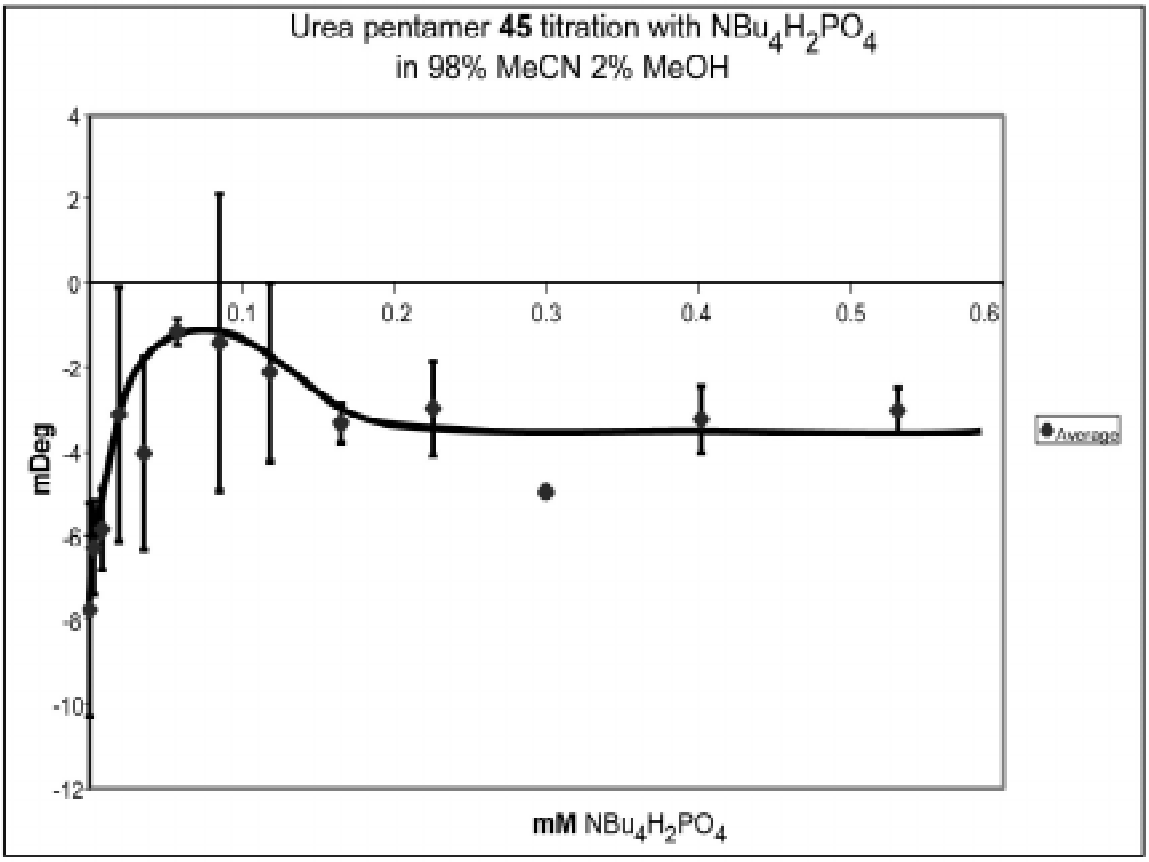

Figure 3.21 CD titration of the pentamer 45.

There appeared to be two different binding constants for pentamer, **45**, detectable in acetonitrile. The first appeared around 0.02 mM, phosphate and the second around 0.2 mM. The concentration was ~0.01 M pentamer. In water with Na_2PO_4, this pentamer had no detectable change in its CD signature. Binding for this molecule seemed improbable in water, but comparison to the amide pentamer augmented the argument that binding was present in acetonitrile. Titration had significant drift due to error in the measurement of CD spectra. Error bars are included in Figures 3.22 and 3.23 for CD measurements in the titration of amide pentamer **45** and **40**. Error was calculated for each measurement, and appears in graph to ± 2 standard deviations. Each data point was measured

three times and the standard error calculation was made for determination of the error. This titration was repeated 2X with both shown on the graph below.

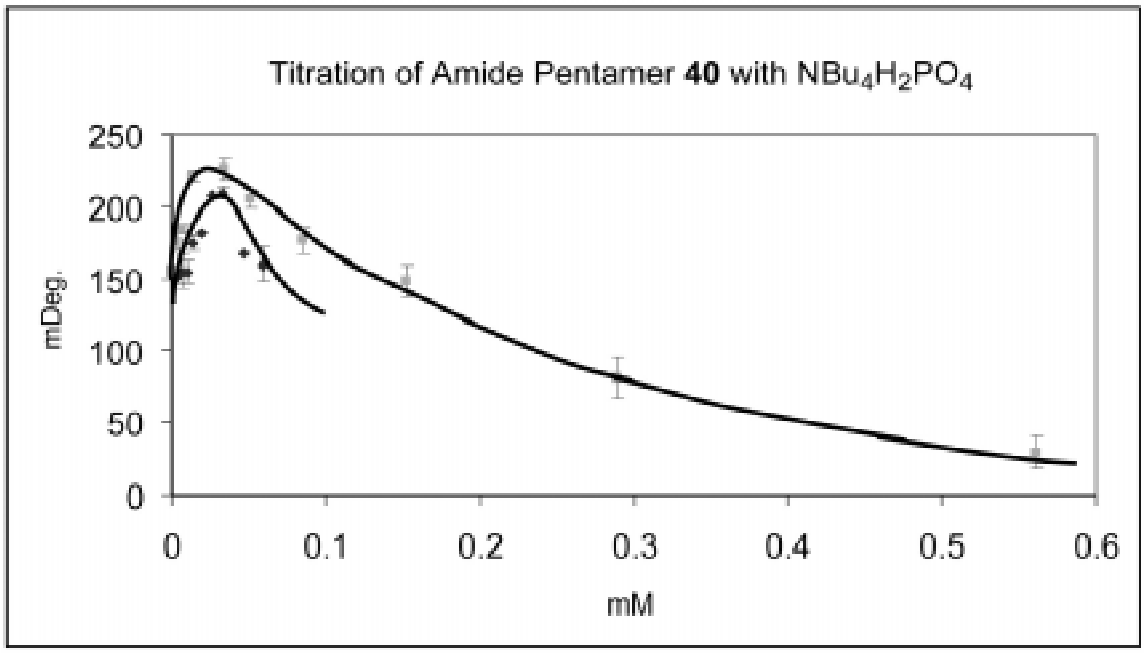

Figure 3.22 CD titration of pentamer (40).

Pentamer **40** was titrated under the same conditions as pentamer **45,** but gave a greater CD response. The response for **40** was enhanced for the second binding constant by a precipitation phenomenon that did not occur for **45**. The binding constant for pentamer **40** was similar for similar concentrations of oligomer and phosphate versus those for pentamer **45**. The first and second binding constants occurred at 0.02 mM and 0.2 mM. Error bars for CD data of pentamer **40** are similar in absolute value to those for **45**.

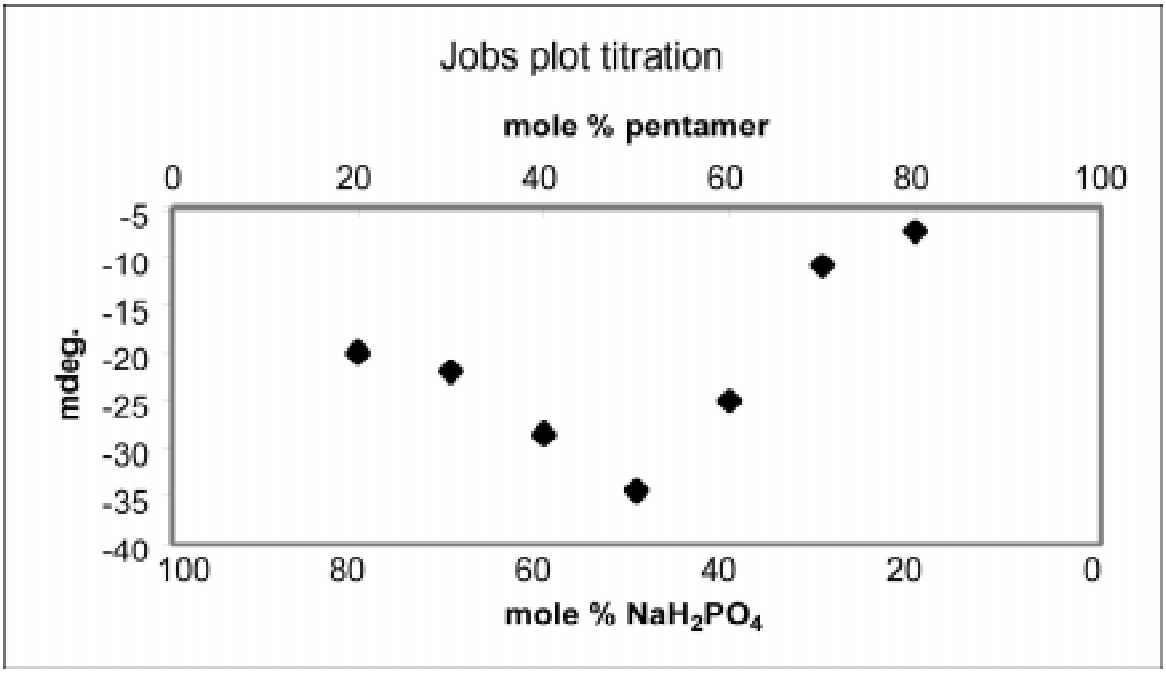

Figure 3.23 Jobs plot for amide pentamer (40).

Jobs plots are useful tools to determine the stoichiometry of binding for a particular binding curve. In the Job's plot the total concentration of the host and the guest are not varied, but the ratio between the two is. The ratio with the maximum observable is the stoichiometric ratio for the binding constant of interest. In the above Jobs plot, the maximum observable occurred at a ratio of 0.5/0.5 H_2PO_4/pentamer. Therefore, the binding constant of 0.02 mM corresponds to a 1: 1 binding stoichiometry of phosphate to pentamer.

Binding stoichiometry for pentamers appeared to vary between the two concentration regions in the two titration plots. The binding constant was similar for **45** and **40,** so there is no reason to believe there is variation between the two pentamers. Jobs plot data for pentamer **40** were collected at concentrations between 0.02 and 0.08 mM pentamer. Total concentration of the anion and the pentamer was kept constant at 0.1 mM. This range of concentrations puts the

titration after the endpoint of the first binding constant and before the midpoint of the second binding constant. This implies that the first binding constant was the predominant factor in the determination for the Jobs plot stoichiometry.

3.5.2 Experimental method for determination of the binding of C_2 symmetric hosts, 40 and 45, to phosphate by circular dichroism spectrometry.

Pentamer **40** (3.0 mg, 4.7 µmol) was dissolved in 50 mL of a 1/49 mixture of methanol/acetonitrile to give a 9.5×10^{-5} M solution of **40**. This was solution **A**. Another solution consisted of tetrabutylammonium dihydrogenphosphate (39.1 mg, 115 mmol) in 100 mL of a 1/49 mixture of methanol/acetonitrile, respectively, to give a 1.2×10^{-3} M solution of phosphate. This was solution **B**. The phosphate solution **B** was added to **A** in with an autopipette in µL increments. Solution was mixed in the CD cuvette. CD spectra for the solution in this cuvette were scanned 2x between 250 and 200 nm and recorded. Data was monitored along the peaks for both pentamers. Nitrogen was flowing though the spectrometer at a rate of 20-30 mL/minute. A standard error calculation of

Equation 3.1 $$s = \sqrt{\sum_{i=1}^{N} \frac{(x_i - \bar{x})^2}{N-1}}$$

was used to calculate the error in three measurements of CD data. Another titration was done but at different concentrations of phosphate so was not included in the calculation. Individual error calculations were done on each point in the other titration.

3.5.3 NMR titration of oligomers

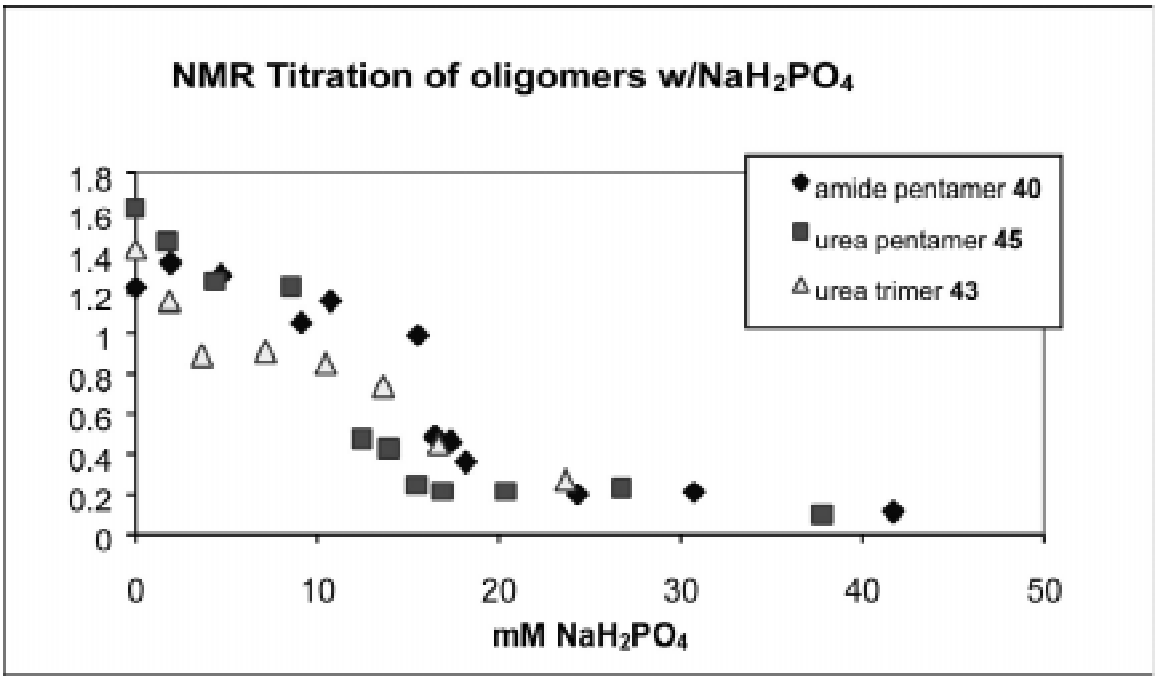

Figure 3.24 NMR titration of oligomers with NaH_2PO_4, monitoring the protic ammonium peak

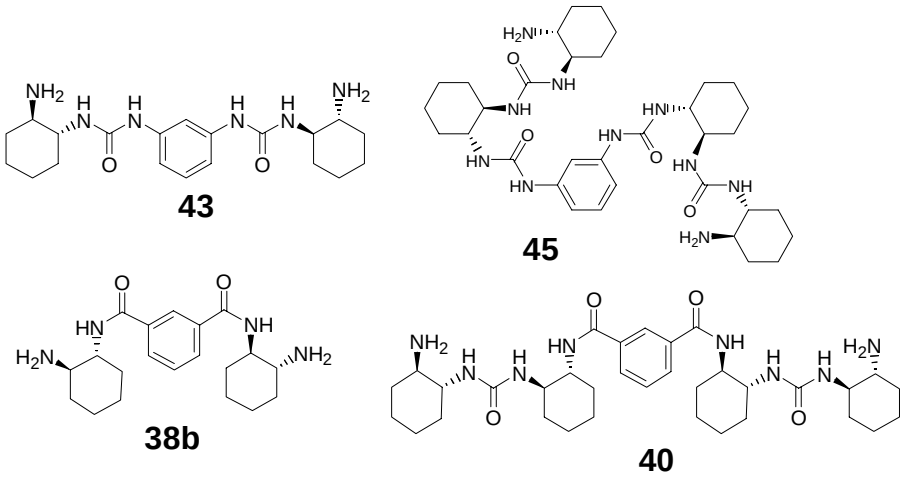

Figure 3.25 Oligomers tested for binding to phosphate by NMR methods

NMR titration of the oligomers verified the binding constants obtained through CD titration methods. Four oligomers (**38b**, **40**, **43**, and **45**) tested positive for binding to phosphate by NMR methods. The change in the NH peak

height and subsequent disappearance of that peak indicated a change in the chemical shift of the peak. The peak was not detected elsewhere, but evidence indicated that the peak should be found near the water peak and therefore undetectable. The NH peak of interest was the R-NH_3^+ peak for the oligomers. The peak was a single broad peak as a result of fast H^+ exchange that comes with the acidity of the ammonium protons. Amide and urea protons were slightly broadened doublets. Before the titration, the ammonium peak was approximately 1.5-fold the size of the peaks corresponding to the amide and urea protons. This was the expected ratio of protons derived from the structure.

Changes in solvent structure explained the up-field movement of the NH peak. The ammonium protons were solvated in solution by multiple water molecules. Upon binding to phosphate, the water structure was broken and fewer electron-withdrawing hydrogen bonds could form to the oligomer. A more electron-rich proton resulted from this change in solvent structure, and therefore the chemical shift of the proton moves up-field.

The three oligomers, included above in Figure 3.26, have one similar binding constant between 12 and 17 mM. The two urea oligomers **40**, and **43** share another binding constant at 3 mM. The data set for **38b** indicated a binding constant similar to those for the other three oligomers tested. Variability in the data made the results inconclusive.

The urea pentamer, **45**, and trimer, **43**, precipitated in solution, but concentrations remained high enough to determine peak integrations. The

internal reference for the NH proton integration was a phenyl CH proton. Therefore, the precipitation did not bias the results.

3.5.4 Experimental method for the determination of the binding of C_2 symmetric hosts, 40 and 45, to phosphate by ^{1}H NMR.

Two solutions were prepared for this determination. For solution **A**, 11.7 mg of free amine **40** was dissolved in 0.04 mL 1 N HCl, 0.49 mL H_20 and 1.1 mL methanol-d_4. This solution was 71% ^{1}H, 29% ^{2}H for the exchangeable protons, so amides should appear at 71% of the expected height for a solution in an aprotic NMR solvent. For solution **B**, 28.0 mg of NaH_2PO_4 was dissolved in 0.53 mL of H_2O and 1.1 mL methanol-d_4. The concentration of sodium dihydrogen phosphate was 146 mM. Solution **B** was added to solution **A** and the proton NMR spectra was acquired under presaturation conditions. The 90° pulse width was determined for the solvent mixture, and saturation delay time was optimized. Aliquots of solution **B** were added to the NMR sample and shaken. The NMR was shimmed after each change in phosphate molarity. Peaks at chemical shifts 7.8, and 8.3 were integrated and the ratio of the two peaks changed of changing concentrations of NaH_2PO_4. The ratio of the integrations of the two peaks was monitored over the course of the titration. Care was taken in order to make the integrations consistent over the course of the titration.

The above titration was repeated for pentamer **45**. The solvent conditions of solution **A** were matched for solution **C**, which contained 8.3 mg (12.4 µmol) of 45 in 0.028 mL of 1 M HCl, 0.340 mL of DI water and 0.742 mL of methanol-d_4

for a total of 1.11 mL solution of 11.2 mM concentration. Solution **B** was also used for this titration. Peaks at 6.0 and 7.8 were used to monitor the titration.

3.6 Synthetic procedures and data

3.6.1 (1R, 2R)-1-(*N*-*t*-butyloxycarbonylamino)-2-aminocyclohexane (31)[29]

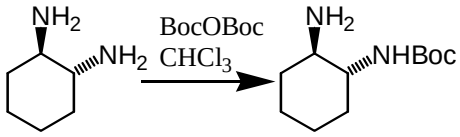

30 **31**

Figure 3.26 (1R, 2R)-1-(*N*-*t*-butyloxycarbonylamino)-2-aminocyclohexane (31)

(1R, 2R)-(+)-*trans*-1,2-diaminocyclcohexane, **30,** was resolved to optically pure (R,R) or (S,S) by a literature procedure.[30] The optically pure diamine is also available commercially, but expense prohibits buying this material in bulk. To a cooled solution of **30** (3.36 g, 29.5 mmol) in CH_2Cl_2 (100 mL) was added a solution of Boc anhydride (3.0 g, 13.7 mmol) in CH_2Cl_2 (100 mL) slowly over a period of 4h. The reaction mixture stirred overnight at RT. Water (25 mL) was added in order to dissolve the precipitate. After separation, the organic phase was concentrated under reduced pressure and the residue dissolved in ethyl acetate (25 mL). Water (25 mL) was added, the mixture was acidified to pH=5 with 2N HCl and the bis-protected diamine was extracted with ethyl acetate (2 x 20 mL). The aqueous phase was adjusted to pH=10 with NaOH and extracted it into ethyl acetate (3 x 20 mL). The combined organic layer was dried (Na_2SO_4) and evaporated under reduced pressure to yield **31** (1.87g, 8.72 mmol, 30%

based on the starting diamine). Spectral properties of the product were identical to those previously reported in the literature.[29]

3.6.2 Synthesis of N-(2-amino-cyclohexyl)-2,2,2-trifluoroacetamide (32)[31]

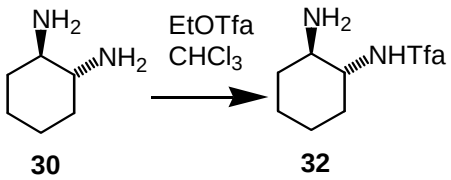

30 **32**

Figure 3.27 Synthesis of N-(2-amino-cyclohexyl)-2,2,2-trifluoroacetamide (32)

To a cooled solution of (1R, 2R)-(+)-*trans*-1,2-diaminocyclcohexane (2.0g, 17.5 mmol) in CH_2Cl_2 (100 mL) was added a solution of ethyl trifluoroacetate (0.94 mL, 7.97 mmol) in CH_2Cl_2 (50 mL) very slowly over a period of 4h. The reaction mixture stirred overnight at RT. Water (25 mL) was added and after separation, the organic phase was concentrated under reduced pressure and the residue dissolved in ethyl acetate (25 mL) and water (25 mL). The mixture was acidified to pH 5 with 2N HCl, and the bis-protected diamine was extracted with ethyl acetate (2 x 20 mL). The aqueous phase was adjusted to pH ~9 with Na_2CO_3 and extracted it into ethyl acetate (3 x 20 mL). The combined organic layer was dried (Na_2SO_4) and on evaporation a white solid **32** as a white solid (0.87g, 4.14 mmol, 24% based on the starting diamine).

3.6.3 Synthesis of dimer (33)

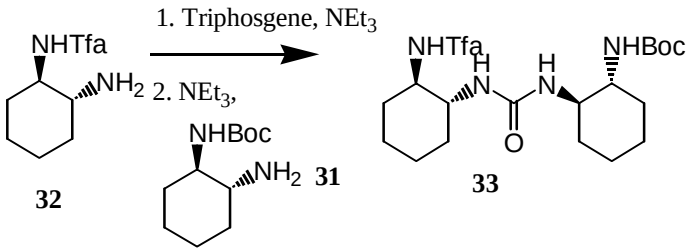

Figure 3.28. Dimer forming reaction

(1R)-1-triflouroacetamido-(2R)-2-aminocyclohexane (2.04 g, 9.71mmol) was dissolved in 40 mL $CHCl_3$, 6 mL acetonitrile, and 3 mL triethylamine. This solution was added to a solution of triphosgene (1.05 g, 3.53 mmol) in 14 mL $CHCl_3$ at a rate of 20 mL/h for the first two hours and 30 mL/h for the second hour. During the addition the reaction was kept at a temperature of 15 to 20 ˚C by the addition of small amounts of ice into a large ice bath. After addition was complete the reaction was stirred for an additional 20 min The (1R)-1-butoxycarbamate-(2R)-2-aminocyclohexane (2.08 g, 9.70 mmol) was dissolved in 12 mL $CHCl_3$ and 2.2 mL triethylamine. This solution was added quickly in one portion to the reaction to the previous reaction. The reaction was allowed to stir overnight, and worked up with 2.0 mL methanol. The remaining $CHCl_3$ was removed with a stream of nitrogen. Trifluoroacetamide **32** and butoxycarbamate **31** protected diamines were removed by 3 extractions with a 10/15 solution of saturated ammonium chloride and distilled water. Then basified with aqueous sodium carbonate. The resulting organic layer was purified by crystallization from ethyl acetate and methanol. The resulting crystals were thin needles that partially

melted and turned brown at 241-242 °C. Subsequent crystallizations from the same mother liquor also gave crystals of good purity.

^{1}H-NMR (400 MHz; $CDCl_3$) δ 8.32 (1H, d), 5.24 (1H, d), 4.72 (1H, d), 4.5 (1H, b) 3.62 (1H, m), 3.42 (1H, m), 3.35 (1H, m), 3.26 (1H, m), 2.22 (1H, d), 1.95 (2H, t), 1.82 (1H, d), 1.71 (8H, m), 1.43(9H, s) 1.1-1.4 (8H, m). ^{13}C-NMR (100.4 MHz; $CDCl_3$ + 3 drops CD_3OD) δ 159.3, 157.6 (q, J=37.4 Hz), 156.9, 115.9 (q, J=287 Hz), 79.3, 56.5, 54.3, 54.1, 51.8, 32.9, 32.6, 32,3, 31.1, 28.2, 24.9, 24.8, 24.7, 24.2. MALDI (MNa^+) 473 (M-Boc+2H) 351. *Anal. Calcd.* For $C_{20}H_{33}F_3N_4O_4$ C, 53.32; H, 7.38; N, 12.44 found C, 53.15, H, 7.27, N, 12.32. IR: 3320.7(s), 3276.1(m), 2940.6(s), 2856.4(m), 1700(s), 1685.1(m), 1639.7(s), 1450.3(w), 1367.2(w), 1322.6(m), 1276.2(w), 1253.1(w), 1181.6(s)

3.6.4 Synthesis of amide (37)

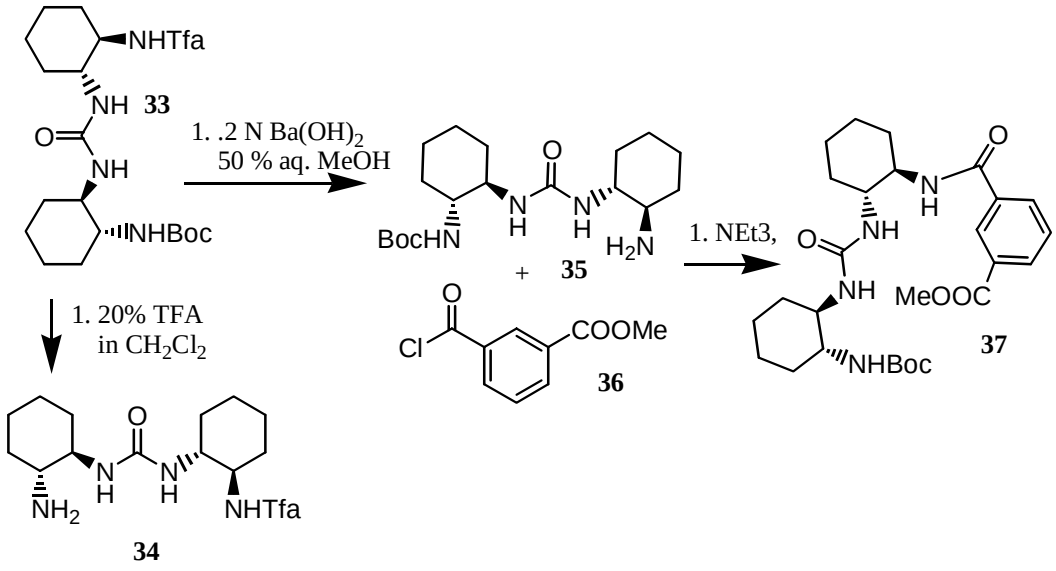

Figure 3.29 Synthesis a differentially protected oligomer.

To make the mono-deprotected dimer **35** the di-protected dimer **33** (0.6946 g, 1.542 mmol) was refluxed for 2 h in 10 mL of 1 M LiOMe in MeOH

with 10% distilled water, and then evaporated under vacuum. The residue was then dissolved with heating in EtOAc and distilled water. The aqueous layer was removed and the organic was acidified with saturated NH_4Cl. The organic layer was extracted 6X with saturated NH_4Cl. The combined aqueous layers were basified with Na_2CO_3 (aq.) to pH 10. Extraction was done with EtOAc 3X. **35** was obtained clean and was used as obtained in the next step (365.5 mg, 1.031 mmol, 67%).

Methyl,hydrogen isophthalate (50.0 mg, 0.278 mmol), prepared from the dimethyl ester by a literature method[32], was stirred in 5 mL distilled $CHCl_3$ and 80 µL of oxalylchloride. N_2 was allowed to flow over the reaction. Upon addition of two drops of DMF, gas evolved from the reaction, and within 10 min the reaction was complete. This reaction was evaporated under vacuum and restored to normal pressure under N_2.

To the acid chloride a solution of amine **35** (92.1 mg, 0.260 mmol), NEt_3 (280 µL) was added drop wise at 0˚C. The reaction was stirred for 2 h and diluted with 5 mL $CHCl_3$, and worked up with 2.5 mL portions of $NaHCO_3$, and distilled water. Product was crystallized from MeOH, EtOAc, and hexane. Crude material was dissolved in MeOH, diluted with EtOAc, and precipitated with hexane, gave 54.7 mg (0.106 mmol, 41%) of clean amide **37**.

^{1}H-NMR (400 MHz; $CDCl_3$) δ 8.48 (1H, dt), 8.15 (1H, dt), 8.03 (1H, dt), 7.56 (1H, td), 3.70 (1H, m), 3.60 (1H, dt), 3.40 (1H, m), 3.26 (1H, m), 2.10 (1H, b), 1.95 (2H, bm), 1.82 (2H, b), 1.65 (1H, b), 1.5 (2H, bm) 1.4 (12H, bm), 0.9-1.4 (4H, m). ^{13}C-NMR (100.4 MHz; drops CD_3OD small amount of $CDCl_3$) δ 171.6,

170.5, 163.9, 161.2, 139.1, 136.1, 135.7, 134.5, 132.6, 132.3, 82.8, 59.8, 58.8, 57.4, 56.8, 55.8, 52.1, 4.12, 36.8, 36.6, 35.9, 31.8, 29.1, 28.7 MALDI (MNa^+) 473 (M-Boc+2H) 351*Anal. Calcd.* For $C_{27}H_{40}N_4O_4$ C, 62.77; H, 7.80; N, 10.84 found C, 62.51, H, 7.77, N, 10.62.

3.6.5 Synthesis of trimer diamide (38):

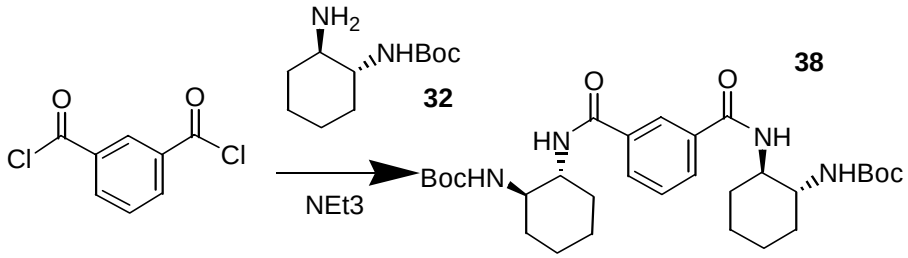

Figure 3.30 Synthesis of trimer diamide 38.

Isophthalic acid (87.9 mg, 0.529 mmol) was stirred in 5 mL methylene chloride. Oxalyl chloride (130 µL, 1.72 mmol) was added under nitrogen pressure. Three drops of dry DMF caused the reaction to bubble vigorously, and the isophthalic acid to dissolve. After 1 h the reaction was evaporated under vacuum and dissolved in 5 mL methylene chloride again. **32** (288.9 mg, 1.348 mmol) was added under nitrogen, and stirred overnight. The reaction stirred overnight at RT. Reaction was worked up with 3 mL brine and 10 mL EtOAc, then 1 N HCl until the aqueous extract was acidic. The organic layer was dried with Na_2SO_4 (anhydrous) and was crystallized with ethyl acetate and hexane.

^{1}H-NMR (400 MHz; CD_3OD) δ 8.23 (1H, s), 8.18 (2H, d), 7.87 (2H, d), 7.46 (1H, t), 6.65 (2H, d), 3.70 (2H, m), 3.38 (2H, m), 1.80 (4H, t), 1.67 (4H, m), 1.2-1.4 (5H, m), 1.22 (18H, s) ^{13}C-NMR (100.4 MHz; $DMSO_{d6}$) δ 169.1, 158.8, 136.2, 131.5, 129.5, 127.7, 80.2, 56.2, 55.1, 33.7, 33.4, 28.9, 26.4, 26.1 *Anal. Calcd.* for

$C_{30}H_{46}N_4O_6$ C, 64.49; H, 8.30; N, 10.03; O, 17.18 found C, 64.47; H, 8.45; N, 9.91 IR: 3335.5(s), 3307.6(s), 2970.1(m), 2935.7(s), 2856.9(m), 1685.2(s), 1647.5(s), 1582.4(w), 1530.2(s), 1449.9(w), 1365.5(m), 1322.9(m), 1283.1(m), 1246.2(w), 1170.4(s), 1016.6(m)

3.6.6 Synthesis of pentamer diamide (39)

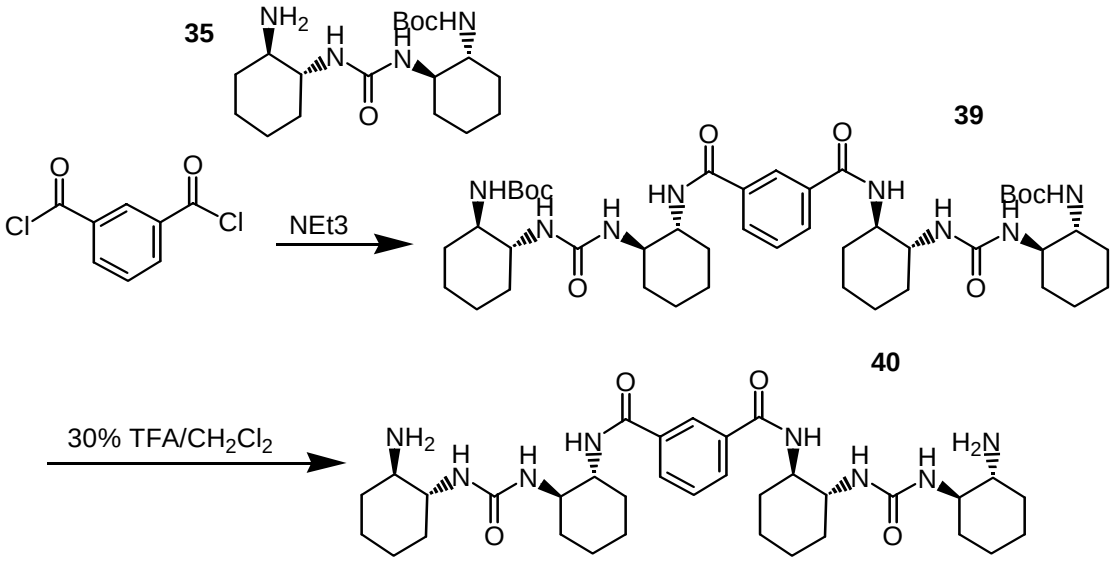

Figure 3.31 Synthesis of pentamer diamide 39, 40.

Isophthalic acid (163.1 mg, 0.9818 mmol) was stirred in 5 mL methylene chloride. Oxalyl chloride (600 µL, 7.9 mmol) was added under nitrogen pressure. Four drops of dry DMF caused the reaction to bubble vigorously, and the isophthalic acid to dissolve. After 1 h the reaction was evaporated under vacuum and dissolved in 5 mL methylene chloride again. **35** (494.2 mg, 1.394 mmol) was dissolved with 10 mL $CHCl_3$ and 500 µL NEt_3 and added under nitrogen to the isophthaloyl chloride, and stirred overnight. The reaction stirring overnight proceded under RT conditions. Reaction was worked up with 3 mL brine and 10 mL EtOAc, then 1 N HCl until the aqueous extract was acidic. The organic layer

was dried with Na_2SO_4 (anhydrous) and was crystallized with ethyl acetate and hexane. The crystals of **39** could be deprotected by submission to a solution of 30% TFA in methylene chloride giving the free amine **40** upon workup.

^{1}H-NMR (400 MHz; CD_3OD) δ 8.12 (1H, s), 7.84 (2H, d), 7.58 (1H, t), 3.98 (2H, m), 3.84 (2H, m), 1.98 (5H, dt), 1.81 (4H, m), 1.49 (4H, m), 1.40 (4H, b), 1.28 (1H, m), 1.22 (2H, b); EA: *Anal. Calcd.* For $C_{44}H_{70}N_8O_8$ C, 62.98; H, 8.41; N, 13.35; O, 15.25, found C, 62.63; H, 8.48; N, 13.07; IR (KBr Pellet): 3332.6(s), 2932.9(s), 2856.1(m), 2605.1 (w), 2498.1(w), 1686.4(s), 1531.5(s), 1449.5(w), 1366.2(w), 1319.3(m), 1280.1(w), 1174.0(m), 1040.6(w) ^{13}C-NMR (50 MHz, 750 µL $CDCl_3$, 100 µL CD_3OD) 167.7, 159.8, 157.0, 134.7, 130.4, 128.7, 79.4, 77.5, 55.5, 55.1, 53.6, 53.3, 33.1, 33.0, 32.9, 32.3, 28.4, 25.2, 24.9, 18.9

3.6.7 Synthesis of trimer (43)

To a solution of 1,3-phenylene diisocyanate (0.1g, 0.63mmol) in CH_2Cl_2 (2 mL) was added the **31** or **32** (0.268g, 1.25 mmol) stirred for 10 min A white gel was formed was washed with the ether. A white solid **42a / 42b** was obtained in quantitative yield.

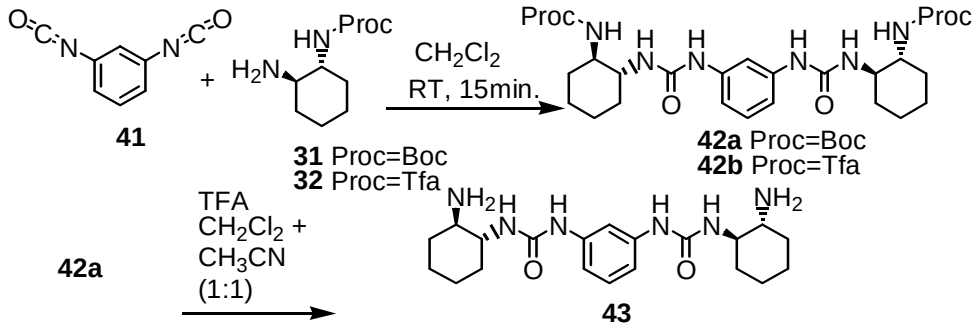

Figure 3.32 Synthesis of trimer 43

1-((1R,2R)-1-N-*t*-butyloxycarbonylamino-2-cyclohexyl)-3-[3-(3-(1R, 2R)-1-N-*t*-butyloxycarbonylamino-2-cyclohexylureido) phenyl] urea [**42a**]:

^{1}H NMR (400MHz, $CDCl_3$ + CD_3OD at 40^{o}C): 7.23 (t, 1H, J=2.0 Hz), 7.18(t, 1H, J=8.0 Hz), 7.06(dd, 2H, J=8.0, 2.0 Hz), 3.44(m, 2H), 3.20 (m, 2H), 2.0 (m, 4H), 1.78 (m, 4H), 1.37 (s, 18H), 1.15 -1.34 (m, 8H) ^{13}C NMR (100MHz, $CDCl_3$ + CD_3OD at 40^{o}C): 157.5, 157.0, 139.8, 129.0, 112.5, 108.8, 78.5, 54.3, 53.0, 33.3, 26.8, 24.2.

1-((1R,2R)-1-N-(2-amino-cyclohexyl)-2,2,2-trifluoroacetamide)-3-[3-(3-(1R, 2R)-1-N-*t*-butyloxycarbonylamino-2-cyclohexylureido)phenyl] urea [**42b**]:

^{1}H NMR (400MHz, $DMSO_{d6}$): 9.18 (d, 2H), 8.18 (bs, 2H), 7.15 (t, 1H, J=2.01Hz), 6.9-7.2 (m, 3H), 5.95 (d, 2H), 3.55-6.20 (m, 4H), 1.6-2.00 (m, 8H), 1.2-1.7 (m, 8H). ^{13}C NMR (50MHz, $DMSO_{d6}$): 156.4, 155.7, 155.2, 140.7, 128.8, 118.9, 110.8, 107.0, 53.8, 51.6, 32.6, 31.0, 24.5, 24.2

1-((1R,2R)-1-amino-2-cyclohexyl)-3-[3-(3-(1R, 2R)-1-N-amino-2-cyclohexyl ureido) phenyl] urea [42]: To a solution of **42a** (87.0 mg, 0.15 mmol) in chloroform: acetonitrile (3.0 mL, 1: 1) was added a solution of trifluoroacetic acid (25 µl, 0.33 mmol) at RT and stirred for 2h. Triethylamine (46 µl, 0.33 mmol) was added to the reaction mixture to neutralize the TFA. It was then washed with the brine. The organic phase was dried (Na_2SO_4) and on evaporation a white solid was obtained (.12 mmol, 47mg, 79%).

The compound **43** can also obtained by deprotecting **42b** by its reaction with the $Ba(OH)_2$ in quantitative yield.

^{1}H NMR (400MHz, D_2O + DCl): 7.29 (1H, t, J=2.4 Hz), 7.23 (t, 1H, J=8.4 Hz), 6.96 (dd, 2H, J=8.4, 2.4 Hz), 3.56-366 (m, 2H), 2.95-3.08 (m, 2H), 1.68-2.08 (m, 8H), 1.20-1.50 (m, 4H) ^{13}C NMR (50 MHz, CD_3OD): 158.2, 141.2, 130.3, 114.4, 112.4, 56.7, 56.3, 34.9, 33.8, 26.6, 25.8.

3.6.8 Synthesis of pentamer (44)

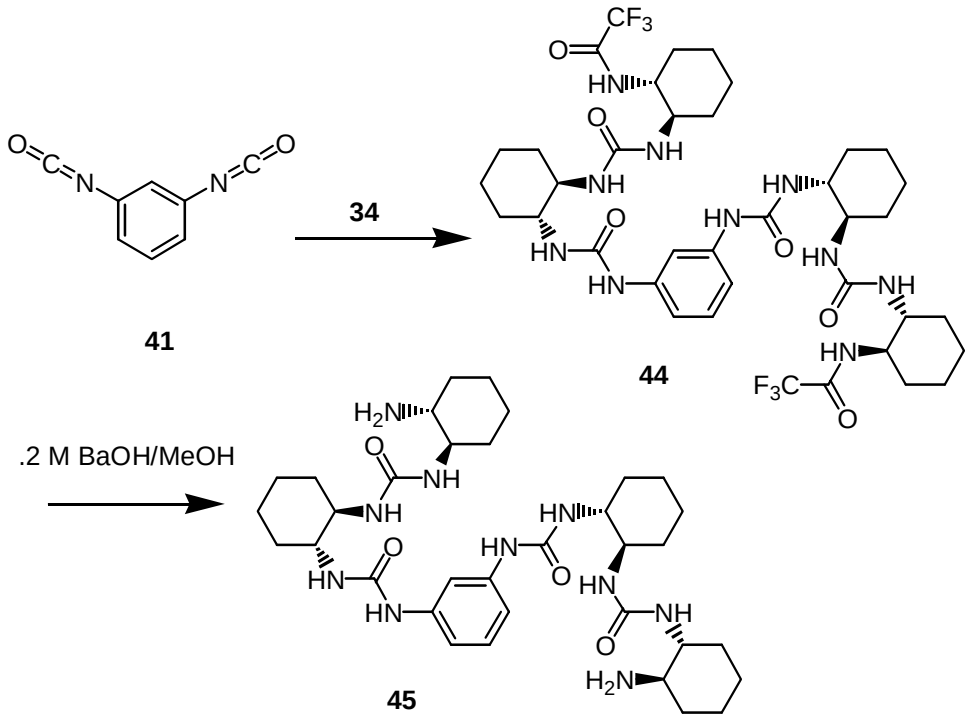

Figure 3.33 Synthesis of Pentamer 44, 45

To the solution of dimer (**34**) in chloroform was added the 1,3-phenylene diisocyanate (**41)** in one lot. It was stirred for 10 min at RT. The solvent was removed and the residual thick gel was triturated with the dry ether to give the white solid in quantitative yield.

^{1}H NMR (400 MHz, $DMSO_{d6}$): 9.29 (d, 2H, J=7.2 Hz), 8.14 (bs, 2H), 7.35 (bs, 1H), 6.94-7.30 (m, 3H), 5.8-6.00 (m, 5.56), 3.20-3.45 (m, 8H), 1.75-1.96 (m 8H), 1.56-1.68 (m, 8H), 1.10-1.40 (m, 16H). ^{13}C NMR (50MHz, $DMSO_{d6}$): 158.5,

156.0, 155.6, 154.9, 140.8, 128.6, 110.4, 106.7, 55.2, 52.7, 52.3, 51.5, 32.2, 30.7, 24.2, 24.0. IR (KBr Pellet) cm^{-1}: 3320.9(s), 2936.3(s), 2859.5(w), 1702.4(m), 1649.6(m), 1562.3(s), 1492.9(w), 1317.8(w), 1317.8(w), 1206.0(s)

3.7 Addendum

3.7.1 Future work

Work on this project will continue with the synthesis of more oligomers of **29**. Solution phase synthesis of these oligomers is being pursued using p-nitrophenylchloroformate as an activating agent. The p-nitrophenylcarbamate intermediates are more stable than the isocyanate intermediate produced through the phosgene equivalents triphosgene and carbonyldiimidazole. If the stability of the p-nitrophenylcarbamate intermediates is high enough then they will be purified, and reacted pure with another free amine. Under these conditions purity of the products should be high.

Oligomers will be studied under cosolvent conditions to determine if the materials will form helical structures. If it can be shown that the oligomers do form a helix, oligomers of varying length will be analyzed for helix formation. Coopertivity in the formation of the helix can be established through establishing a pattern of increasing ability to form a helix in solution.

3.7.2 Membrane sensors

Berrocal *et al.* tested the *t*-Boc-protected pentamer **39** for use as an ionophore in a liquid membrane sensor system. In this paradigm an ionophore acts as an embedded binding site that changes the electric potential across a membrane in the presence of the appropriate analyte above threshold

concentration. A first evaluation of these compounds as ionophores in anion-selective electrodes, indicated some selectivity for sulfate among the tested hydrophilic anions. However, the response was much larger to more hydrophobic anions such as salicylate and thiocyanate. Hopefully, with a longer oligourea a more selective ionophore can be found.

3.8 Conclusion

Analysis of the oligomer **29** was encouraging for further development of the project. Modeling studies indicated the preference for β-structure from the RC plots but did not rule out the possibility of α-helix formation. A structure that can mimic the 2-state structure of proteins will be exciting to investigate, and may uncover what characteristics are unique to proteins. The preference for β-structure was surprising. Comparisons with the structurally related cyclohexane β-amino acid led to the assumption that the materials would be helical. However, the presence of the β-state does not indicate that these materials will not bind to oxoanions as planed. The helix was the second largest energetic local minimum. In addition, oxoanions present multiple hydrogen bond acceptors and the modeled materials were stable and flexible in a Monte Carlo simulation in chloroform. Hopefully, cosolvents like TFE and HFIP that induce helicity in peptides will induce similar conformational changes in oligoureas.

Binding was indicated by the NMR and CD analyses. Two separate binding constants were found in both the NMR and the CD analysis. Additional measurements of the binding with a less acidic anion are required to discount the possibility of acid base reactions influencing the results, and decrease error

measurements that might cast doubt upon the binding determination. Modeling studies suggest a mechanism for the increased CD absorbance upon formation of the 1: 1 complex of phosphate and the amide pentamer versus the complex of phosphate and the urea pentamer. We have found a mechanism of creating a foldamer that should exploit the additive powers of multiple weak hydrogen bonds, by creating a foldamer that could do what most *de novo* binding molecules do not do. Strongly bind to an oxoanion.

We synthesized two derivatives of 2-aminobenzimidazole that have an intramolecular hydrogen bond in a conjugated CN system. The synthesis methodology was simple if not high yielding. Products required only 1 or 2 steps to get from starting material to product. The compounds were not complex for either material, but showed interesting dynamics.

The hydrogen bonds that were studied showed a complexity that defies the common perception that the intramolecular hydrogen bond is a simple tether linking the hydrogen bond donor and acceptor. Weak hydrogen bonds were found in guanidinobenzimidazole, that had an effect on the bond order of a conjugated system. In **1d,e** another conjugated system was found with similar dynamics, but was stericly inhibited from forming an intramolecular hydrogen bond. The carboxamidine NH hydrogen atom was postulated to have very slow proton exchange due to the higher pKa of the carboxamidine moiety. This presented the opportunity to investigate hydrogen bonds in general.

Two different alkylation patterns were analyzed for differences and similarities in the dynamic rate of exchange of alkyl and benzo protons in an

effort to determine the mechanism and effect of the intramolecular hydrogen bond for this conjugated system. A system was made for which the guanidine nitrogen atoms are either primary or secondary to limit the number of mechanisms that explain an apparent change in the bond order of these guanidinobenzimidazole derivatives.

These studies provided a realistic vision of what to expect of intramolecular hydrogen bonds in the control of *de novo* designed conformations. It was found that, the six-centered intramolecular hydrogen bonds studied here were not necessarily stable enough to be used for the design of compounds needing conformational stability. In **1d,e** the sigma bond at N1-C11 has hindered rotation from the steric barrier present in a totally planar conformation. Molecules **1b,c** had no hindered rotation at C2-N10 except for the intramolecular hydrogen bond. It appeared that the more planar molecule had an increased effect upon the bond order of the conjugated system.

3.9 References

(1) Eliel, E. L.; Wilen, S. H. *Chiroptical Properties*; Eliel, E. L. and Wilen, S. H., Ed.; John Wiley & Sons, Inc.: New York, 1994, pp 991-1118.

(2) Greenfield, N.; Fasman, G. D. *Biochemistry* **1969**, *8*, 4108-4116.

(3) Gellman, S. H. *Acc. Chem. Res.* **1998**, *31*, 173-180.

(4) Appella, D. H.; Christianson, L. A.; Karle, I. L.; Powell, D. R.; Gellman, S. H. *J. Am. Chem. Soc.* **1996**, *118*, 13071-13072.

(5) Hamuro, Y.; Geib, S. J.; Hamilton, A. D. *J. Am. Chem. Soc.* **1996**, *118*, 7529-7541.

(6) Tesmer, J. J. G.; Klem, T. J.; Deras, M. L.; Jo, D. V.; Smith, J. L. *Nature Structural Biology* **1996**, *3*, 74-87.

(7) Ramachandran, G. N.; Sasisekharan, V. *J. Mol. Biol.* **1963**, *7*, 95-99.

(8) Murthy, V. L.; Srinivasan, R.; E., D. D.; Rose, G. D. *J. Mol. Biol.* **1999**, *291*, 313-327.

(9) Seebach, D.; Jacobi, A.; Rueping, M.; Gademann, K.; Ernst, M.; Jaun, B. *Helv. Chim. Acta.* **2000**, *83*, 2115-2140.

(10) Porter, E. A.; Wang, X.; Lee, H. S.; Weisblum, B.; Gellman, S. H. *Nature* **2000**, *404*, 298-298.

(11) Werder, M.; Hauser, H.; Abele, S.; Seebach, D. *Helv. Chim. Acta.* **1999**, *82*, 1774-1783.

(12) Gin, M. S.; Moore, J. S. *Org. Lett.* **2000**, *2*, 135-138.

(13) Prince, R. B.; Barnes, S. A.; Moore, J. S. *J. Am. Chem. Soc.* **2000**, *122*, 2758-2762.

(14) Prince, R. B.; Brunsveld, L.; Meijer, E. W.; Moore, J. S. *Angew. Chem., Int. Ed. Engl.* **2000**, *39*, 228-230.

(15) Wooley, K. L.; Moore, J. S.; Wu, C.; Yang, Y. *Proc. Natl. Acad. Sci.* **2000**, *97*, 11147-11148.

(16) Baudlier, J. *J. Org. Chem.* **1998**, *63*, 5750-5761.

(17) Schenck, H. L.; Gellman, S. H. *J. Am. Chem. Soc.* **1998**, *120*, 4869-4870.

(18) Saunders, M.; Houk, K. N.; Wu, Y.-D.; Still, W. C.; Lipton, M.; Chang, G.; Guida, W. C. *J. Am. Chem. Soc.* **1990**, *112*, 1419-1427.

(19) Metropolis, N. R., A. W.; Rosenbluth, M. N.; Teller, A. H.; Teller, E. *J. Chem. Phys.* **1953**, *21*, 1087.

(20) Howard, A. E.; Kollman, P. A. *J. Med. Chem.* **1988**, *31*, 1669-1675.

(21) Still, W. C.; Tempczyk, A.; Hawley, R. C.; Hendrickson, T. *J. Am. Chem. Soc.* **1990**, *112*, 6127-6129.

(22) Amidon, G. L.; Yalkowsky, S. H.; Anik, S. T.; Valvani, S. C. *J. Phys. Chem.* **1975**, *72*, 2239.

(23) Hermann, R. B. *J. Phys. Chem.* **1972**, *76*, 2239.

(24) Mohamadi, F.; Richards, N. G.; Guida, W. C.; Liskamp, R.; Lipton, M.; Caufield, C.; Chang, G.; Hendrickson, T.; Still, W. C. *J. Comput. Chem.* **1990**, *11*, 440.

(25) Pappu, R. V.; Srinivasan, R.; Rose, G. D. *Proc. Natl. Acad. Sci. U.S.A.* **2000**, *97*, 12565-12570.

(26) Walgers, R.; Lee, T. C.; Cammers-Goodwin, A. *J. Am. Chem. Soc.* **1998**, *120*, 5073-5079.

(27) Sindkhedkar, M. D.; Mulla, H. R.; Cammers-Goodwin, A. *J. Am. Chem. Soc.* **2000**, *122*.

(28) Mulla, H. R.; Cammers-Goodwin, A. *J. Am. Chem. Soc.* **2000**, *122*, 738-739.

(29) Lagriffoule, P.; Wittung, P.; Eriksson, M.; Jensen, K. K.; Norden, B.; Buchardt, O.; Nielsen, P. E. *Chem. Eur. J.* **1997**, *3*, 912-919.

(30) Larrow, J. F.; Jacobsen, E. N. *J. Org. Chem.* **1994**, *59*, 1939--1942.

(31) Xu, D.; Prasad, K.; Repic, O.; Blacklock, T. J. *Tetrahedron Lett.* **1995**, *36*, 7357-7360.

(32) Murakami, Y.; Hara, H.; Okada, T.; Hashizume, H.; Kii, M.; Ishihara, Y.; Ishikawa, M.; Shimamura, M.; Mihara, S.-i.; Kato, G.; Hanasaki, K.; Hagishita, S.; Fujimoto, M. *J. Med. Chem.* **1999**, *42*, 2621-2632.

Appendices

A.1 Crystal data and structure refinement for 1c, 1d, 33.

Compound	1c	1d	33
Empirical formula	$C_{14}H_{21}N_5$	$C_{14}H_{21}N_5$	$C_{20}H_{33}N_4O_4F_3$
Formula weight	259.36	259.35	450.5
Temperature (K)	173(1)	173(1)	145(1)
Wavelength (Å)	0.71073	0.71073	0.71073
Crystal system, space group	Monoclinic, P 21/n	Orthorhombic, P na21	Triclinic, P 1
Unit cell dimensions			
a(Å)	9.6450(10)	18.066(4)	4.9590(10)
b(Å)	7.7760(10)	10.234(2)	11.218(2)
c(Å)	18.874(3)	22.275(5)	11.410(2)
$\alpha(^o)$	90	90	109.04(2)
$\beta(^o)$	95.559(10)	90	91.77(2)
$\gamma(^o)$	90	90	101.38(2)
$V(Å^3)$	1408.9(3)	4118.4(14)	585.09(19)
Z, Calculated density (Mg/m^3)	4, 1.223	8, 1.121	1, 1.279
Absorption coefficient (mm^{-1})	0.077	0.075	0.105
F(000)	560	1504	240
Crystal size (mm)	0.28 x 0.24 x 0.12	0.44 x 0.30 x 0.30	0.60 x 0.10 x 0.03
θ range for data collection	2.29 to 25.00	1.83 to 22.50	1.90 to 25.00
Limiting indices	-11≤h≤11, -9≤k≤9, -22≤l≤22	-19≤h≤19, -11≤k≤11, -23≤l≤23	-5≤h≤5, -13≤k≤13, -13≤l≤13
Reflections collected / unique	9104 / 2479 [R(int) = 0.0548]	19888 / 5371 [R(int) = 0.0762]	4031 / 4031 [R(int) = 0.0420]
Completeness	to θ = 25.00, 99.9%	to θ = 22.50, 99.9%	to θ = 25.00, 100%
Absorption correction	None	None	None
Refinement method	Full-matrix least-squares on F^2	Full-matrix least-squares on F^2	Full-matrix least-squares on F^2

Data / restraints / parameters	2479 / 48 / 177	5371 / 417 / 451	4031 / 267 / 281
Goodness-of-fit on F^2	1.092	1.116	1.076
Final R indices [I>2sigma(I)]	R1 = 0.0676, wR2 = 0.1381	R1 = 0.0737, wR2 = 0.1638	R1 = 0.0535, wR2 = 0.0865
R indices (all data)	R1 = 0.0870, wR2 = 0.1466	R1 = 0.0908, wR2 = 0.1728	R1 = 0.0729, wR2 = 0.0918
Absolute structure parameter	NA	0	-0.9(7) [meaningless !]
Extinction coefficient	0.007(3)	NA	0.027(3)
Largest diff. peak and hole (e $Å^{-3}$)	0.455 and -0.248	0.228 and -0.239	0.197 and -0.151

A.2 Crystal data and structure refinement for 1g.

Compound	
Empirical formula	C14 H21 N5
Formula weight	259.36
Temperature (K)	173(1) K
Wavelength (Å)	0.71073 A
Crystal system, space group	"Monoclinic, P 21/c"
Unit cell dimensions	
a(Å)	8.0810(3)
b(Å)	21.1140(7)
c(Å)	9.6270(3)
$\alpha(^{o})$	90 deg.
$\beta(^{o})$	114.2021(14)
$\gamma(^{o})$	90 deg.
$V(Å^3)$	1498.21(9)
Z, Calculated density (Mg/m^3)	4, 1.150
Absorption coefficient (mm^{-1})	0.073
F(000)	560
Crystal size (mm)	0.26 x 0.25 x 0.20
θ range for data collection	1.93 to 27.49 deg.

Limiting indices	-10<=h<=10 -27<=k<=26 -12<=l<=12
Reflections collected / unique	11517 / 3457
Completeness	100.00%
Absorption correction	Semi-empirical from equivalents
Refinement method	Full-matrix least- squares on F^2
Data / restraints / parameters	3457 / 0 / 177
Goodness-of-fit on F^2	1.032
Final R indices [I>2sigma(I)]	R1 = 0.0497 wR2 = 0.1146
R indices (all data)	R1 = 0.0784 wR2 = 0.1262
Absolute structure parameter	NA
Extinction coefficient	0.014(2)
Largest diff. peak and hole (e $Å^{-3}$)	.294 and -.284

A.3 Crystal coordinates (X 10^4) for 33.

	x	y	z	U(eq)
C(1)	6083(5)	1003(2)	6220(2)	26(1)
C(2)	4826(5)	508(2)	7231(2)	28(1)
C(3)	4542(6)	-942(2)	6860(2)	40(1)
C(4)	2849(6)	-1652(2)	5608(2)	45(1)
C(5)	4000(6)	-1143(3)	4605(2)	41(1)
C(6)	4283(5)	308(2)	4979(2)	35(1)
C(1')	7568(5)	2966(2)	12615(2)	28(1)
C(2')	6493(5)	3413(2)	11588(2)	28(1)
C(3')	7482(5)	4869(2)	11938(2)	37(1)
C(4')	6653(6)	5595(3)	13207(3)	42(1)
C(5')	7653(6)	5123(3)	14206(2)	40(1)
C(6')	6667(5)	3664(2)	13863(2)	35(1)
N(7)	6426(4)	1207(2)	8435(2)	30(1)
C(8)	5356(5)	1950(2)	9419(2)	26(1)
N(9)	7276(4)	2717(2)	10384(2)	31(1)
O(10)	2869(3)	1942(2)	9439(1)	31(1)
N(11)	6472(4)	2389(2)	6587(2)	28(1)
C(12)	8969(5)	3176(2)	7008(2)	27(1)
O(13)	8782(3)	4408(2)	7527(2)	41(1)
C(14)	11308(5)	5435(2)	8068(3)	37(1)
O(15)	11122(3)	2807(2)	6907(2)	40(1)
C(16)	12772(6)	5173(3)	9109(3)	47(1)
C(17)	10166(6)	6639(3)	8576(4)	79(1)
C(18)	13079(5)	5544(3)	7040(3)	43(1)
N(19)	6677(4)	1563(2)	12253(2)	31(1)
C(20)	8438(5)	796(2)	12030(2)	34(1)
C(21)	7193(6)	-647(3)	11530(3)	43(1)
O(22)	10943(4)	1153(2)	12165(2)	60(1)
F(23)	8365(3)	-1267(2)	12134(2)	82(1)
F(24)	4500(3)	-953(2)	11609(2)	55(1)
F(25)	7582(4)	-1130(2)	10339(2)	84(1)

A.4 Crystal coordinates (X 10^4) for (1c)

	x	y	z	U(eq)
N(1)	469(2)	-509(2)	8024(1)	27(1)
C(2)	434(2)	571(3)	7472(1)	27(1)
N(3)	1671(2)	1437(3)	7459(1)	30(1)
C(4)	3929(3)	1303(3)	8265(1)	36(1)
C(5)	4522(3)	448(3)	8862(1)	38(1)
C(6)	3777(3)	-766(3)	9213(1)	36(1)
C(7)	2408(3)	-1158(3)	8982(1)	30(1)
C(8)	1794(2)	-322(3)	8380(1)	25(1)
C(9)	2565(2)	893(3)	8030(1)	26(1)
N(10)	-580(2)	899(3)	6943(1)	31(1)
C(11)	-1773(3)	50(3)	6902(1)	29(1)
N(12)	-2709(2)	354(3)	6325(1)	34(1)
N(13)	-2101(2)	-1072(3)	7404(1)	36(1)
C(14)	-2313(3)	1555(4)	5759(1)	41(1)
C(15)	-3965(3)	-684(3)	6151(1)	36(1)
C(16)	-3677(3)	-2583(3)	6033(1)	44(1)
C(17)	-5099(3)	-340(4)	6627(2)	49(1)
C(18)	-1879(3)	571(4)	5121(2)	61(1)
C(19)	-3401(3)	2869(4)	5561(2)	52(1)

A.5 Crystal coordinates (X 10^4) for (1d)

	x	y	z	U(eq)
N(1A)	2078(2)	1736(4)	263(2)	43(1)
C(2A)	2475(3)	2124(5)	761(2)	43(1)
N(3A)	3183(2)	2354(4)	638(2)	42(1)
C(4A)	3849(3)	2240(5)	-363(2)	47(1)
C(5A)	3757(3)	1953(5)	-965(2)	54(1)
C(6A)	3071(3)	1566(6)	-1188(3)	62(2)
C(7A)	2454(3)	1461(6)	-814(2)	53(1)
C(8A)	2559(3)	1732(5)	-220(2)	40(1)
C(9A)	3239(3)	2131(4)	17(2)	38(1)
N(10A)	2172(2)	2227(5)	1298(2)	61(1)
C(11A)	1293(3)	1483(5)	252(2)	41(1)
N(12A)	1154(2)	189(4)	343(2)	54(1)
C(13A)	422(3)	-393(5)	327(3)	54(1)
C(14A)	368(4)	-1298(8)	-214(4)	103(2)
C(15A)	273(4)	-1114(7)	901(3)	96(2)
N(16A)	801(2)	2348(4)	171(2)	49(1)
C(17A)	1032(3)	3697(5)	42(3)	64(2)
C(18A)	637(5)	4597(7)	452(4)	127(3)
C(19A)	871(4)	4014(7)	-597(3)	80(2)
N(1B)	4558(2)	1969(4)	2201(2)	41(1)
C(2B)	4968(3)	2408(5)	1723(2)	43(1)
N(3B)	5681(2)	2533(4)	1838(2)	45(1)
C(4B)	6381(3)	2098(5)	2803(2)	47(1)
C(5B)	6285(3)	1719(5)	3393(2)	51(1)
C(6B)	5595(3)	1376(6)	3616(2)	56(1)
C(7B)	4964(3)	1434(5)	3264(2)	49(1)
C(8B)	5062(3)	1826(5)	2674(2)	42(1)
C(9B)	5748(3)	2179(5)	2440(2)	41(1)
N(10B)	4652(2)	2682(5)	1186(2)	57(1)
C(11B)	3768(3)	1798(5)	2234(2)	40(1)
N(12B)	3592(2)	521(4)	2252(2)	50(1)
C(13B)	2853(3)	50(5)	2434(2)	56(1)
C(14B)	2761(4)	-1350(7)	2255(4)	119(3)
C(15B)	2761(3)	198(8)	3106(3)	84(2)
N(16B)	3310(2)	2717(4)	2250(2)	42(1)
C(17B)	3554(3)	4080(5)	2307(2)	49(1)
C(18B)	3352(3)	4556(6)	2934(3)	70(2)
C(19B)	3199(4)	4900(6)	1819(3)	88(2)
O(1C)	2638(3)	3161(6)	5472(2)	111(2)
O(2C)	1636(2)	1954(4)	5351(2)	92(2)
C(1C)	1965(4)	3045(6)	5490(3)	76(2)

C(2C)	1437(4)	4046(6)	5658(4)	107(2)
C(3C)	2080(5)	819(8)	5181(4)	116(3)
C(4C)	2065(5)	642(9)	4575(3)	132(3)
O(1D)	4770(3)	-1557(5)	2174(3)	121(2)
O(2D)	5665(2)	-2798(4)	2532(2)	73(1)
C(1D)	5414(4)	-1774(7)	2237(3)	81(2)
C(2D)	6039(4)	-988(7)	2006(4)	106(2)
C(3D)	5102(4)	-3619(8)	2782(4)	103(2)
C(4D)	5460(4)	-4690(7)	3098(4)	112(3)

A.6 Crystal coordinates (X 10^4) for (1g)

	x	y	z	U(eq)
N(1)	5441(2)	2338(1)	5901(1)	29(1)
C(2)	4685(2)	2594(1)	4476(2)	26(1)
N(3)	4758(2)	2196(1)	3420(1)	27(1)
C(4)	5935(2)	1074(1)	3696(2)	36(1)
C(5)	6671(2)	594(1)	4740(2)	41(1)
C(6)	7042(2)	677(1)	6273(2)	43(1)
C(7)	6701(2)	1246(1)	6821(2)	38(1)
C(8)	5966(2)	1727(1)	5772(2)	28(1)
C(9)	5556(2)	1648(1)	4220(2)	27(1)
N(10)	4008(2)	3191(1)	4330(1)	30(1)
C(11)	2704(2)	3376(1)	3020(2)	29(1)
N(12)	1948(2)	3017(1)	1764(1)	32(1)
N(13)	2057(2)	3973(1)	2974(1)	35(1)
C(14)	2595(2)	4375(1)	4325(2)	35(1)
C(15)	2226(3)	5059(1)	3819(2)	51(1)
C(16)	1637(2)	4180(1)	5325(2)	45(1)
C(17)	447(2)	3192(1)	333(2)	35(1)
C(18)	1062(2)	3616(1)	-647(2)	48(1)
C(19)	-404(2)	2588(1)	-499(2)	49(1)

A.7 NOSEY spectrum for (1d)

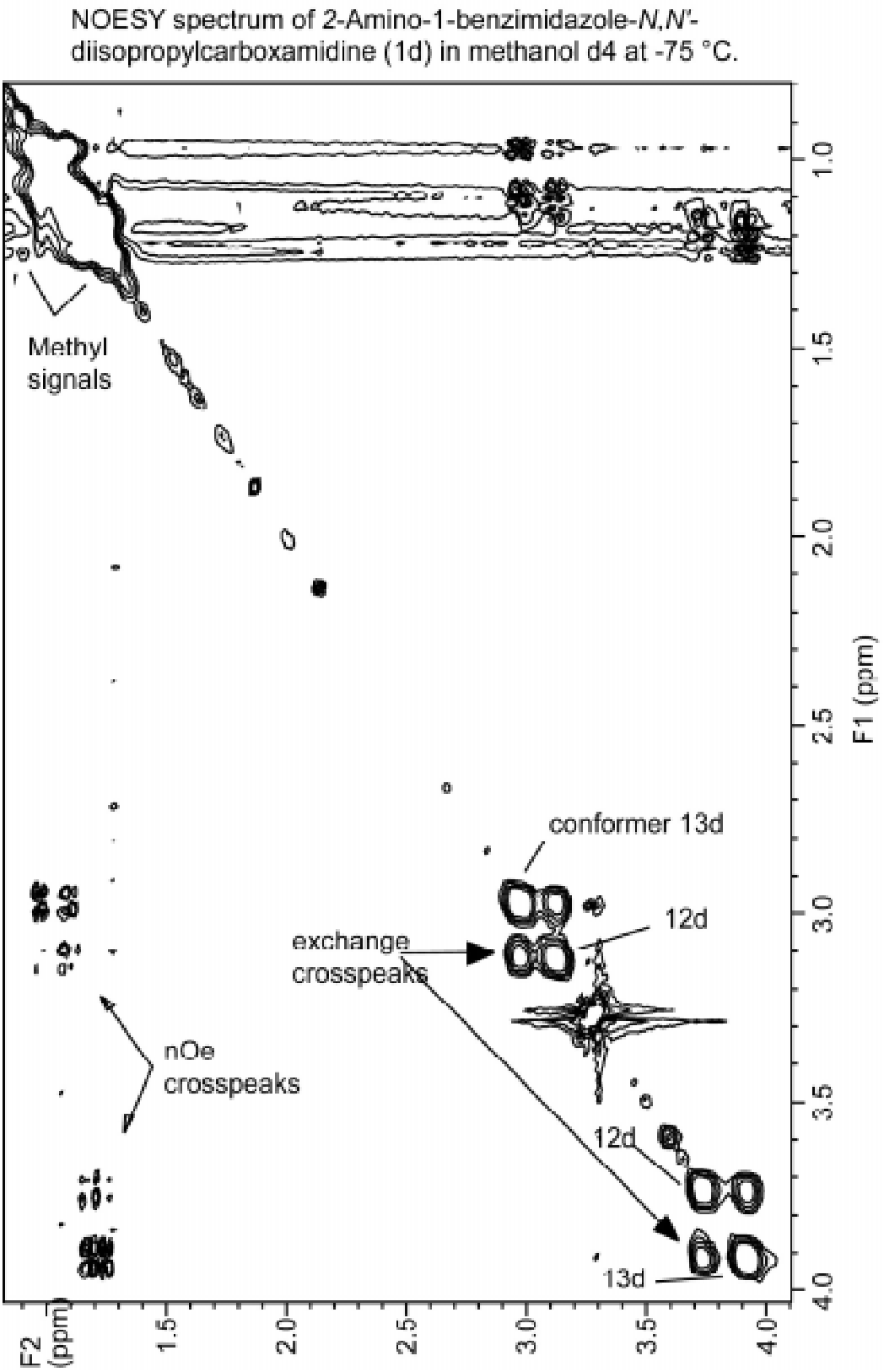

A.8 *N*-(1H-benzoimidazol-2-yl)-*N'*,*N'*-dimethyl-guanidine ^{1}H NMR (300 MHz; acetone)

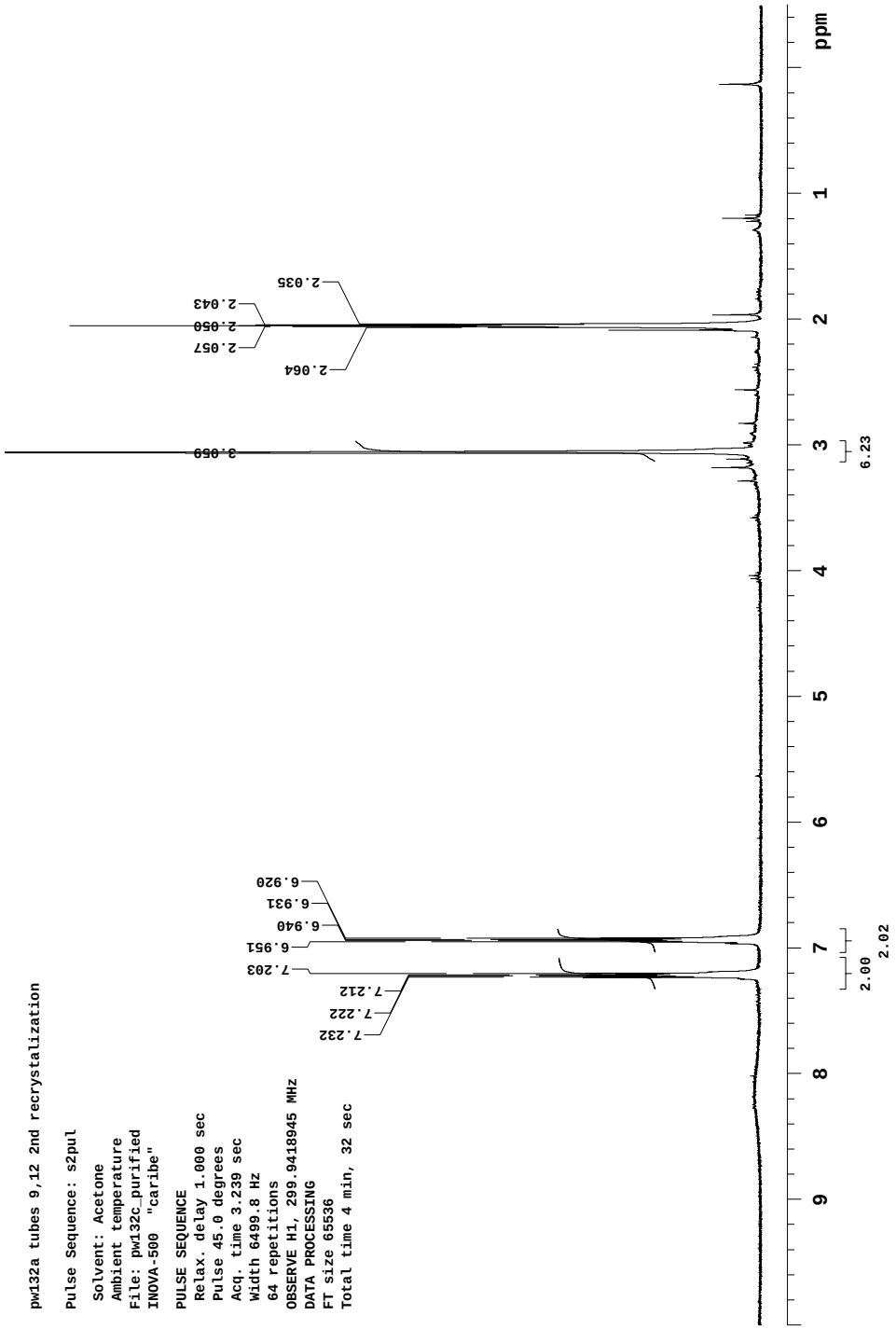

A.9 *N*-(1H-benzoimidazol-2-yl)-*N'*,*N''*-dimethyl-guanidine ^{13}C NMR (75.4 MHz; MeOH)

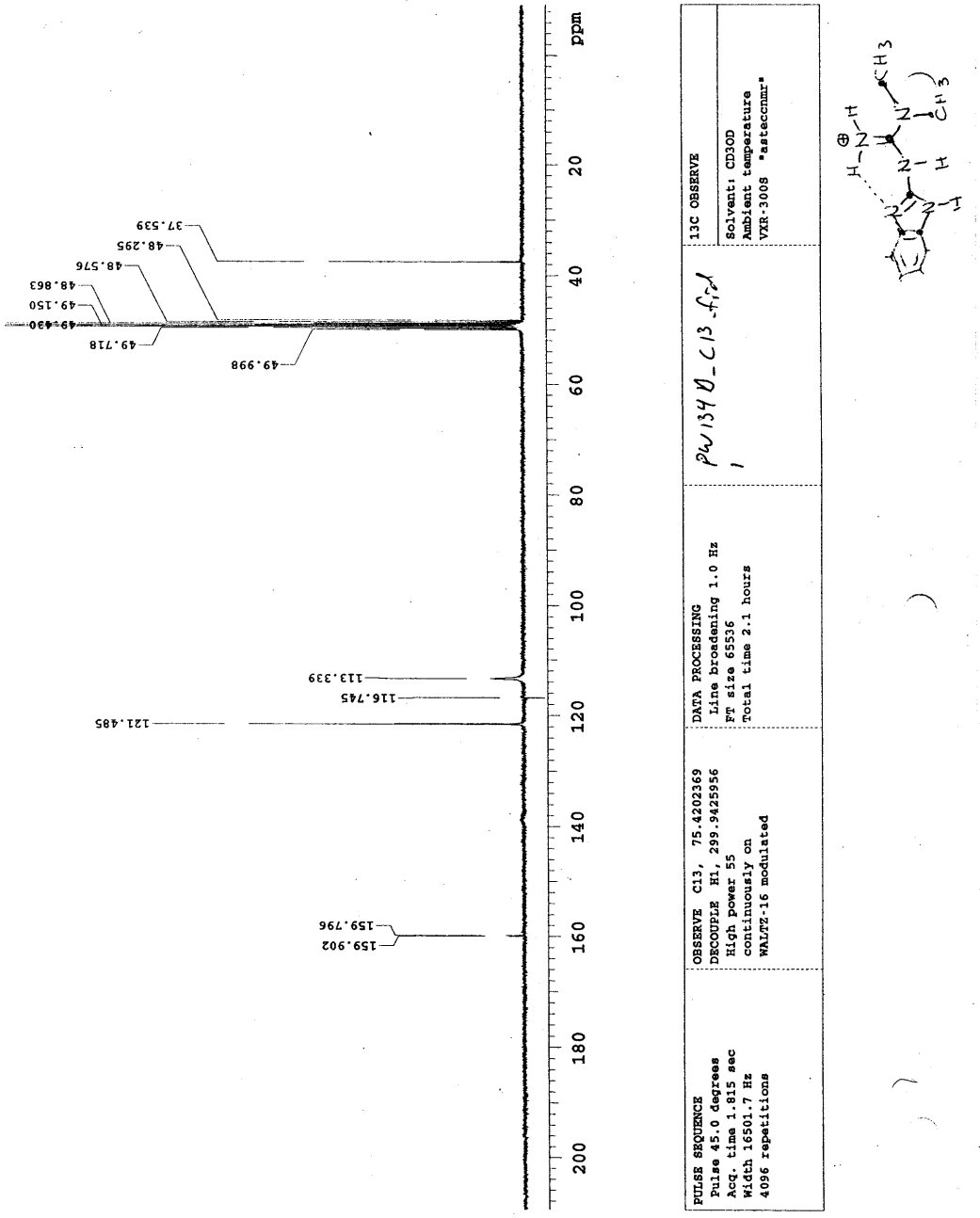

A.10 2-Amino-1-benzimidazole-*N,N'*-diisopropylcarboxamidine ^{1}H NMR (300 MHz; $CDCl_3$)

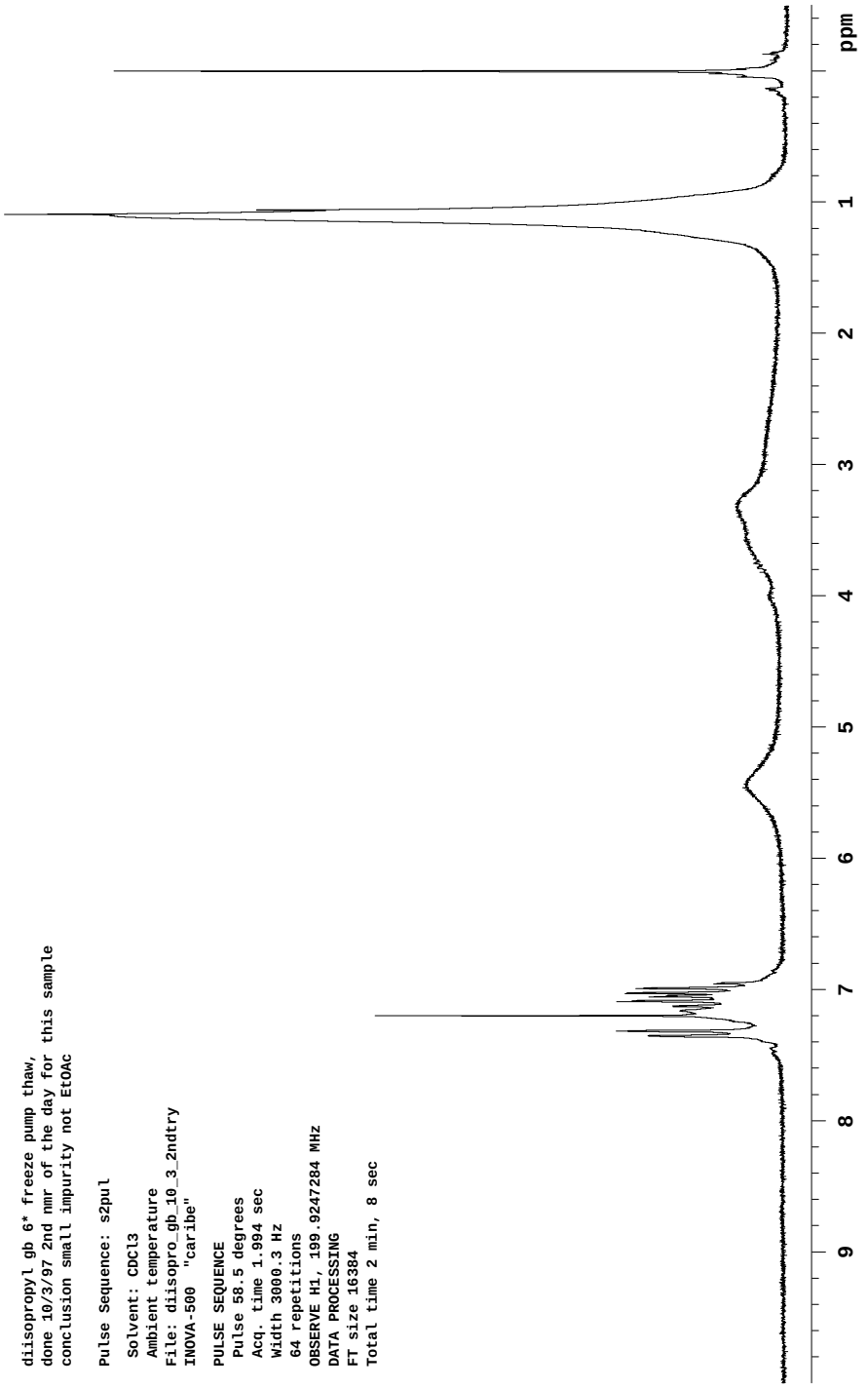

A.11 2-Amino-1-benzimidazole-*N,N'*-diisopropylcarboxamidine ^{13}C NMR (75.4 MHz; $CDCl_3$)

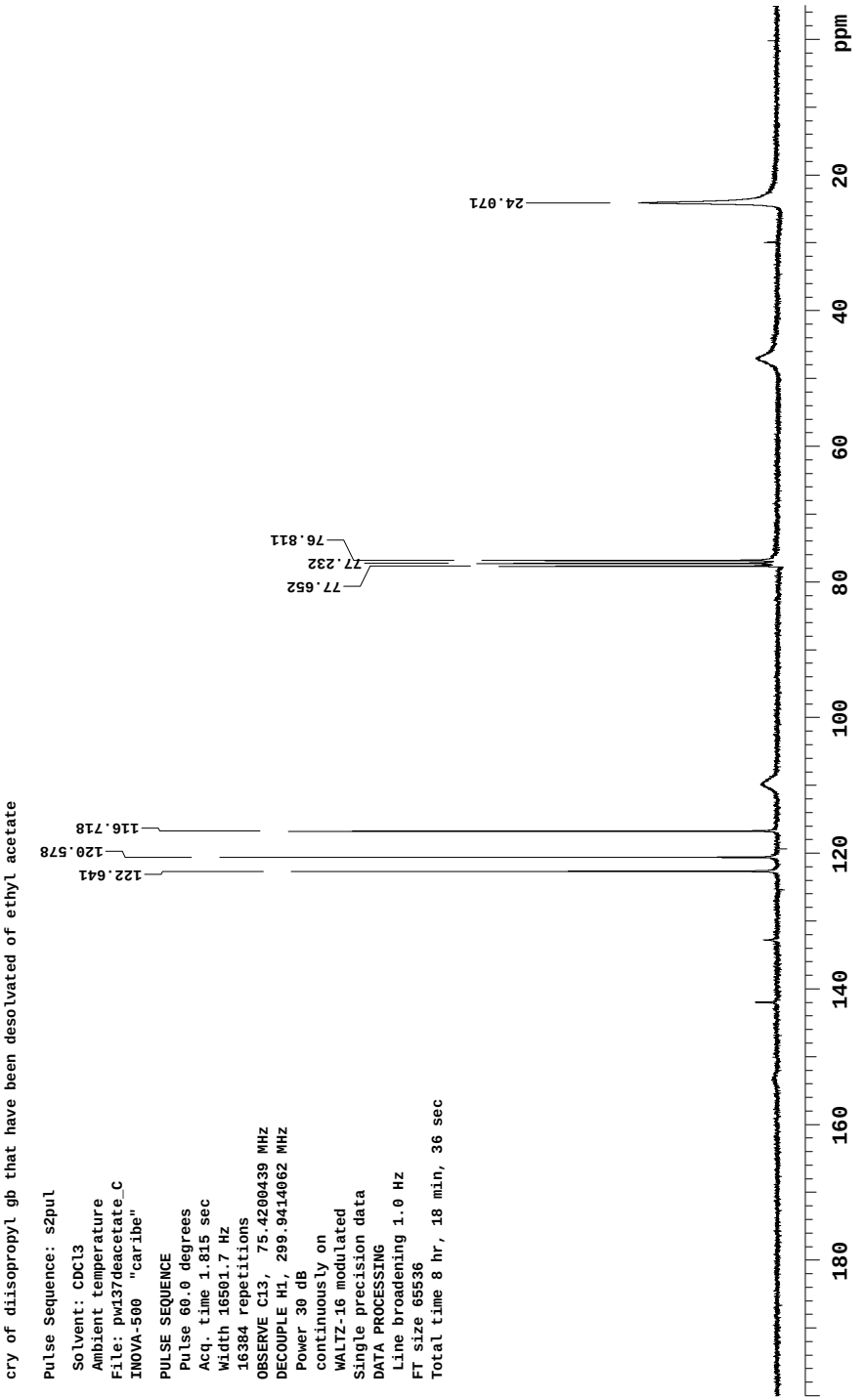

A.12 *N*-(1H-benzoimidazol-2-yl)-*N'*,*N''*-diisopropyl-guanidine ^{1}H NMR (300 MHz; $CDCl_3$)

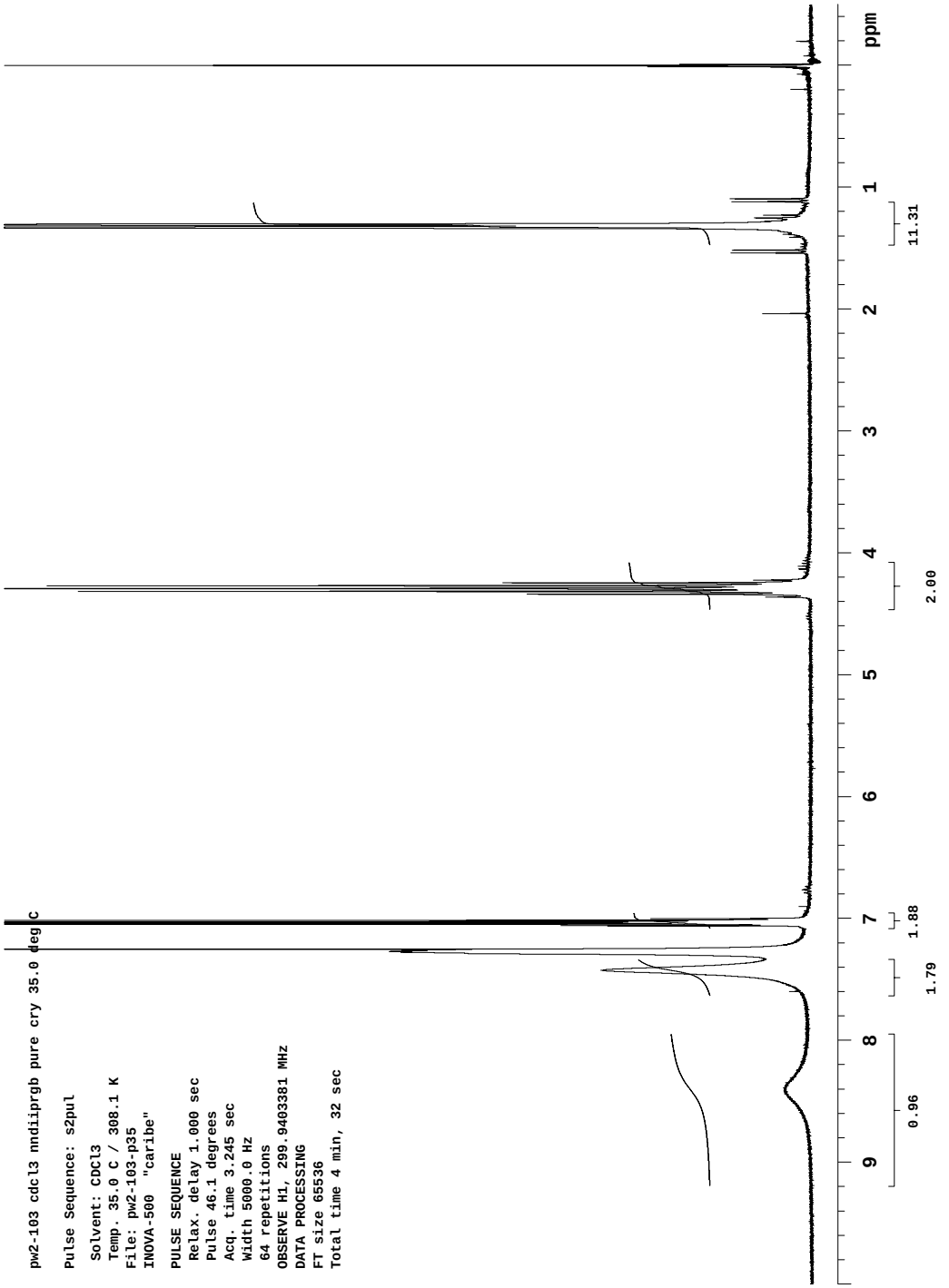

A.13 *N*-(1H-benzoimidazol-2-yl)-*N'*,*N''*-diisopropyl-guanidine ^{13}C NMR (75.4 MHz; Benzene)

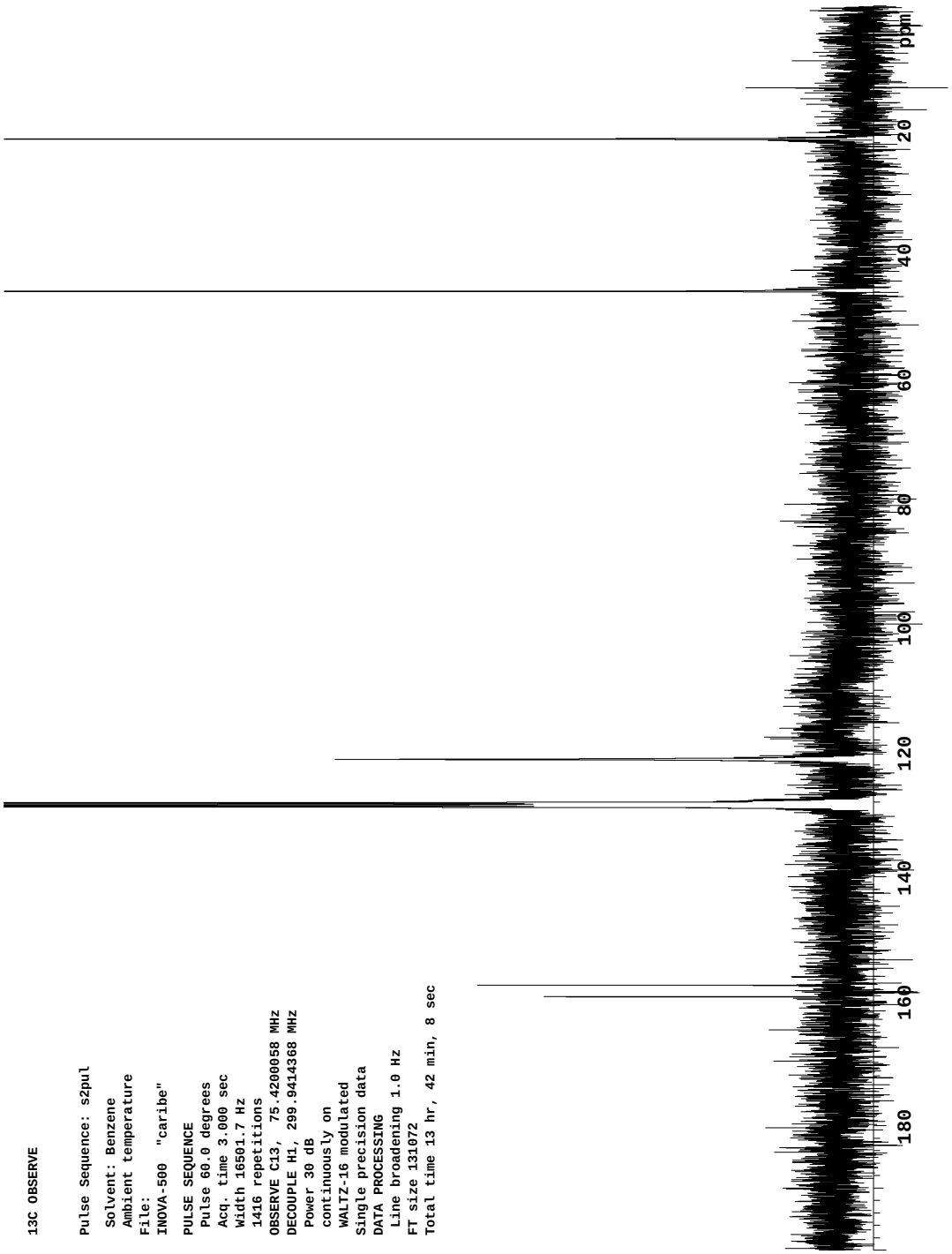

A.14 2-Amino-1-benzimidazole-*N',N'*-ditolylcarboxamidine ^{1}H NMR (300 MHz; $CDCl_3$)

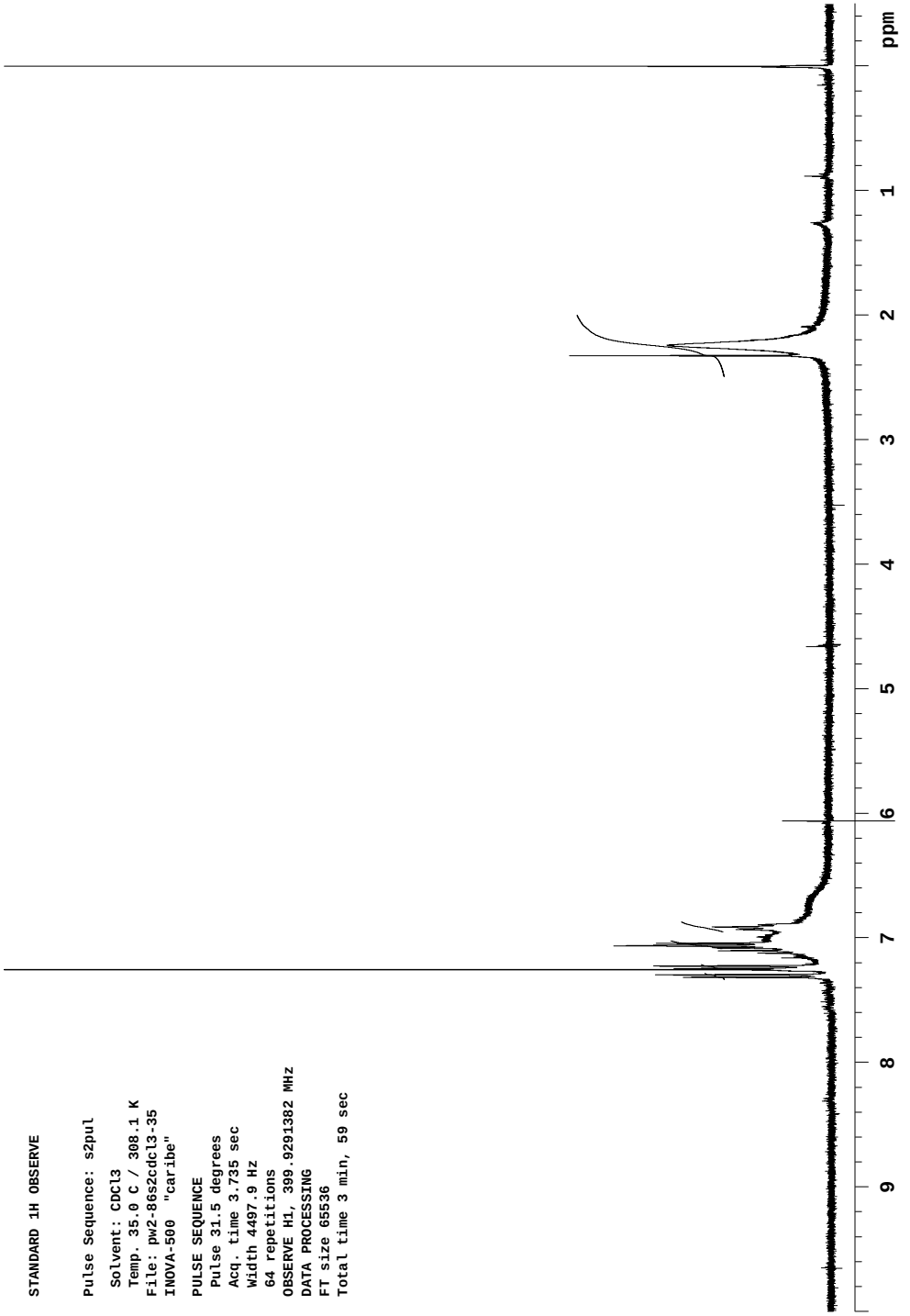

A.15 2-Amino-1-benzimidazole-*N',N'*-ditolylcarboxamidine ^{13}C NMR (75.4 MHz; $CDCl_3$)

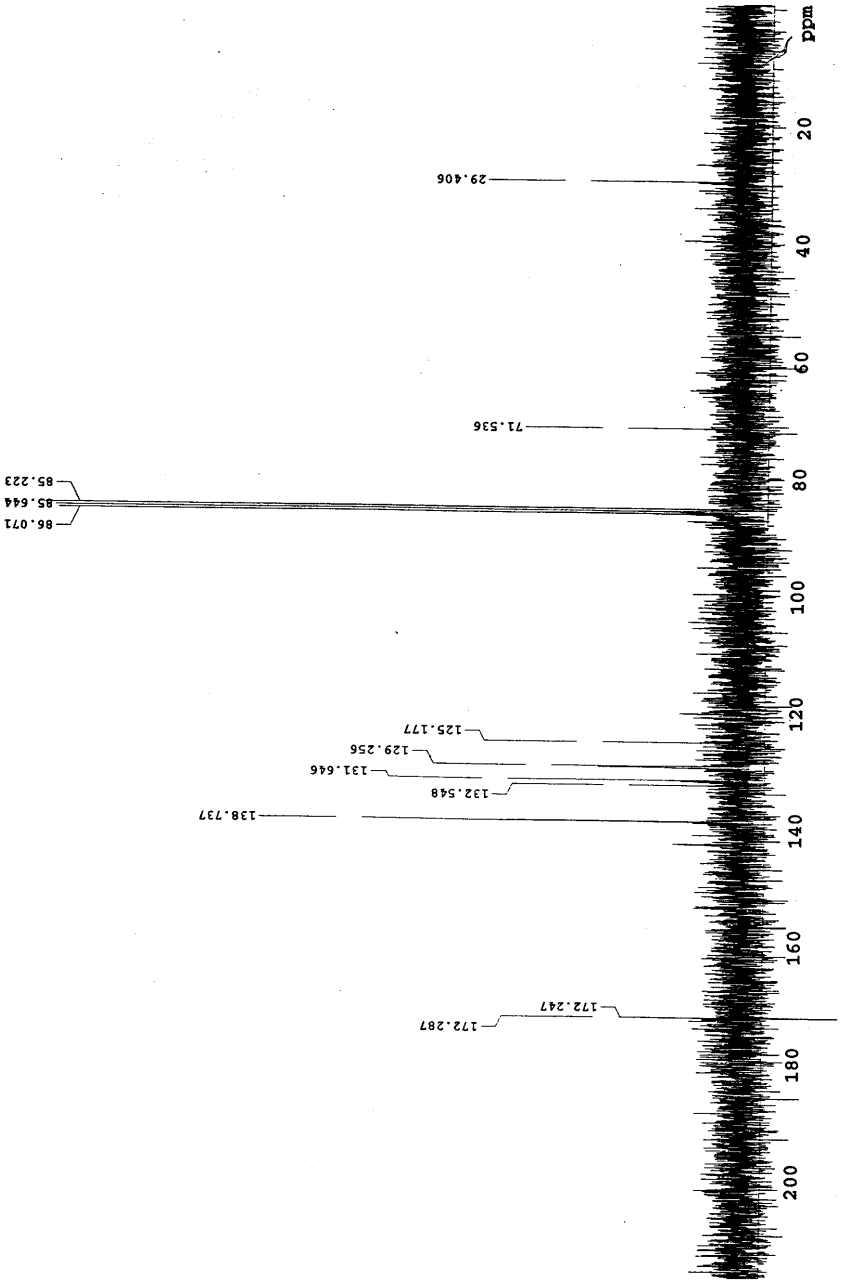

A.16 *N*-(1H-benzoimidazol-2-yl)-*N',N"*-diisopropyl-guanidine (1g) ^{13}C NMR (100 MHz; CD_3OD)

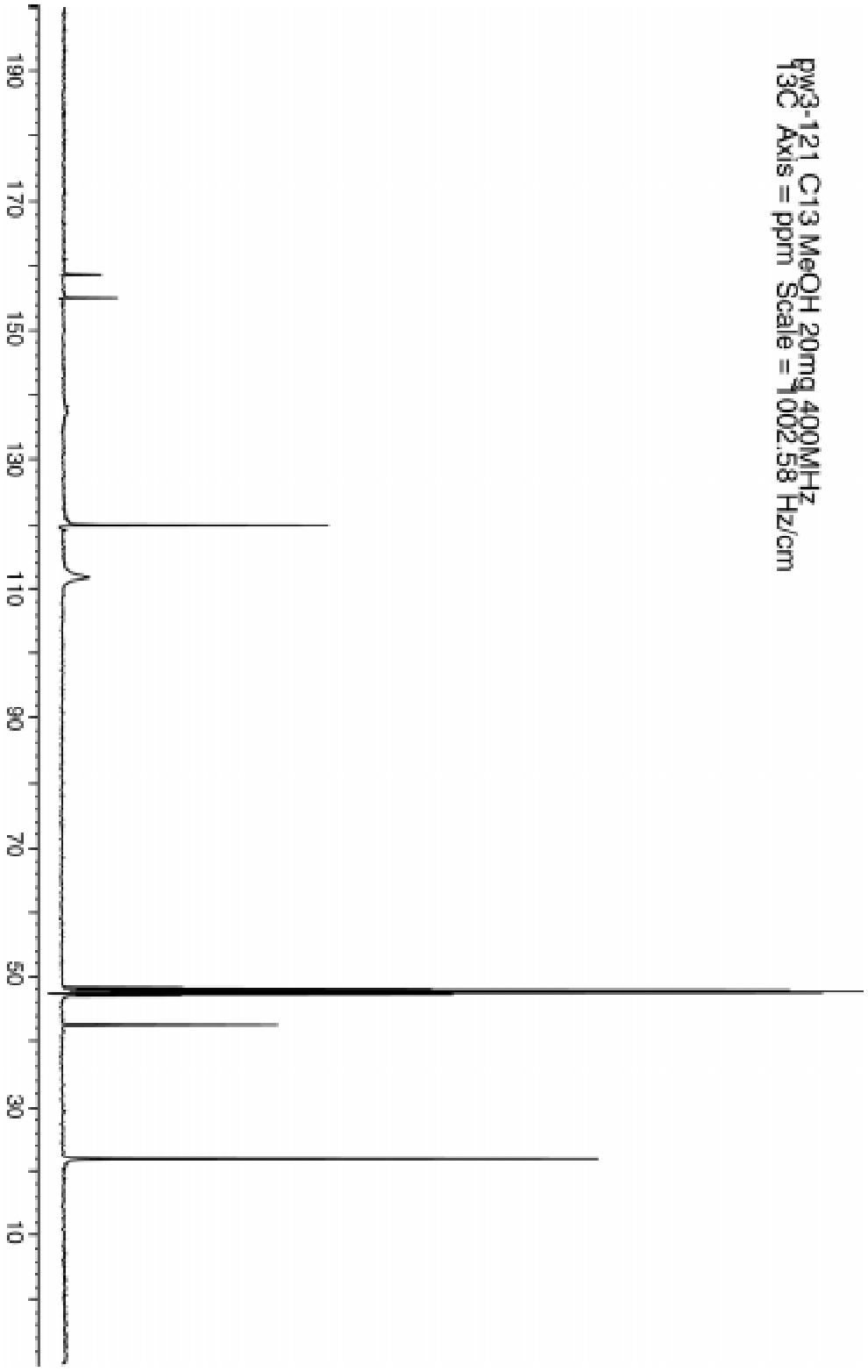

A.17 *N*-(1H-benzoimidazol-2-yl)-*N',N"*-diisopropyl-guanidine (1g) ^{13}C NMR (399.7 MHz; CD_3OD)

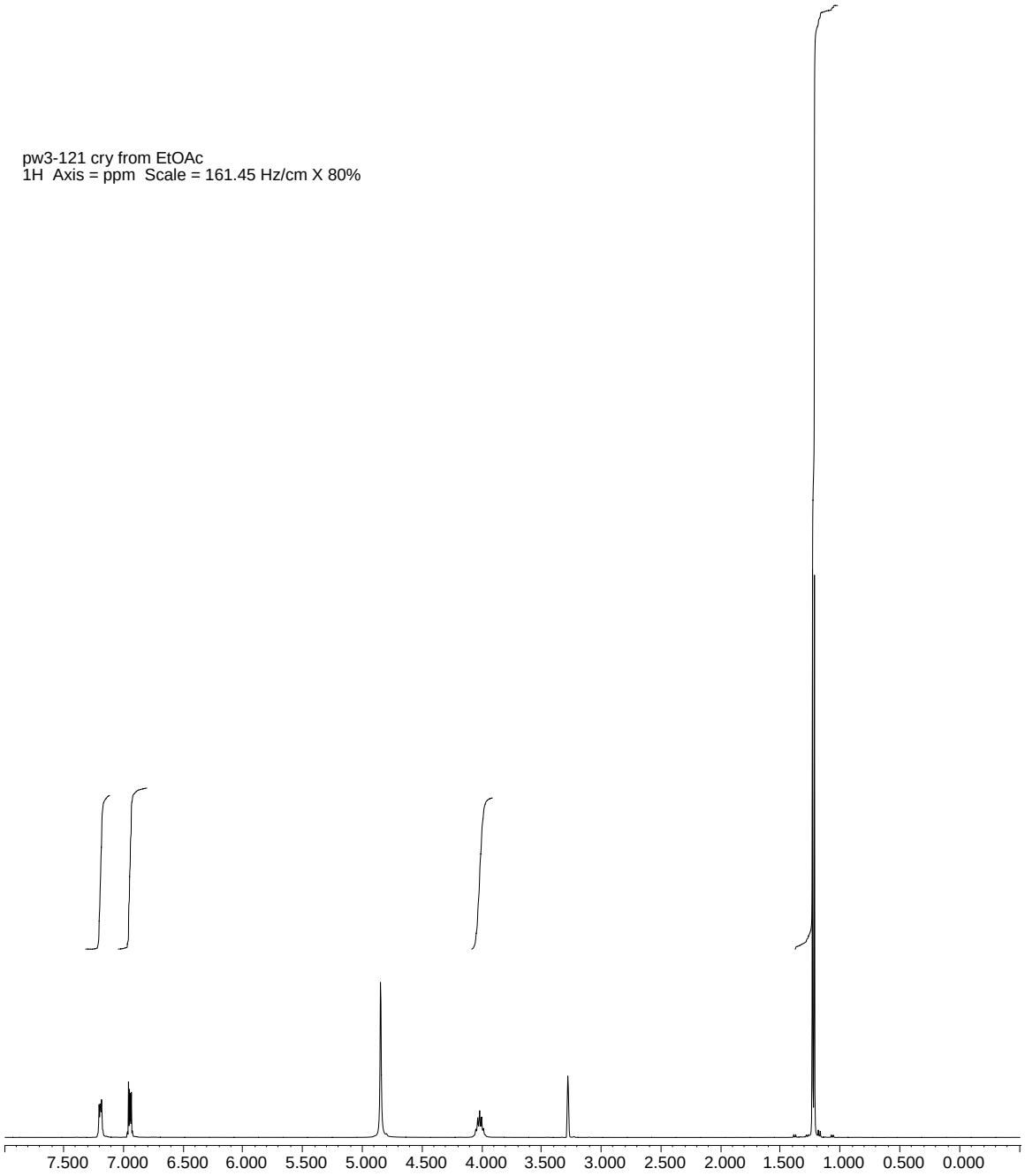

A.18 (33) ^{1}H NMR (399.7 MHz; $CDCl_3$)

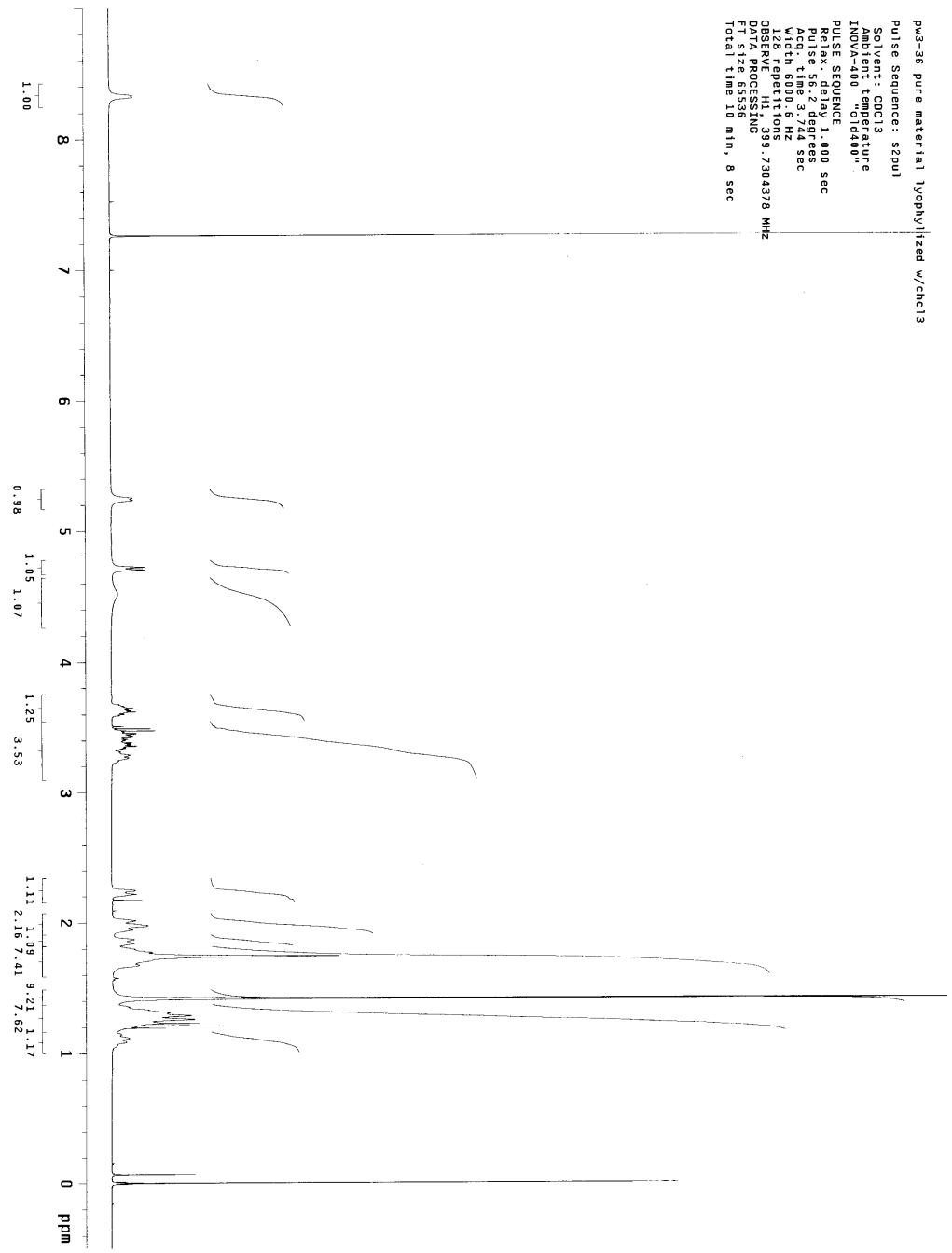

A.19 (33) ^{13}C NMR (100.5 MHz; $CDCl_3$)

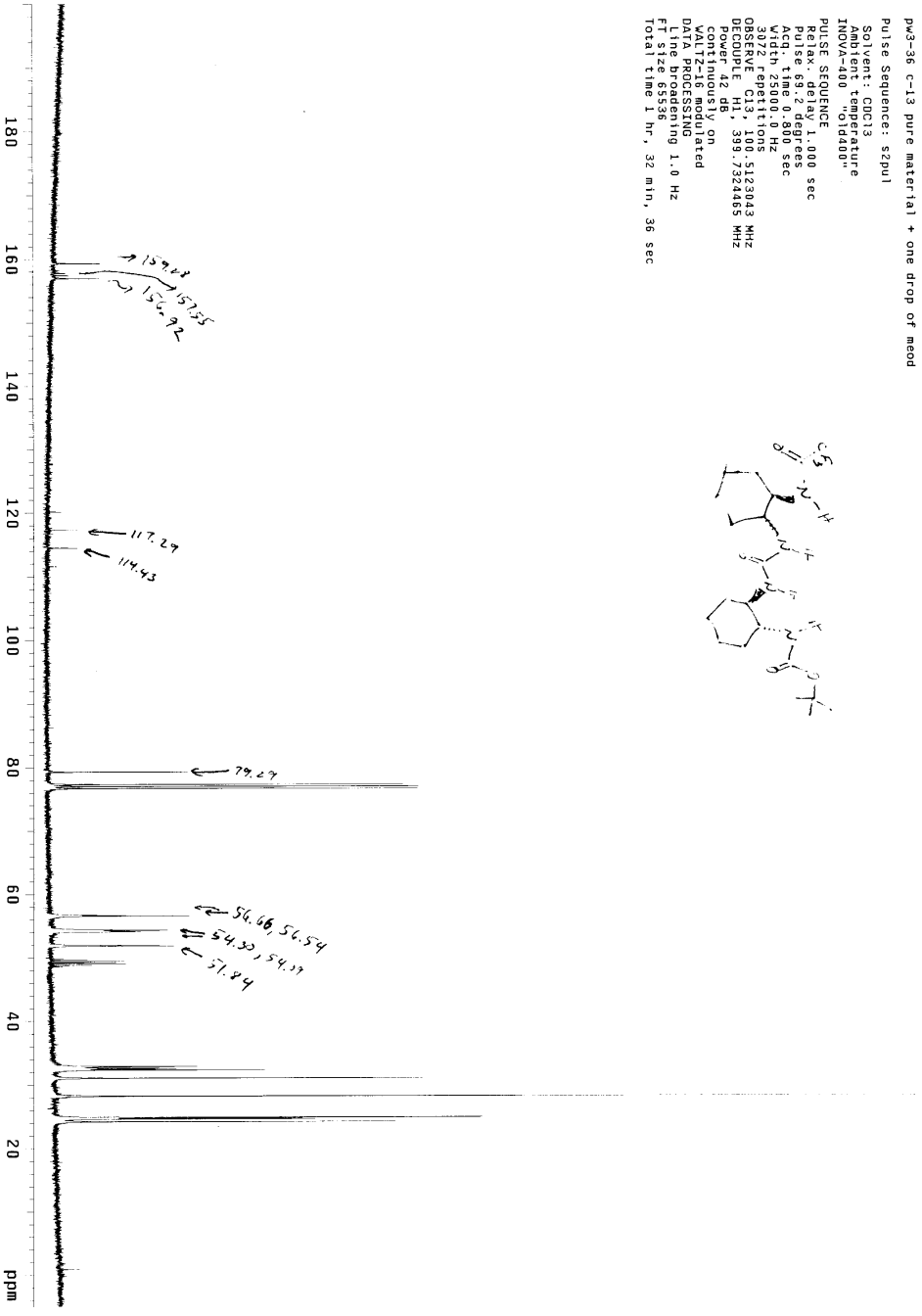

A.20 (39) ^{1}H NMR (199.9 MHz; $CDCl_3$)

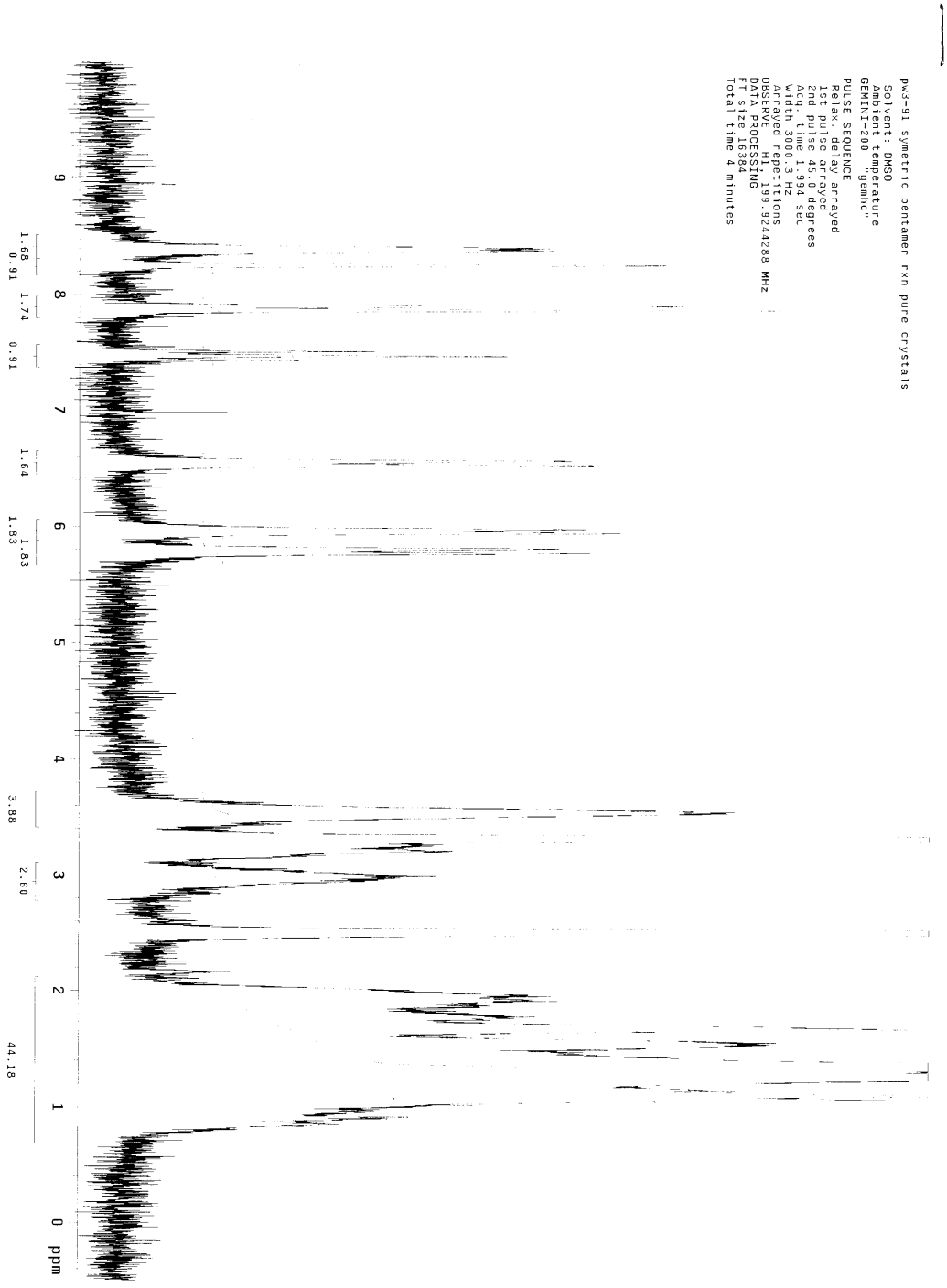

A.21 (39) ^{13}C NMR (50.3 MHz; $DMSO_{d6}$)

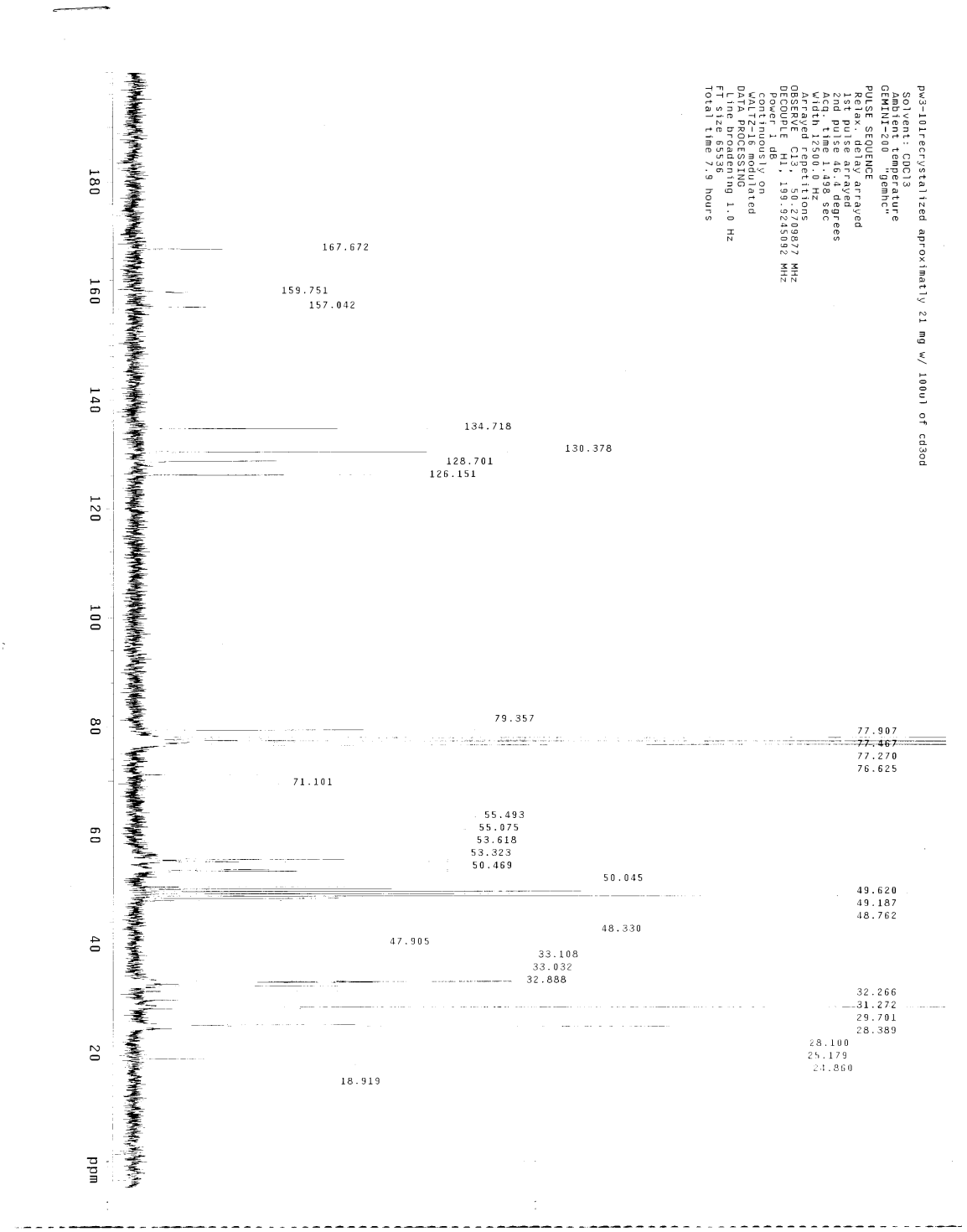

Bibliography

(1) Acerete, C.; Catalan, J.; Sanchez-Cabezudo, M. *Heterocycles* **1987**, *26*, 1581-1586.

(2) Amidon, G. L.; Yalkowsky, S. H.; Anik, S. T.; Valvani, S. C. *J. Phys. Chem.* **1975**, *72*, 2239.

(3) Appella, D. H.; Christianson, L. A.; Karle, I. L.; Powell, D. R.; Gellman, S. H. *J. Am. Chem. Soc.* **1996**, *118*, 13071-13072.

(4) Asano, T.; Furuta, H.; Hofmann, H.-J.; Cimiraglia, R.; Tsuno, Y.; Fujio, M. *J. Org. Chem.* **1993**, *58*, 4418-4423.

(5) Asano, T.; Okada, T.; Herkstroeter, W. G. *J. Org. Chem.* **1989**, *54*, 379-383.

(6) Baudlier, J. *J. Org. Chem.* **1998**, *63*, 5750-5761.

(7) Bauer, V. J.; Fulmor, W.; Morton, G. O.; Safir, S. R. *Tett. Lett.* **1968**, *90*, 6846-6847.

(8) Bedford, G. R.; Taylor, P. J.; Webb, G. A. *Magn. Reson. Chem.* **1995**, *33*, 383-388.

(9) Bidwell, L. M.; McManus, M. E.; Gaedigk, A.; Kakuta, Y.; Negishi, M.; Pedersen, L.; Martin, J. L. *J. Mol. Biol.* **1999**, *293*, 521-530.

(10) Caira, M. R. *Top. Curr. Chem.* **1998**, *198*, 164-208.

(11) Caira, M. R.; Watson, W. H.; Vogtle, F.; Muller, W. *Acta Crystallogr.* **1984**, *C40*, 1047.

(12) Charmant, J. P. H.; Lloyd-Jones, G. C.; Peakman, T. M.; Woodward, R. L. *Eur. J. Org. Chem.* **1999**, *1999*, 2501-2510.

(13) Contreras, R.; Andrade-Lopez, N.; Ariza-Castolo, A. *Heteroatom Chemistry* **1997**, *8*, 397-410.

(14) Eilingsfield, H.; Neubaur, G.; Seefelder, M.; Weidinger, H. *Chem. Ber.* **1964**, *97*, 1232-1245.

(15) Eliel, E. L.; Wilen, S. H. *Chiroptical Properties*; Eliel, E. L. and Wilen, S. H., Ed.; John Wiley & Sons, Inc.: New York, 1994, pp 991-1118.

(16) Folmer, B. J. B.; Sijbesma, R. P.; Kooijman, H.; Spek, A. L.; Meijer, E. W. *J. Am. Chem. Soc.* **1999**, *121*, 9001-9007.

(17) Forés, M.; Duran, M.; Solá, M. *J. Phys. Chem. A.* **1999**, *103*, 4525-4532.

(18) Frisch, M. J.; Trucks, G. W.; Schlegel, H. B.; Scuseria, G. E.; Robb, M. A.; Cheeseman, J. R.; Zakrzewski, V. G.; Montgomery, J. A.; Stratmann, R. E.; Burant, J. C.; Dapprich, S.; Millam, J. M.; Daniels, A. D.; Kudin, K. N.; Strain, M. C.; Farkas, O.; Tomasi, J.; Barone, V.; Cossi, M.; Cammi, R.; Mennucci, B.; Pomelli, C.; Adamo, C.; Clifford, S.; Ochterski, J.; Petersson, G. A.; Ayala, P. Y.; Cui, Q.; Morokuma, K.; Malick, D. K.; Rabuck, A. D.; Raghavachari, K.; Foresman, J. B.; Cioslowski, J.; Ortiz, J. V.; Stefanov, B. B.; Liu, G.; Liashenko, A.; Piskorz, P.; Komaromi, I.; Gomperts, R.; Martin, R. L.; Fox, D. J.; Keith, T.; Al-Laham, M. A.; Peng, C. Y.; Nanayakkara, A.; Gonzalez, C.; Challacombe, M.; Gill, P. M. W.; Johnson, B. G.; Chen, W.; Wong, M. W.; Andres, J. L.; Head-Gordon, M.; Replogle, E. S.; Pople, J. A. *Gaussian 98 (Revision A.6)*; Gaussian, Inc.: Pittsburgh PA, 1998.

(19) Gallivan, J. P.; Dougherty, D. A. *J. Am. Chem. Soc.* **2000**, *122*, 870.

(20) Gellman, S. H. *Acc. Chem. Res.* **1998**, *31*, 173-180.

(21) Gilli, G.; Bertolasi, V.; Gilli, P.; Ferretti, V. *J. Chem. Soc., Perkin Trans. 2* **1997**, 945-952.

(22) Gilli, G.; Bertolassi, V.; Gilli, P.; Ferretti, V. *Chem. Eur. J.* **1996**, *2*, 925-934.

(23) Gilli, G.; Gilli, P.; Bertolassi, V.; Ferretti, V. *J. Am. Chem. Soc.* **1994**, *116*, 909-15.

(24) Gin, M. S.; Moore, J. S. *Org. Lett.* **2000**, *2*, 135-138.

(25) Gould, I. R.; Kollman, P. A. *J. Am. Chem. Soc.* **1994**, *116*, 2493-2499.

(26) Graubaum, H.; Martin, D.; Csunderlik, C.; Glatt, H.-H.; Bacaloglu, R.; Malurea-Munteanu, M. *Z.Chem.* **1984**, *24*, 57-58.

(27) Greenfield, N.; Fasman, G. D. *Biochemistry* **1969**, *8*, 4108-4116.

(28) Gung, B. W.; Zhu, Z.; Zou, D.; Everingham, B.; Oyeamalu, A.; Crist, R. M.; Baudlier, J. *J. Org. Chem.* **1998**, *63*, 5750-5761.

(29) Hamuro, Y.; Geib, S. J.; Hamilton, A. D. *J. Am. Chem. Soc.* **1996**, *118*, 7529-7541.

(30) Heilmayer, W.; Sterk, H.; Kollenz, G. *Tetrahedron* **1998**, *54*, 8025-8034.

(31) Hermann, R. B. *J. Phys. Chem.* **1972**, *76*, 2239.

(32) Hodgson, P.; Lloyd-Jones, G. C.; Murray, M.; Peakman, T. M.; Woodward, R. L. *Chem. Eur. J.* **2000**, *6*, 4451-4460.

(33) Howard, A. E.; Kollman, P. A. *J. Med. Chem.* **1988**, *31*, 1669-1675.

(34) Howard, S. T.; Platts, J. A. *J. Org. Chem.* **1998**, *63*, 3568-3571.

(35) Huang, B.; Parquette, J. R. *Org. Lett.* **2000**, *2*, 239-242.

(36) Huang, B.; Parquette, J. R. *J. Am. Chem. Soc.* **2001**, *123*, 2689-2690.

(37) Kataoka, H. *2-(3N-substituted guanidino)benzimidazole derivatives*; Taisho Pharm.: Japan, 1962; Vol. 64, pp 19629d.

(38) Kawasaki, T.; Tokuhiro, M.; Kimizuka, N.; Kunitake, T. *J. Am. Chem. Soc.* **2001**, *123*, 6792-6800.

(39) Kessler, H.; Leibfritz, D. *Tetrahedron Lett.* **1970**, 1423-1426.

(40) Kim, B. H.; Cho, S. G.; Ha, T.-K. *J. Org. Chem.* **1999**, *64*, 5036-5041.

(41) King, F. E.; Acheson, R. M.; Spensley, P. C. *J. Chem. Soc.* **1948**, 1366-1371.

(42) Lagriffoule, P.; Wittung, P.; Eriksson, M.; Jensen, K. K.; Norden, B.; Buchardt, O.; Nielsen, P. E. *Chem. Eur. J.* **1997**, *3*, 912-919.

(43) Larrow, J. F.; Jacobsen, E. N. *J. Org. Chem.* **1994**, *59*, 1939--1942.

(44) Ledvina, P. S.; Yao, N.; Choudhary, A.; Quiocho, F. A. *Proc. Natl. Acad. Sci. USA* **1996**, *93*, 6786–6791.

(45) Lluch, J. M.; Garcia-Viloca, M.; Gelabert, R.; González-Lafont, À.; Moreno, M. *J. Am. Chem. Soc.* **1998**, *120*, 10203-9.

(46) Ma, J. C.; Dougherty, D. A. *Chem. Rev.* **1997**, *97*, 1303-1324.

(47) Macedo-Ribeiro, S.; Hemrika, W.; Renirie, R.; Wever, R.; Messerschmidt, A. *J. Biol. Inorg. Chem.* **1999**, *4*, 209-219.

(48) Marullo, N. P.; Wagener, E. H. *Tetrahedron Lett.* **1969**, 2555-2558.

(49) McDonald, D. Q.; Still, W. C. *Tetrahedron Lett.* **1992**, *33*, 7743-7746.

(50) Metropolis, N. R., A. W.; Rosenbluth, M. N.; Teller, A. H.; Teller, E. *J. Chem. Phys.* **1953**, *21*, 1087.

(51) Mohamadi, F.; Richards, N. G.; Guida, W. C.; Liskamp, R.; Lipton, M.; Caufield, C.; Chang, G.; Hendrickson, T.; Still, W. C. *J. Comput. Chem.* **1990**, *11*, 440.

(52) Mulla, H. R.; Cammers-Goodwin, A. *J. Am. Chem. Soc.* **2000**, *122*, 738-739.

(53) Murakami, Y.; Hara, H.; Okada, T.; Hashizume, H.; Kii, M.; Ishihara, Y.; Ishikawa, M.; Shimamura, M.; Mihara, S.-i.; Kato, G.; Hanasaki, K.; Hagishita, S.; Fujimoto, M. *J. Med. Chem.* **1999**, *42*, 2621-2632.

(54) Murthy, V. L.; Srinivasan, R.; E., D. D.; Rose, G. D. *J. Mol. Biol.* **1999**, *291*, 313-327.

(55) Ngola, S. M.; Dougherty, D. A. *J. Org. Chem.* **1998**, *63*, 4566-4567.

(56) Pappu, R. V.; Srinivasan, R.; Rose, G. D. *Proc. Natl. Acad. Sci. U.S.A.* **2000**, *97*, 12565-12570.

(57) Perrin, C. L.; Nielson, J. B. *Annu. Rev. Phys. Chem.* **1997**, *48*, 511-44.

(58) Perrin, C. L.; Ohta, B. K. *J. Am. Chem. Soc.* **2001**, *123*, 6520-6526.

(59) Porter, E. A.; Wang, X.; Lee, H. S.; Weisblum, B.; Gellman, S. H. *Nature* **2000**, *404*, 298-298.

(60) Prince, R. B.; Barnes, S. A.; Moore, J. S. *J. Am. Chem. Soc.* **2000**, *122*, 2758-2762.

(61) Prince, R. B.; Brunsveld, L.; Meijer, E. W.; Moore, J. S. *Angew. Chem., Int. Ed. Engl.* **2000**, *39*, 228-230.

(62) Ramachandran, G. N.; Sasisekharan, V. *J. Mol. Biol.* **1963**, *7*, 95-99.

(63) Recker, J.; Tomcik, D. J.; Parquette, J. R. *J. Am. Chem. Soc.* **2000**, *122*, 10298-10307.

(64) Saunders, M.; Houk, K. N.; Wu, Y.-D.; Still, W. C.; Lipton, M.; Chang, G.; Guida, W. C. *J. Am. Chem. Soc.* **1990**, *112*, 1419-1427.

(65) Schenck, H. L.; Gellman, S. H. *J. Am. Chem. Soc.* **1998**, *120*, 4869-4870.

(66) Seebach, D.; Jacobi, A.; Rueping, M.; Gademann, K.; Ernst, M.; Jaun, B. *Helv. Chim. Acta.* **2000**, *83*, 2115-2140.

(67) Sindkhedkar, M. D.; Mulla, H. R.; Cammers-Goodwin, A. *J. Am. Chem. Soc.* **2000**, *122*.

(68) Solà, M.; Luque, F. J.; Forés, M.; Duran, M.; Orozco, M. *J. Phys. Chem. A* **1999**, *103*, 4525-32.

(69) Steel, P. J. *J. Heterocycl. Chem.* **1991**, *28*, 1817-18.

(70) Still, W. C.; Tempczyk, A.; Hawley, R. C.; Hendrickson, T. *J. Am. Chem. Soc.* **1990**, *112*, 6127-6129.

(71) Tesmer, J. J. G.; Klem, T. J.; Deras, M. L.; Jo, D. V.; Smith, J. L. *Nature Structural Biology* **1996**, *3*, 74-87.

(72) Tóth, G.; Szöllösy, A.; Almásy, A.; Podányi, B.; Hermecz, I.; Breining, T.; Mészáros, Z. *Org. Mag. Res.* **1983**, *21*, 687-693.

(73) Wachter-Jurcsak, N.; Detmer, C. A. *Org. Lett.* **1999**, *1*, 795-8.

(74) Walgers, R.; Lee, T. C.; Cammers-Goodwin, A. *J. Am. Chem. Soc.* **1998**, *120*, 5073-5079.

(75) Watson, W. H.; Galloy, J.; Grossie, D. A.; Voegtle, F.; Mueller, W. M. *J. Org. Chem.* **1984**, *49*, 347-53.

(76) Weiner, S. J.; Kollman, P. A.; Case, D. A.; Singh, U. C.; Ghio, C.; Alagona, G.; Profeta, S.; Weiner, P. *J. Am. Chem. Soc.* **1984**, *106*, 765-784.

(77) Werder, M.; Hauser, H.; Abele, S.; Seebach, D. *Helv. Chim. Acta.* **1999**, *82*, 1774-1783.

(78) Wildes, P. D.; Pacifici, J. F.; Irick, G.; Whitten, D. G. *J. Am. Chem. Soc.* **1971**, *93*, 2004.

(79) Wooley, K. L.; Moore, J. S.; Wu, C.; Yang, Y. *Proc. Natl. Acad. Sci.* **2000**, *97*, 11147-11148.

(80) Xu, D.; Prasad, K.; Repic, O.; Blacklock, T. J. *Tetrahedron Lett.* **1995**, *36*, 7357-7360.

(81) Zoltewicz, J. A.; Maier, N. M.; Fabian, W. M. F. *J. Org. Chem.* **1998**, *63*, 4985-4990.

Vita

Peter G. Willis was born on the 18th of Febuary, 1972 in Ames, Iowa USA. He got his high school diploma from Berea Community High School in Berea, KY in May 1990. He received a Bachelors of the Arts degree from Berea College, in Berea, KY in May 1994. In Berea, he worked as a teaching assistant, and as a research assistant testing the oxidative properties of quinuclidine and dabco bromine complexes. He was awarded the J. Stanton King Award, given to the top two science majors at Berea College for their contribution to excellent academics at Berea College in 1994. From 1995 to 1996 he worked as a formulations chemist for ICC Chemicals in Cincinnati, OH. In January of 1996 he joined the chemistry department at the University of Kentucky. For the last two years he has been a participant in the National Science Foundation - IGERT program with the fellowship that comes with this program.

Publications resulting from this work

1. Peter Willis, Marlon Jones, Milind Sindkhedkar, and Arthur Cammers-Goodwin. "Molecular Recognition with Chiral Oligourea Foldamers." (In progress)

2. Peter, G. Willis and Arthur Cammers-Goodwin* "Conformation of Guanidinobenzimidazole, Strain, Planarity and a Intramolecular Hydrogen Bond" (In progress)

Publications not included in this work

1. Christopher B. Martin, Hormuzd R. Mulla, Peter G. Willis, and Arthur Cammers-Goodwin*; "Derivatives of N-Benzyl-2-phenylpyridinium Bromide, Minimalist Models for Face-to-Face, Center-to-Edge -Stacking in Water", *J. Org. Chem.*; **1999**; 64; 7802-7806.